

**Lifetime prediction for solder die-attach
in power applications by means
of primary and secondary creep**

**Von der Fakultät für Maschinenbau, Elektrotechnik und
Wirtschaftsingenieurwesen der Brandenburgischen
Technischen Universität Cottbus
zur Erlangung des akademischen Grades eines Doktor-Ingenieurs
genehmigte Dissertation**

vorgelegt von

Dipl.-Ing.
Sylvain Déplanque

geboren am 01.06.1979 in Lille (Frankreich)

Vorsitzender: Professor Dr.-Ing. habil. V. Michailov

Gutachter: Professor Dr.-Ing B. Viehweger

Gutachter: Professor Dr.rer.nat.habil. B. Michel

Tag der Mündlichen Prüfung: 04. Dezember 2007

Summary

The objective of this thesis was to accurately check and improve the models existing for eutectic solder alloys used in simulation tools. Creep deformation, which is the most important deformation mode of solders, of two solder alloys, the widely used eutectic SnPb and the environmentally friendly alternative solder alloy SnAgCu was tested. It was shown that it is necessary to model two different stages of this high temperature induced mechanism: To improve the current material definition, primary creep must be implemented in the FE-software in addition to the existing secondary creep models. This thesis shows how it is possible to test creep behaviour under cyclic loading conditions with a test specimen of novel design. So, primary creep was observed and reoccurs cyclically under such test conditions. Furthermore, steady state creep is also always observed. A Constitutive equation combining both primary and secondary creep was given and verified. This model was implemented in FE-code *Ansys*, and after performing different kinds of simulation, the necessity of simulating primary creep was demonstrated. In order to achieve reliability information by FE-simulation of solder die attach, the creep-fatigue behaviour with the mean of crack propagation must be modeled. Various kinds of chips on copper substrate (power-transistors) were thermally tested, and different methods were used to investigate crack propagation. These methods were scanning acoustic microscopy and microstructure analysis by optical microscopy. The influence of damage on thermal behaviour (i.e. the thermal resistance of the device) was also assessed. These results were compared with the simulation results in order to build a lifetime prediction model based on crack propagation analysis.

Zusammenfassung

Das Ziel dieser Arbeit war es, die schon vorhandenen Modelle für die Lötstellensimulation zu verbessern. Da das Kriechen für die Verformung von Lötlegierungen der wichtigste Mechanismus ist, wurde das Kriechverhalten für zwei Lötlegierungen untersucht. Es handelt sich dabei um die weltweit bekannten Legierungen eut. SnPb und das umweltverträglichere SnAgCu. Es ist empfehlenswert zwei Bereiche dieses Hoch-Temperatur Mechanismus zu modellieren. Um die bisherigen Werkstoffmodelle verbessern zu können, ist das primäre Kriechen zusätzlich zu den bestehenden sekundären Kriechmodellen in FE-Programme zu implementieren. Diese Arbeit zeigt, wie das Kriechen unter zyklischer Belastung mit einer neuen Prüfkörpergeometrie untersucht werden kann. Unter solchen Randbedingungen ist erneut primäres Kriechen zu beobachten. Weiterhin wurde immer auch stationäres Kriechen beobachtet. Eine Zustandsgleichung, bestehend aus primärem und sekundärem Kriechen, wurde entwickelt. Dieses Modell wurde in den FE-Code Ansys implementiert, und nach der Durchführung von verschiedenen Packagingsimulationen wurde ebenfalls festgestellt, dass das primäre Kriechen unbedingt berücksichtigt werden muss. Um eine Lebensdauerprognose von flächigen Lötstellen zu erreichen, müssen die Kriechermüdung sowie der Rissfortschritt modelliert werden. Einige Testdemonstratoren (Leistungstransistor auf Kupfer) wurden thermo-mechanisch geprüft (Temperaturschock und Temperaturwechsel). Durch zwei verschiedene Methoden (Ultraschallmikroskopie und Gefügeanalyse) wurde die Rissinitiierung und der Rissfortschritt untersucht. Der Einfluss der Schädigung auf das thermische Verhalten des Testobjektes (thermischer Widerstand des Bauelements) wurde ebenfalls bewertet. Diese experimentellen Ergebnisse wurden mit den Simulationsergebnissen verglichen, um ein neues Lebensdauermodell basierend auf der Rissfortschrittanalyse zu bauen. Eine sehr gute Übereinstimmung erlaubt nun die Zuverlässigkeitsvorhersage von flächig aufgelöteten Chips im Bereich der Leistungselektronik.

Danksagung

Zuerst möchte ich meinem Doktorvater Herrn Prof. Viehweger von der Technischen Universität Cottbus für die Betreuung der Dissertation, stete Diskussionsbereitschaft und die Schaffung einer sehr motivierenden Arbeitsatmosphäre danken.

Für die Übernahme eines zweiten Gutachtens spreche ich Herrn Prof. Bernd Michel vom Fraunhofer Institut für Zuverlässigkeit und Mikrointegration in Berlin meinen Dank aus. Herr Prof. Bernd Michel hat als Abteilungsleiter die Arbeit von Beginn an fachlich und organisatorisch begleitet.

Des weiteren danke ich Herrn Prof. Michailov für die Übernahme des Prüfungsvorsitzes.

Ein herzliches Dankeschön gilt auch meinem Gruppenleiter Herrn Dr. Wolfgang Nüchter von der Firma Robert Bosch GmbH für die hervorragende und sehr engagierte Betreuung der Dissertation.

Herrn Dr. Bernhard Wunderle vom Fraunhofer Institut für Zuverlässigkeit und Mikrointegration in Berlin, der die Dissertation in Berlin betreut hat, möchte ich für die sehr interessante Diskussion herzlich danken.

Die Einbindung in die Abteilung CR/APJ bei Robert Bosch unter der Leitung von Herrn Dr. Schmitz trug zum Gelingen der Arbeit bei. Besonders die Zusammenarbeit mit Herrn Manfred Spraul bereitete mir viel Freude. Ich danke auch allen Kollegen der Gruppe APJ3, besonders Herrn Rainer Holz und Thomas Ruczyka für die sehr gute Zusammenarbeit.

Unterstützung in jeder Hinsicht erfuhr ich von meinen Kollegen der Abteilung Mechanical Reliability and Micromaterials des Fraunhofer IZM. Besonders danke ich Herrn Dr. Hans Walter, Herrn Dr. Rainer Dudek, Herrn Dr. Ralph Schacht, Herrn Dr. Olaf Wittler, Herrn Daniel May, Herrn Jürgen Hussack, Frau Astrid Gollhardt, Dr. Dietmar Vogel, Herrn Dr. Faust, Herrn Florian Schindler, Frau Kreissig, .

Ich bedanke auch Jean-Marc, Maryse, Laurie, Ambroise, Jean und Armelle für ihren Geduld.

Nicht zuletzt danke ich meiner Frau Adèle für das Verständnis und den notwendigen Rückhalt, den sie mir während der Promotion geben konnte.

Contents

| | |
|--|------------|
| Summary | i |
| Zusammenfassung | iii |
| Danksagung | v |
| 1 Introduction and motivations | 1 |
| 2 Theoretical background | 3 |
| 2.1 Elasticity, plasticity and creep | 3 |
| 2.1.1 tensile stress and strain | 3 |
| 2.1.2 multiaxiale stress and strain | 4 |
| 2.1.3 elasticity and plasticity | 7 |
| 2.1.4 creep | 9 |
| 2.2 model describing elasticity,plasticity and creep | 11 |
| 2.2.1 elastic model | 11 |
| 2.2.2 plastic model | 12 |
| 2.2.3 creep models | 13 |
| 2.2.4 chaboche Model | 16 |
| 2.2.5 Anand's Model | 17 |
| 2.3 lifetime prediction | 18 |
| 2.3.1 stress-life analysis | 18 |
| 2.3.2 strain-life analysis | 20 |
| 2.3.3 accumulated creep strain methods | 21 |
| 2.3.4 energy based methods | 21 |
| 2.3.5 crack propagation analysis | 22 |

| | | |
|----------|--|-----------|
| 3 | Creep Test Sample | 23 |
| 3.1 | An overview of different creep test specimens | 23 |
| 3.1.1 | The folk-shape specimen test | 24 |
| 3.1.2 | The ring-and-plug test specimen | 25 |
| 3.1.3 | The single lap test specimen | 30 |
| 3.1.4 | The double lap test specimen | 30 |
| 3.1.5 | The grooved-lap test specimen | 31 |
| 3.2 | comparison between the different test specimens | 32 |
| 3.2.1 | mechanical load | 32 |
| 3.2.2 | thermal load | 34 |
| 3.3 | improvement of the test specimen | 35 |
| 3.3.1 | new kind of test sample | 35 |
| 3.3.2 | fabrication and investigation of the test sample | 37 |
| 4 | Development of new creep constitutive equations | 40 |
| 4.1 | creep tests | 40 |
| 4.2 | steady-state creep | 45 |
| 4.2.1 | SnPb | 45 |
| 4.2.2 | SnAgCu | 46 |
| 4.3 | primary creep | 48 |
| 5 | Implementation of creep laws in FE-codes | 52 |
| 5.1 | Fortran Subroutine | 52 |
| 5.1.1 | different kind of subroutines | 52 |
| 5.1.2 | Computation of the creep strain | 53 |
| 5.1.3 | from an equivalent stress and strain to a stress and strain tensor | 53 |
| 5.2 | New algorithm | 55 |
| 5.2.1 | stepwise creep test and implementation in the subroutine | 55 |
| 5.2.2 | detection of the change of stress direction | 60 |
| 5.3 | verification of the subroutine | 61 |
| 5.3.1 | verification of the algorithm | 61 |
| 5.3.2 | comparison between analytical and FE-calculation | 62 |
| 5.3.3 | verification through a tensile test | 63 |
| 5.4 | influence of the primary creep | 64 |
| 5.4.1 | shear test | 64 |
| 5.4.2 | flip-chips | 64 |
| 5.4.3 | PBGA | 66 |
| 5.5 | conclusion | 67 |

| | |
|--|------------|
| 6 Lifetime Prediction of Die Attaches | 68 |
| 6.1 Scanning Acoustic Microscopy (SAM), principe and application | 68 |
| 6.2 Test Vehicle | 70 |
| 6.2.1 test devices, geometry and soldering | 70 |
| 6.2.2 experimental procedure | 71 |
| 6.3 Thermal behavior | 74 |
| 6.4 crack growth | 77 |
| 6.5 FE-Model | 78 |
| 6.6 results | 80 |
| 6.7 verification test | 88 |
| 6.8 conclusion | 91 |
| Bibliography | 93 |
| Curriculum Vitae | 101 |

Chapter 1

Introduction and motivations

Power electronics are more more used in the automotive industry. In Surface mounting technology, the use of miniaturized power devices increases. Power electronics is used in electronic motor control units, braking systems, air- conditioning systems, and for those systems, the demand is the same: higher efficiency, more compactness, lower price and higher reliability. In this case it is no longer acceptable to perform long thermal cycling tests to get the lifetime of electronic components. For accuracy in the development process, simulation tools and particularly the finite element method [1] are used to estimate the lifetime of power devices soldered on bare copper substrate (i.e. Die attach). Indeed, the thermal behavior of this kind of devices, cyclicly loaded, could be strongly influenced by the damage of the solder joint, even more that the electrical behavior. This thesis purposes a full model of solder joints for lifetime prediction of chip on copper board. Two different material behaviors were investigated:

- a model describing the deformation of solder joints under thermo-mechanical load.
- a model describing the crack propagation in the chip on copper board solder joints (die attaches).

It will be shown in this thesis, that it is important to describe the solder joints behavior (i.e. creep) and to implement it in finite element codes like Ansys. In the literature ([2–6]), a lot of creep models describing the steady-state creep are available for SnPb and SnAgCu (the two alloys that were investigated) but only Schubert [7] investigated both the primary and the secondary creep. To accurate existing simulation tools, it will be shown, that the primary creep can not be neglected in all simulations as expected. In this thesis, the creep behavior will be investigated under reversal load conditions and a model describing primary and secondary creep will be presented (from experimental and theory sides). The difficulty is to permit a FE-code to use such kind of creep model in its computation process. A method to implement the constitutive equations readable by the FE-codes are presented. The influence of primary creep of some electronic packagings (Flip-chip and PBGA) will be briefly presented.

For electronic packagings like flip-chip, PBGAs, their reliability has been the object of longstanding research work (e.g. [2, 8–22]).

As far as Chips on Copper board is concerned, this experience and information is lacking: Some authors describe the behavior of Chips on other Substrate [23], but no one gives a

model of crack propagations on die attaches based on Finite element simulations. This need for lifetime assessment is important to reduce the development time and the cost for testing new packages in the future. As for solder joint reliability assessment, Finite Element simulations coupled with thermal cycling tests of test-specimens have been used to analyze their average crack initiation and growth in order to make statements of general validity and to extrapolate the results to new designs and material combinations [24].

Some authors have used the amount of plastic deformation accumulated within one thermal cycle as failure criterion [25, 26]. Others have simulated the creep strain [10, 13, 27, 28] or dissipated energy [11] within the framework of thermally induced low cycle fatigue and used a Coffin-Manson type of approach [29, 30]. This allows an analysis of influence and comparison of different load and material combinations with respect to solder joint reliability and permits subsequent lifetime prediction [3, 13, 31]. Alternatively some papers also suggest an approach based on fracture mechanical means [32–34]. The model which will be presented is based on observation of crack initiation and growth, which was modeled as an function of the accumulated creep strain.

Chapter 2

Theoretical background

This chapter will present the definitions of materials behaviors and particularly of solder joints. To begin, some notions like stress, strain and the associated notations have to be presented. These notions will be used in the rest of the thesis. The elasticity, plasticity and the creep are phenomena which occur in solder joint. Some models that can be used for solder joints describing those phenomena, will be explained and presented. In the second part of this chapter, the lifetime and crack growth models will also be discussed. The models which are here presented are very important, particularly the creep models, because they are conditioning the test conditions, which will be performed to develop the creep laws (for example to develop a Garafalo creep laws or a Chaboche model, creep test conditions are different).

2.1 Elasticity, plasticity and creep

Here the principal deformation type of solder joints are shown. before developing the term of elasticity, plasticity and creep, the terms stress, strain and tensor are discussed, because they are needed to describe the state of material.

2.1.1 tensile stress and strain

To understand and to model the behavior of materials, two concepts are used. They correspond to physical phenomena. To explain what is the stress and the strain, it is common to describe the deformation of a cylindrical test specimen loaded in tension. In tension, the length of this test specimen increases, but its diameter reduces. Engineering stress is the applied load divided by the original cross section area (the unit is the N/m^2 but the N/mm^2 or MPa is more useful).

$$S = \frac{F}{A_0} \quad (2.1)$$

where F is a force in Newton and A_0 a surface in m^2 . True stress is defined by dividing the applied load by the actual real cross section:

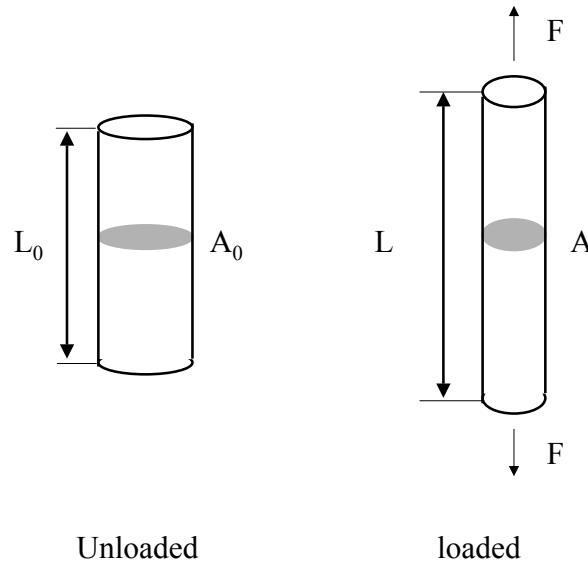


Figure 2.1. *cylindrical test specimen under tension*

$$\sigma = \frac{F}{A} \quad (2.2)$$

Engineering strain is the total change of the cylinder length divided by the original cylinder length:

$$\varepsilon = \frac{L - L_0}{L_0} \quad (2.3)$$

True strain is calculated from the instantaneous cylinder length:

$$\varepsilon = \int_{L_0}^L \frac{\delta L}{L} = \ln \frac{L}{L_0} \quad (2.4)$$

The difference between the engineering and true stress strain can be illustrated by the conventional stress-strain curve of a tensile test. The figure 2.2 shows the difference between the plotted true stress strain curve and the engineering stress strain curve.

In the rest of this thesis only the true stress and strain notations will be used.

2.1.2 multiaxiale stress and strain

The notations which were presented are only significant in uniaxial tensile case. When a volume is deformed, internal forces arise as a reaction to a change of the geometry. The figure 2.3 is representing a small area ΔA with a normal vector n is taken in a plane passing through this body, with a resultant force ΔP acting on it. The stress vector is defined at this point as:

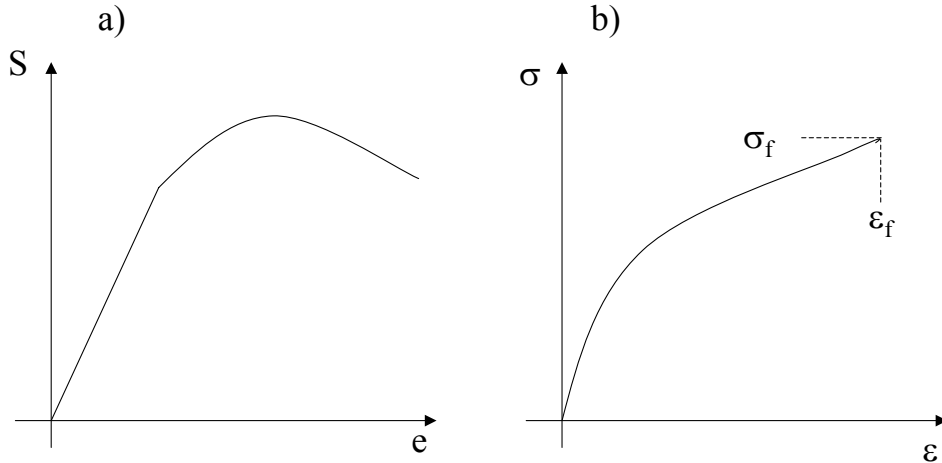


Figure 2.2. Fig. a) engineering stress strain curve Fig. b) true stress strain curve

$$P^{(n)} = \lim_{\Delta A \rightarrow 0} \frac{\Delta P}{\Delta A} = \frac{dP}{dA} \quad (2.5)$$

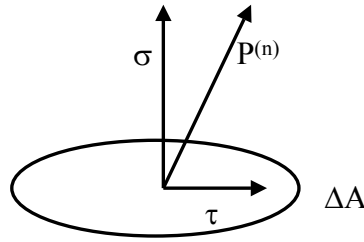


Figure 2.3. stress definition as a combination of the shear and the tensile stress

The vector $P^{(n)}$ is composed by two components, one normal to the plane, called the normal stress σ , one tangent to the plane, called the shearing stress τ . In a tridimensional problem, to specify the stress state at a point it is necessary to prescribe stresses referred to three mutually perpendicular planes passing through this point. To specify the three perpendicular to the axis areas (in a cartesian system x,y,z) $\Delta A^{(x)}$, $\Delta A^{(y)}$ and $\Delta A^{(z)}$, considering an infinitesimal tetrahedron composed by three coordinate plane and an inclined plane in this coordinate system with a normal vector n , the stress vector $P^{(n)}$ is specified by three stress vectors $P^{(x)}$, $P^{(y)}$ and $P^{(z)}$ acting on the faces of the tetrahedron:

$$P^{(n)} = P^{(x)} + P^{(y)} + P^{(z)} \quad (2.6)$$

Each stress vector can be decomposed into three components, one tensile stress and two shear stress. The complete stress state at a point is then composed by nine quantities. The representation of this three quantities is called a stress tensor and can be written as follow:

$$\sigma_{ij} = \begin{pmatrix} \sigma_x & \tau_{yx} & \tau_{zx} \\ \tau_{xy} & \sigma_y & \tau_{zy} \\ \tau_{xz} & \tau_{yz} & \sigma_z \end{pmatrix} \quad (2.7)$$

The equilibrium of forces requires that:

$$\tau_{ij} = \tau_{ji} \quad (2.8)$$

It means that only 6 components are necessary to describe the stress state of materials.

The stress tensor can easily be decomposed into a stress axiator, $\sigma_m \delta_{ij} + \delta_{ij}$, and the stress deviator s_{ij} :

$$\sigma_{ij} = \sigma_m \delta_{ij} + s_{ij} \quad (2.9)$$

where δ_{ij} is the Knoeler-delta and σ_m denotes the mean value of the stress diagonal (also called the mean stress).

$$\sigma_m = \frac{1}{3}(\sigma_x + \sigma_y + \sigma_z) \quad (2.10)$$

The stress deviator is then:

$$s_{ij} = \begin{pmatrix} \sigma_x - \sigma_m & \tau_{yx} & \tau_{zx} \\ \tau_{xy} & \sigma_y - \sigma_m & \tau_{zy} \\ \tau_{xz} & \tau_{yz} & \sigma_z - \sigma_m \end{pmatrix} \quad (2.11)$$

To make the calculation easier, a scalar can be used to reduce a stress tensor to a single value. This scalar is the equivalent stress also called the Von-Mises stress:

$$\sigma_{eq} = \sigma_{vm} = \frac{1}{\sqrt{2}}((\sigma_x - \sigma_y)^2 + (\sigma_y - \sigma_z)^2 + (\sigma_x - \sigma_z)^2 + 6(\tau_{xy}^2 + \tau_{yz}^2 + \tau_{zx}^2))^{\frac{1}{2}} \quad (2.12)$$

It is also possible to define the strain for a 3D environment. The infinitesimal strain-displacement relationships can be summarized as:

$$\varepsilon_{ij} = \frac{1}{2} \left(\frac{\partial u_i}{\partial x_j} + \frac{\partial u_j}{\partial x_i} \right) \quad (2.13)$$

where u is the displacement vector, x the coordinate, and the two indices i and j can range over the three coordinates 1, 2, 3 in three dimensional space. Expanding the equation 2.13 for each coordinate direction gives:

$$\varepsilon_x = \varepsilon_{xx} = \frac{\partial u}{\partial x} \quad (2.14)$$

$$\varepsilon_y = \varepsilon_{yy} = \frac{\partial v}{\partial y} \quad (2.15)$$

$$\varepsilon_z = \varepsilon_{zz} = \frac{\partial w}{\partial z} \quad (2.16)$$

$$\varepsilon_{zy} = \varepsilon_{yz} = \frac{1}{2} \left(\frac{\partial w}{\partial y} + \frac{\partial v}{\partial z} \right) \quad (2.17)$$

$$\varepsilon_{zx} = \varepsilon_{xz} = \frac{1}{2} \left(\frac{\partial u}{\partial z} + \frac{\partial w}{\partial x} \right) \quad (2.18)$$

$$\varepsilon_{xy} = \varepsilon_{yx} = \frac{1}{2} \left(\frac{\partial v}{\partial x} + \frac{\partial u}{\partial y} \right) \quad (2.19)$$

the small strain tensor is written:

$$\varepsilon_{ij} = \begin{pmatrix} \varepsilon_x & \varepsilon_{yx} & \varepsilon_{zx} \\ \varepsilon_{xy} & \varepsilon_y & \varepsilon_{zy} \\ \varepsilon_{xz} & \varepsilon_{yz} & \varepsilon_z \end{pmatrix} = \begin{pmatrix} \varepsilon_x & \frac{1}{2}\gamma_{yx} & \frac{1}{2}\gamma_{zx} \\ \frac{1}{2}\gamma_{xy} & \varepsilon_y & \frac{1}{2}\gamma_{zy} \\ \frac{1}{2}\gamma_{xz} & \frac{1}{2}\gamma_{yz} & \frac{1}{2}\varepsilon_z \end{pmatrix} \quad (2.20)$$

Analogously to the equation 2.11 the e_{ij} is the strain deviator

$$e_{ij} = \begin{pmatrix} \varepsilon_x - \varepsilon_m & \varepsilon_{yx} & \varepsilon_{zx} \\ \varepsilon_{xy} & \varepsilon_y - \varepsilon_m & \varepsilon_{zy} \\ \varepsilon_{xz} & \varepsilon_{yz} & \varepsilon_z - \varepsilon_m \end{pmatrix} \quad (2.21)$$

Where $\varepsilon_m = \frac{1}{3}(\varepsilon_x + \varepsilon_y + \varepsilon_z)$ is the mean strain. As shown in equation 2.12 an equivalent strain can be defined:

$$\varepsilon_{eq} = \frac{\sqrt{2}}{2(1+\nu)} ((\varepsilon_x - \varepsilon_y)^2 + (\varepsilon_y - \varepsilon_z)^2 + \varepsilon_x \varepsilon_z) + 6(\varepsilon_{xy}^2 + \varepsilon_{yz}^2 + \varepsilon_{zx}^2))^{\frac{1}{2}} \quad (2.22)$$

2.1.3 elasticity and plasticity

A typical stress strain curve was discussed in section 2.1.1. An another stress strain tensile curve is also presented in figure 2.4. It is assumed that for this tensile diagram, the creep does not occur. The diagram begins with a straight line from the origin O to the point A, which means that the relationship between the stress and the strain in the initial region is linear (see 2.2.1). It is the domain of the elasticity. The slope of the straight line is called the elastic modulus also called the young's modulus. The point A is called the yield point, and R_e the yield stress that is commonly described as end of the elasticity or proportional stress strain relationship. Beginning at this point, considerable elongation of the test specimen occurs. This elongation occurs till the point B. This point is called the ultimate stress (R_m). This part of the curve describes the plasticity of the material and occurs till the fracture of material. Material that undergoes a large plasticity domain are classified in the ductile materials. The other are brittle. The solder alloys like SnAgCu and SnPb are very ductile. Let us now consider what is happening when the load is removed during a tensile test, in contrary of the standard tensile test, for which the load is applied till the fracture. When we applied a load to a material from the point O to the point A and this load is removed, the material follows the same curve during the loading and the unloading phase (see figure 2.5 fig a). It is the elasticity. In this case it is a linear elasticity. Now suppose that this same material is loaded to a higher level that the point B is reached on the stress strain curve (see figure 2.5 fig b). During the unloading the material follows the straight line BC. This line is parallel to the initial portion of the

stress-strain curve, that is the tangent to the curve at the origin. At the point C the stress goes back to zero, but residual strain or permanent strain is observed. Between the points B and C the material is partially elastic. Between the point O and A the material is elastic and now permanent strain can occur. When the point E is reached, the material will be permanent deformed. This point E is the elastic limit. The characteristic of a material by which it undergoes inelastic strains beyond the strain at the elastic limit is known as the plasticity. the elastic region on the curve (from O to E) is followed by the plastic region. When large deformations occur in a ductile material loaded into the plastic region, the material is said to undergo the plastic flow (strain hardening). Now suppose that the material is reloaded after such an unloaded (see figure 2.5 fig c). The new loading begins at point C and continues upward to point B. The material then follows the original stress strain curve. Both elasticity and plasticity are not dependant to the time. In the case of solder joints, the elastic region is very small and the plastic region difficult to measure because of the occurrence of creep, which is a time-dependant plasticity. Some authors [35,36] describe the plasticity with the theory of the dislocations. They show that at a certain level of stress the dislocations occur and they are irreversible without a stress in the opposite direction. In a crystal, there are always slip. In such crystal the lattice defects tend to accumulate at slip planes. These defects are the dislocations. In the case of pure plasticity, the dislocation density increases as the solder alloy is strained plastically. The flow stress is the stress require to deform plastically an alloy further. The increase of dislocation density is also accompanied by the increase in the the flow stress.

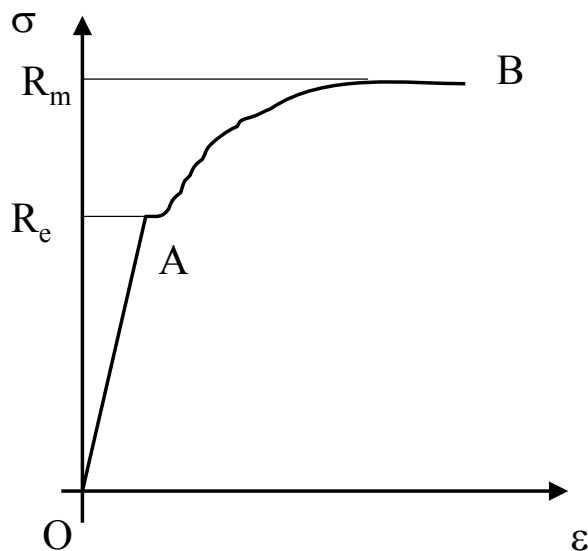


Figure 2.4. *stress-strain diagram for a typical metallic alloy in tension*

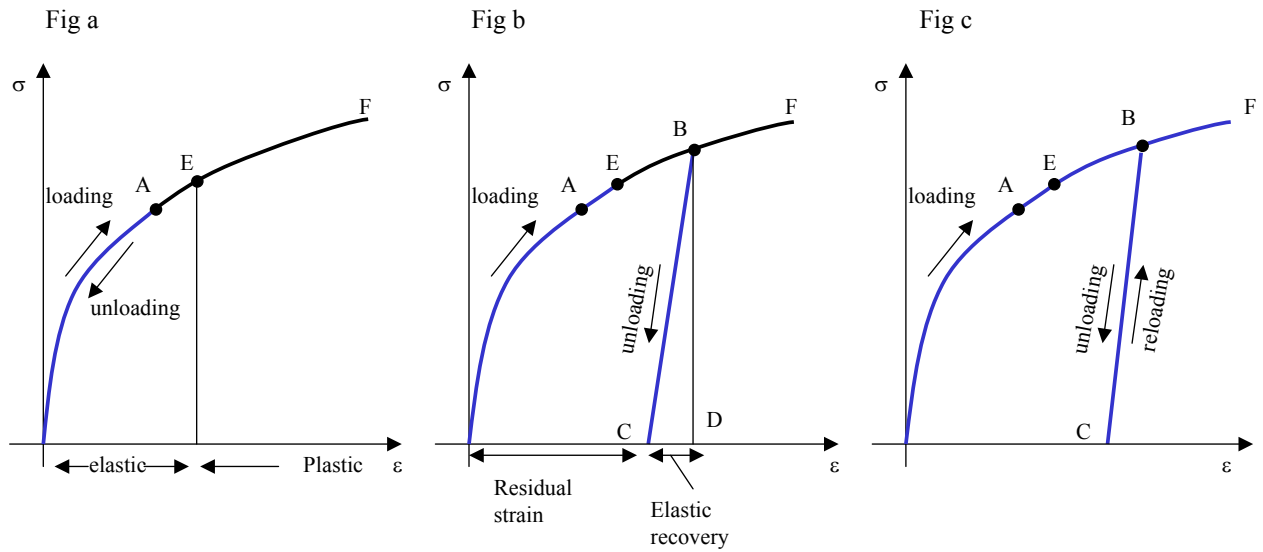


Figure 2.5. stress-strain diagrams of solder alloy illustrating elastic behavior (fig a) and partially elastic behavior (fig b). fig c shows the reloading raising the elastic limit.

2.1.4 creep

The creep is typically a plasticity which occurs at high temperature. It appears when this temperature is greater roughly than $0.4 T_m$ where T_m is the melting point in Kelvins. There are a lot of authors which described the creep but most of them [37–40] as a high temperature plasticity which is time dependant and is currently associated to a deformation at a constant stress level and at a constant temperature. The curve describing this deformation as a time function until the fracture of material is called a creep curve at constant stress level. An alternative to this curve is the creep curve at constant strain rate. These both kind of curves are presented in figure 2.6. For both curves, three regions are designed. The stage I on the creep curve is the primary creep, where the creep strain $\dot{\epsilon} = d\epsilon/dt$ is decreasing with increasing of the creep strain or time (fig a). In fig b, the solder alloy hardens, resulting in increasing flow of stresses. For solder alloys, in fig a the creep rate decreases to a constant value. This value is called the steady-state creep rate and describes the stage II of the creep called the secondary creep, also called steady-state creep. In fig b) the stress is increasing to a certain stress level called the steady-state stress. After the secondary creep and due to the increasing of cavities and/or crack in alloys, the creep rate increases continuously until the fracture (see fig a). This regime is termed the tertiary creep and always leads to fracture. For this reason, and because only a thermo-cycle is calculated for lifetime prediction, the tertiary creep can be neglected, because occurs only some cycles before cracking and fracture.

For some solder alloys which are different from the SnPb and SnAgCu (see Chapter IV) the secondary creep is not observable. Since the creep is thermally and not only stress activated, the time dependant and high temperature plasticity occurs also for a stress level under the yield stress. Since it depends on thermal activation (see below) the strain rate given at a certain stress is extremely temperature sensitive. Unlike the independent

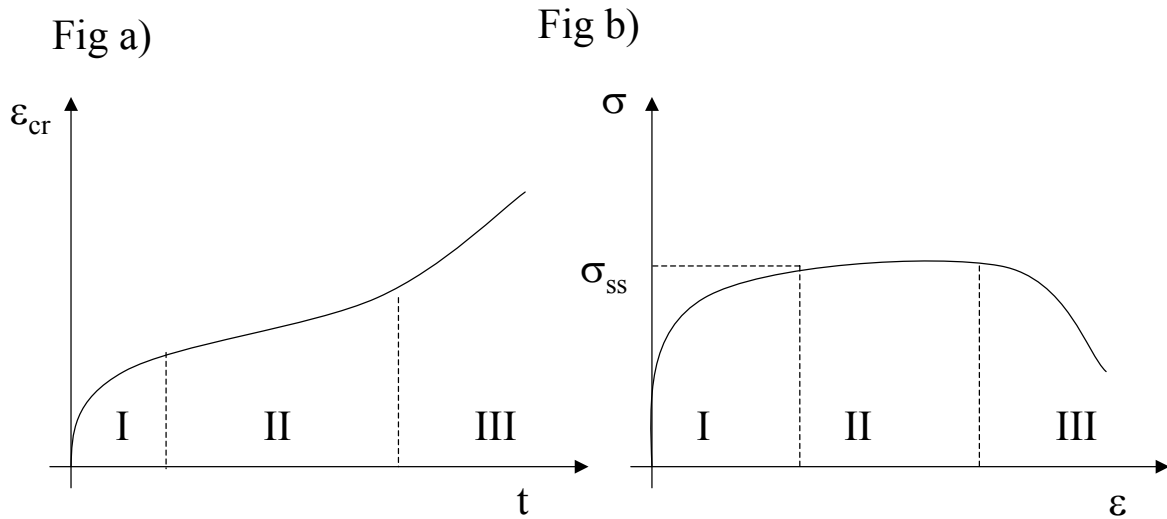


Figure 2.6. Fig. a) constant true stress creep behavior curve of solder alloys Fig. b) creep curve at constant strain rate. The stress steady state for the secondary creep is represented by σ_{ss}

plasticity (see 2.1.3), the creep is not only dependant to the stress level but also to the temperature. During creep the flow stress is closed to the zero value, and no stress increase is necessary to further the plastic deformation (see figure 2.6 a). In this case the dislocation density at a given strain is a function of the temperature. It increases when the temperature increases. It is possible that the thermal energy aids an applied stress in overcoming the energy barrier, which is necessary for dislocation occurrence. An another probable factor in the control of the motion of dislocations under constant stress and temperature is the intersection of dislocations. Alloys contain a network of dislocation referred as a forest of dislocations. At low temperature a slip dislocation can not go through an another dislocation (intersection). But the thermal energy can aid the applied stress in driving a dislocation through another and through a forest of dislocations [41]. The second effect of dislocation intersection is the apparition of jogs on dislocations. These jogs can move by slip along dislocations, but also climbs in the direction of screw dislocations. After this jog climbs or glides, results the creation of a vacancy. This jog climbs and glides and the resulting creation are thermally activated and can help the movement of dislocations. This creation of vacancies is not always due to the mechanical load, but can also occur because of the atomic diffusion, which is also thermal-dependant. All these mechanisms can explain why creep is thermally activated, but the creep is not only due to the density of dislocations that increases with the time.

Since the most solder alloys are polycrystalline, the dislocation theory of the grains is not enough to explain the creep of these alloys. Some other authors [42–44] explained creep with mechanisms different from the dislocations in grain. The first most popular is called grain boundary sliding, which causes a reorganization of the metal microstructure and creep, this phenomenon is also called superplasticity, during which the elongation of metal

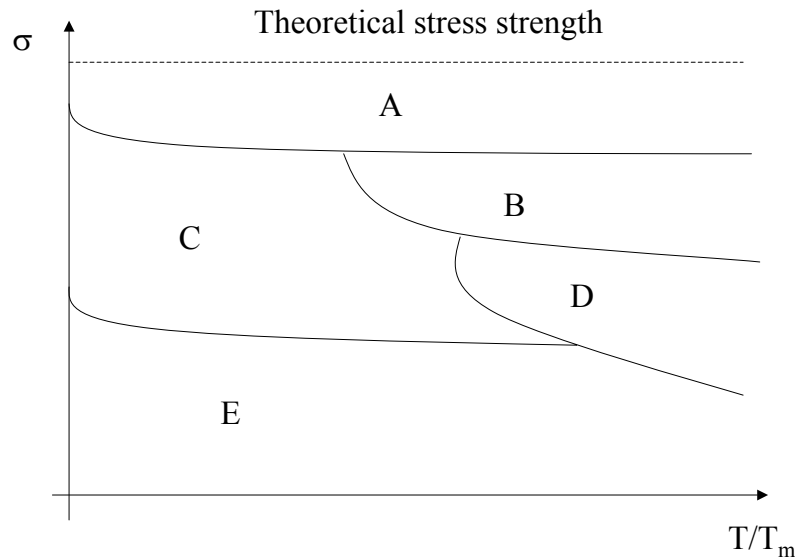


Figure 2.7. Map of creep deformation. A- dislocation glide; B- dislocation creep also called power law creep; C- Coble creep; D- Nabarro-Herring creep E- elastic deformation

can be extraordinary large.

Another model has been proposed by Nabarro and Herring. The self diffusion in grain can produce a plastic flow if matter is carried from grain boundaries. In this model the grain boundaries are considered to be sources and sinks for vacancies. In this kind of creep the creep rate will be hardly dependant on the grain sizes. That explains why the creep rate is significantly depending on the solder joint microstructure (see section IV).

The grain boundary diffusion is also known to be viable describing the creep at low stress and temperature level. This form of creep is called Coble creep.

Frost et al. [42] proposes a classification of the different creep mechanisms as a function of the temperature and the stress. This classification is presented on figure 2.7. For solder joints which have a low melting point (about 466K for eutectic SnPb and 491K for SnAgCu) and that the current range of temperature in most of automotive electronic applications is between -40C (233K) and + 150C (423K), the creep deformation occurs in all stages of the solder joint life. The typical deformations of the creep of solder joints are the deformations A, B and D.

2.2 model describing elasticity, plasticity and creep

2.2.1 elastic model

The simple Hooke's law in a case of uniaxial load is given by

$$\varepsilon_{el} = \frac{\sigma}{E} \quad (2.23)$$

where σ is the stress in Pa, E the Young's Modul in Pa and ε the elastic strain. It is possible to generalize this law for the multiaxial case:

$$\varepsilon_{el} = \frac{1 + \nu}{E}\sigma - \frac{\nu}{E}(tr\sigma)I \quad (2.24)$$

where ν is the poisson coefficient, E the Young's modulus in Pa, σ the stress tensor, I the unit tensor, and $tr \sigma$ the trace of σ , which is the sum of the three diagonal components of the stress tensor.

2.2.2 plastic model

A lot of models exist and are implemented in FE-codes (stress hardening, strain hardening, ...). This section deals with the most common. The first easier equation is the strain hardening and was purposed by Ramberg and Osgood:

$$\varepsilon_{pl} = \left(\frac{\sigma}{K}\right)^{\frac{1}{n}} \quad (2.25)$$

where K is the strain hardening coefficient and n is the strain hardening exponent. This equation gives a good description of a lot of alloys, and is largely used for a stress or strain based lifetime prediction by means of FE-calculation. Combining the equations 2.23 and 2.25 the curve shown in figure 2.1.1 can be modeled by the following equation:

$$\varepsilon = \frac{\sigma}{E} + \left(\frac{\sigma}{K}\right)^{\frac{1}{n}} \quad (2.26)$$

In case of endurance calculation, the behavior under cyclic conditions has to be described. The figure 2.8 shows the material response in alternative compression and tension. This is called a hysteresis loop.

from the equation 2.26 the hysteresis loop can be calculated as follow:

$$\Delta\varepsilon = \frac{\Delta\sigma}{E} + 2\left(\frac{\Delta\sigma}{2K}\right)^{\frac{1}{n}} \quad (2.27)$$

An another method to compute the true stress and strain is given by Neuber [45]. This method is particularly useful to describe a stress concentration state, but can also be used as a general method describing the plasticity. Neuber purposed that the local stress and strain could be determined using a stress concentration factor K_t . If the nominal stress and strain are S and e, and σ and ε the true stress a true strain: The neuber rule is given by:

$$\Delta\varepsilon_{true}\Delta\sigma_{true} = K_t\Delta S.\Delta eK_t \quad (2.28)$$

Performing a linear computation, it is possible using this rule to calculate the local plastic stress and strain of the material. Indeed, the left hand side of the equation is the stress strain product for the true elastic-plastic stress and strain. The right hand side of the equation is the stress strain product which would be calculated it the material is only elastic. The original use of this rule, that described the stress concentration at notch,

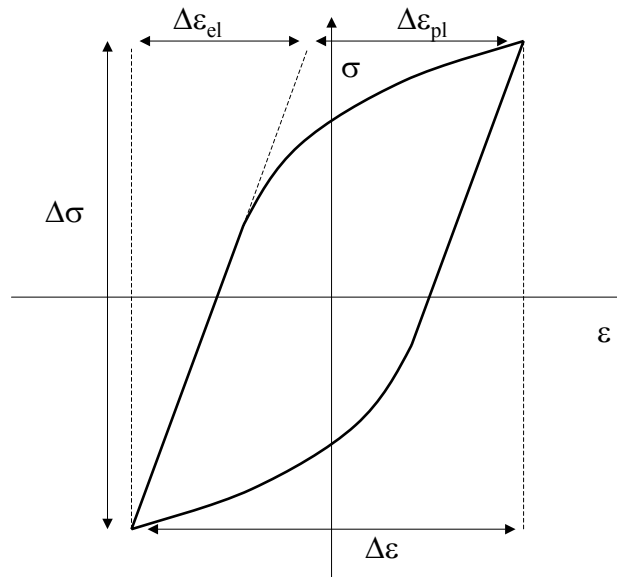


Figure 2.8. *hysteresis loop: stress and strain in compression and tensile test*

can be turned aside to describe the normal plasticity. Indeed, for each elastic stress level, knowing the equation, of the curve (thick curve) describing the elastic-plastic curve, permit to calculate the elastic-plastic stress and strain from an elastic computation. This Neuber theory says the energy deformation for a perfect elastic material is the same that the energy to deform the material plastically. That means that:

$$\varepsilon_{el}\sigma_{el} = \varepsilon_{true}\sigma_{true} \quad (2.29)$$

2.2.3 creep models

To be able to describe both the plasticity and the creep behavior, two approaches can be used:

- To separate the plastic and the creep strain (see [46] and [47]). The equations presented in Section 2.2 can be used to describe the plasticity. Creep equations have to be developed. The difficulty of this method is to separate the time independent plasticity from the creep. (approach 1)
- Use a limited approach which incorporates, with a different viscoplastic potential, a smooth transition between the time-dependant regime (creep) and the time independent one (plasticity). (approach 2)

In this section, a model using the first approach will be presented. Models based on second approach are presented in section 2.2.4 and 2.2.5. The current creep tests are performed at a constant stress and temperature. The majority of the authors [3, 31, 48–53], who developed constitutive laws for solder alloys neglected the primary creep and concentrate

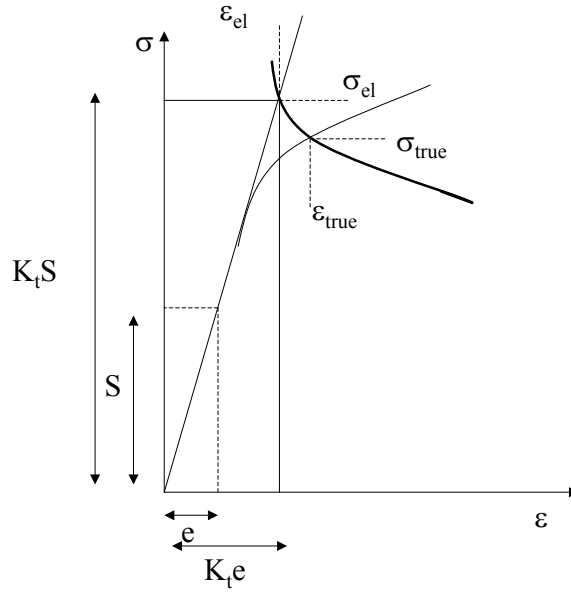


Figure 2.9. *the neuber's rule*

the efforts to describe a good model for secondary creep. In this approach, the mechanical part of the strain ε_{tot} is composed into elastic and plastic and creep and thermal strain.

$$\varepsilon_{tot} = \varepsilon_{el} + \varepsilon_{pl} + \varepsilon_{cr} + \varepsilon_{th} \quad (2.30)$$

The secondary creep as a linear regime can be described by the steady-state creep rate. The authors pre-cited gave the relationship between this creep rate and the temperature and stress. the total strain rate is given by:

$$\dot{\varepsilon}_{tot} = \dot{\varepsilon}_{el} + \dot{\varepsilon}_{pl} + \dot{\varepsilon}_{cr} + \dot{\varepsilon}_{th} \quad (2.31)$$

From equations 2.31 and 2.23 the total strain rate can be written:

$$\dot{\varepsilon}_{tot} = \dot{\varepsilon}_{pl} + \dot{\varepsilon}_{cr} + \frac{\sigma}{E} + \alpha \dot{T} - (\varepsilon_{tot} - \varepsilon_{th} - \varepsilon_{pl} - \varepsilon_{cr}) \frac{dE/dT}{E} \quad (2.32)$$

To calculate creep with this method, it is necessary to introduce a relationship between $\dot{\varepsilon}_{cr}$ and the von Mises Stress, temperature and time. So that the majority of the models only describe the secondary creep, the dependance on time is not necessary.

Temperature-dependant steady-state creep law

It is clear that the secondary creep rate depends on temperature and on stress. The higher the temperature or the stress is, the bigger the creep rate is. Some models dissociate the influence of temperature and stress to describe the creep rate. At constant stress the creep rate only depends on temperature. This is comparable to diffusion process which can be

described through activation energy. Using an Arrhenius equation, the creep rate can be described by (equation 2.33)

$$\dot{\epsilon}_s(T) = A \times e^{\frac{-Q_c}{RT}} \quad (2.33)$$

where $\dot{\epsilon}_s$ is the steady-state creep rate, Q_c is the activation energy for the creep (J/mol), R the universal Gas constant (8,14 J/(mol.K)), A the proportional constant, T the temperature in Kelvin. The activation energy can be different at different Temperature depending on the creep mechanism. The dislocation sliding creep has not the same activation energy than the diffusion creep. For the dislocation sliding and the diffusion process the creep rate i.e. the activation energy depends also strongly on the grain size respectively the microstructure of solder alloys.

Stress-dependant steady-state creep law

At constant temperature, the steady state creep strain can also be described through its dependence on stress by the Norton law (equation 2.34):

$$\dot{\epsilon}_s(\sigma) = C \times \sigma^n \quad (2.34)$$

where σ is the stress in MPa and n the stress exponent. As it was already discussed for the activation energy, the stress exponent also depends on the creep mechanism.

Stress and temperature steady-state creep law

An alternative Norton's law can also describe the temperature dependance:

$$\dot{\epsilon}_s(\sigma, T) = C \times \sigma^n \times T^m \quad (2.35)$$

Unfortunately, this law is not capable to describe a large temperature and stress domain. A better solution is to combine the equation 2.33 and 2.34:

$$\dot{\epsilon}_s(\sigma, T) = C \times \sigma^n \times e^{\frac{-Q_c}{RT}} \quad (2.36)$$

Since for metal and particularly solder alloys, two creep mechanisms commonly occur, and that means that the parameters are not the same at low temperature and stress level as at high temperature and stress level, Garafalo et al. [54] defines the secondary creep rate as follow:

$$\dot{\epsilon}_s(\sigma, T) = A \times [\sinh(C \times \sigma)] e^{\frac{-Q_c}{RT}} \quad (2.37)$$

where A and C are constants from experiment.

Strain or time hardening primary creep law

Using the above notations, primary creep strain can be described as a function of time (time hardening):

$$\dot{\epsilon}_{pr} = C \times \sigma^n \times e^{\left(\frac{-Q}{RT}\right) \times t^{-\alpha}} \quad (2.38)$$

or as a function of strain (strain hardening):

$$\dot{\varepsilon}_{pr} = C \times \sigma^n \times e^{\left(\frac{-Q}{RT}\right) \times \varepsilon_{cr}^{-\beta}} \quad (2.39)$$

where $\dot{\varepsilon}_{pr}$ is the primary creep rate and α , β , n and C are constants and Q is the creep activation energy.

Combining the equation 2.36 and 2.38 a temperature and stress dependant total creep rate law can be developed:

$$\dot{\varepsilon}_{tot} = C \times \sigma^n \times e^{\left(\frac{-Q}{RT}\right)} \times (1 + t^{-\alpha}) \quad (2.40)$$

where $\dot{\varepsilon}_{tot}$ is the total creep rate (sum of primary and secondary creep).

2.2.4 chaboche Model

The Chaboche Model [55] [56] [57] is based on the second approach developed in section 2.2.3.

The mechanical part of the strain ε_m is composed into elastic and plastic and thermal strain.

$$\varepsilon_m = \varepsilon_{el} + \varepsilon_{pl} + \varepsilon_{th} \quad (2.41)$$

To be able to integrate the creep which depends on the time, a time integration is necessary. The total strain rate could be written as the sum of the elastic, plastic and thermal rate:

$$\dot{\varepsilon}_{tot} = \dot{\varepsilon}_{el} + \dot{\varepsilon}_{pl} + \dot{\varepsilon}_{th} \quad (2.42)$$

The thermal extension is given by

$$\varepsilon_{th} = \alpha \times \Delta T \times \delta \quad (2.43)$$

where α is the coefficient of thermal expansion the elastic strain rate could be obtained derivating the equation 2.24

and from 2.32

$$\dot{\varepsilon}_{tot} = \dot{\varepsilon}_{pl} + \frac{\sigma}{E} + \alpha \dot{T} - (\dot{\varepsilon}_{tot} - \dot{\varepsilon}_{th} - \dot{\varepsilon}_{pl}) \frac{dE/dT}{E} \quad (2.44)$$

$\dot{\varepsilon}_{el}$ could be found derivating the equation 2.24. The chaboche model gives the strain rate, based on unified theory:

$$\dot{\varepsilon}_{pl} = \left\langle \frac{|\sigma - \chi| - R}{K} \right\rangle^n \text{sgn}(\sigma - \chi) \quad (2.45)$$

where the Heaviside function $\langle x \rangle = x$, if $x > 0$ and $\langle x \rangle = 0$ when $x = 0$

$$\dot{\chi} = H \dot{\varepsilon}_{pl} - D \chi |\dot{\varepsilon}_{pl}| \quad (2.46)$$

$$\dot{R} = h\dot{\varepsilon}^{pl} - dR|\dot{\varepsilon}^{pl}| \quad (2.47)$$

Where χ and R represent material internal variables, describing the yield stress and the drag stress respectively. K, n, H, D, h, d are parameters to be determined. For the cyclic viscoplasticity and the creep Schmitt et al. [58] introduced a modified model capable to describe the primary, secondary and tertiary creep under temperature and mechanical cycling conditions:

$$\dot{\varepsilon}_{pl} = \left\langle \frac{|\sigma - \alpha| - k}{K} \right\rangle^n \text{sgn}(\sigma - \alpha) \quad (2.48)$$

where α is the back stress. The evolution equations for the back stresses are:

$$\dot{\alpha}_i = \sqrt{2/3} H_i r_i \left(\text{sgn}(\sigma - \alpha) - \sqrt{2/3} \left| \frac{\alpha_i}{r_m} \right|^{\chi+1} \text{sig}(\alpha_i) \right) \dot{p} - R \alpha_i \quad (2.49)$$

$$\alpha = \sum \alpha_i \text{ with } i = 1, 2, \dots, 5 \quad (2.50)$$

$$H_m = c_m (1 - a_m e^{-b_m p}) \quad (2.51)$$

where r is the Norton strain rate exponent, K the viscosity, k the yield stress, χ the ratchening exponent, r_i the saturation limit of the back stress component α_i , α_i, b_i, c_i are parameters for the cyclic plasticity. All these parameters are temperature dependant, that means that these parameters have to be fitted for each measured temperature. The value of the parameters for the other temperatures could be linear interpolated in case of FE-simulation. The great advantage of this model is that the full behavior and not only the creep can be described. A damage model can also be introduced and computed for the simulation of lifetime under thermo-cyclic loading (see [59]). To have a good statistical results, and to be able to determine all of the parameters at 5 Temperatures, The number of tests that have to be performed is very high (it was estimate to 400 for a solder joint). It was not realistic to perform such a job during this work.

2.2.5 Anand's Model

It is convenient in the literature [60–64] to use the Anand model. This is a viscoplastic constitutive model, in which the plasticity and creep are unified and describe by the same set flow and evolutionary relations. This model can be applied to represent the inelastic deformation behavior for solders. The anand's model equations are the following. The flow equation is:

$$\dot{\varepsilon}_{pl} = A e^{-\frac{Q}{R\theta}} \left[\sinh \left(\xi \frac{\sigma}{s} \right) \right]^{\frac{1}{m}} \quad (2.52)$$

and the evolution equation is

$$\dot{s} = \left\{ h_o (|B|)^a \frac{B}{|B|} \right\} \dot{\varepsilon}_{pl} \quad (2.53)$$

where

$$B = 1 - \frac{s}{s^*} \quad (2.54)$$

with

$$s^* = \hat{s} \left[\frac{\dot{\varepsilon}_{pl}}{A} e^{\frac{Q}{RT}} \right]^n \quad (2.55)$$

where T is the temperature in Kelvin, s the effective Cauchy stress, s^* is the saturation value of deformation resistance, \dot{s} the time derivative of s , Q is the activation energy in kJ/mole, R the universal gaz constant, A the pre-exponential factor, ξ the multiplier of stress, m the strain rate sensitivity of stress, h_o the hardening/softening constant, n the strain rate sensitivity of saturation value, a the strain rate sensitivity of hardening or softening. This model was not used to describe the creep behavior, which were measured in chapter 3, because it is not capable to describe the primary creep under reversal condition, and is after Anand [65,66] himself not accurate to describe the creep.

2.3 lifetime prediction

In this section, it will explicitly be presented the different methods that are used to predict lifetime of solder joints with the use of FE-software. For the lifetime prediction of solder joints, 4 classes of models are used:

- the stress based models
- the strain based models
- the energy based models
- the damage models

Most of them are empirical and it is also possible to combine those models together in some cases. The most popular are presented here above.

2.3.1 stress-life analysis

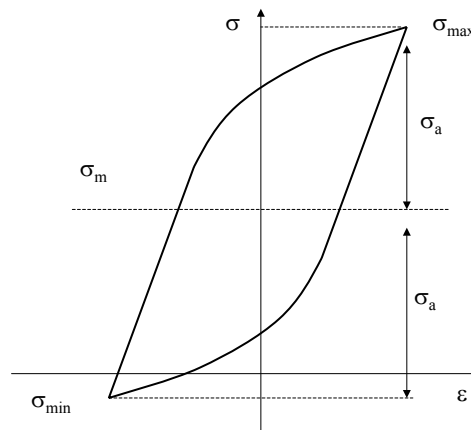


Figure 2.10. *a fatigue hysteresis loop*

It is the method which gives very good results in the elastic and long life field, but is used for predicting lifetime of SnPb. The first work is to know and simplified the load collective.

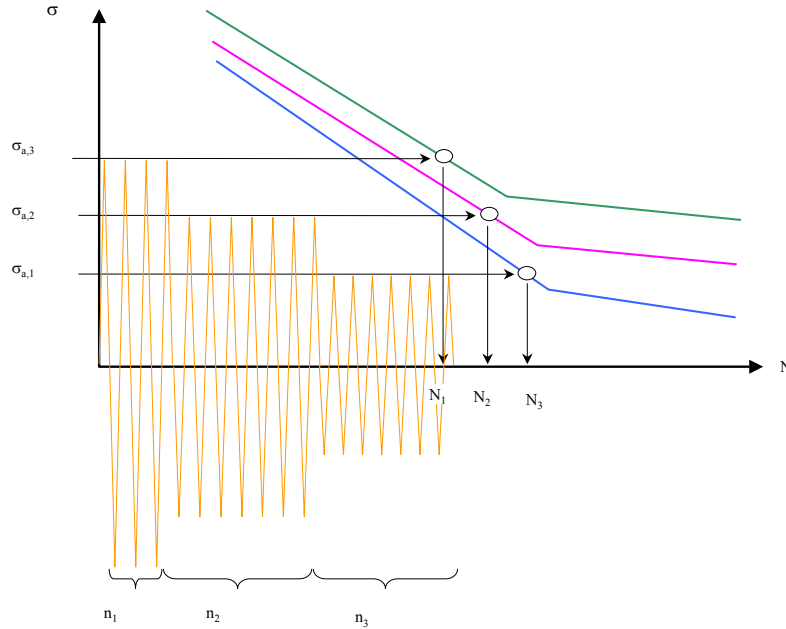


Figure 2.11. calculation of the damage accumulation. Palmgreen-Miner Law.

For each hysteresis loop a stress amplitude a correspondent mean stress can be associated, such as:

$$\sigma_a = \frac{\sigma_{max} - \sigma_{min}}{2} \quad (2.56)$$

$$\sigma_m = \frac{\sigma_{max} + \sigma_{min}}{2} \quad (2.57)$$

For each hysteresis loop x , $\sigma_{a,x}$, $\sigma_{m,x}$ and a number of cycles n_x are calculated. A Wöhler curve (a curve which give the number of cycles to end of life at a constant stress without influence of the mean stress) is used to determine the damage. For each hysteresis loop a corrected Wöhler curve taken care of the mean stress. A lot of rules like the Goodmann or Gerber rules can be used to determine the mean stress influence.

With the load collective, and the calculated Wöhler curve, the fatigue software is able to calculate a damage accumulation with a Palmgreen Miner law, as shown in figure 2.11. The damage for a hysteresis loop x is $d_x = \frac{n_x}{N_x}$. The Palmgreen-Miner law, which calculates the total damage is given by:

$$D = \sum d_x = \sum \frac{n_x}{N_x} \quad (2.58)$$

where n_x is the number of hysteresis loop x , N_x is the number of cycle to failure at a stress $\sigma_{a,x}$, with a mean stress of $\sigma_{m,x}$. When $D=1$, the specimen breaks down. Some authors

found good results using this method, but it does not seem to be good for the thermal cycling test, because the process is not stress control, but temperature controlled. In this case, because of the creep deformation, the stress can not describe the state of the solder joint. The strain has to be used, to calculate failure of solder joints. A strain-life approach is presented in section 2.3.2.

2.3.2 strain-life analysis

The endurance can be expressed as N cycles, but also as $2N_f$ half cycles; or reversals. N_f is the number of cycles, $2N_f$ the number of reversals. Basquin [67] was the first which presented a relationship between the stress amplitude and the endurance:

$$\frac{\Delta\sigma}{2} = \sigma'_f (2N_f)^b \quad (2.59)$$

σ'_f is the fatigue strength, and b the fatigue strength exponent also called the Basquin's exponent. The stress and elastic component of strain are related by (see equation 2.23):

$$\Delta\varepsilon_e = \frac{\Delta\sigma}{E} \quad (2.60)$$

Combining the equation 2.59 and 2.60 The Basquin law can be written so:

$$\frac{\Delta\varepsilon_e}{2} = \frac{\sigma'_f}{E} (2N_f)^b \quad (2.61)$$

Manson [30] and Coffin [29] a relationship between the plastic strain amplitude and endurance can be expressed by:

$$\Delta\varepsilon_{pl} = \varepsilon'_f (2N_f)^c \quad (2.62)$$

where c is the fatigue ductility exponent, and ε'_f is the fatigue ductility coefficient, which is the plastic strain amplitude at $2N_f = 1$ In term of strain amplitude:

$$\frac{\Delta\varepsilon}{2} = \frac{\Delta\varepsilon_{el}}{2} + \frac{\Delta\varepsilon_{pl}}{2} \quad (2.63)$$

From equations 2.60, and 2.62 and 2.64, the strain life relationship is:

$$\frac{\Delta\varepsilon}{2} = \frac{\sigma'_f}{E} (2N_f)^b + \varepsilon'_f (2N_f)^c \quad (2.64)$$

For each ε_x a corresponding endurance N_f can be calculated. knowing the load collective is also possible to calculate the damage D (see equation 2.58)

2.3.3 accumulated creep strain methods

It will be shown in Chapter IV that the creep is really more relevant than the elasticity and the plasticity in solder alloys like SnPb or SnAgCu. The lifetime (1000 to 5000 cycles) of solder can be considered to be short in comparison to the fatigue in the elastic field of steel for example (a lifetime of 10^6 to 10^8 cycles is not exceptional in the automotive industry). The short lifetime of solder joint is due to the high plasticity during thermo-cycles. The phenomenon is also called the creep-fatigue. As shown above the methods based on strain are more accurate for describing the fatigue in term of plasticity. For thermo-cycles such as presented in Chapter VI, the solder joint is only damaged by the creep and the plasticity. The elasticity term of the fatigue is not relevant. So the Coffin-Manson [29, 30] equation which gives a relationship between the expected number of cycles to failure and the plastic strain is:

$$N_f = C_1 (\Delta\varepsilon_{pl})^{C_2} \quad (2.65)$$

where $\Delta\varepsilon_{pl}$ is the plastic strain amplitude, N_f the number of cycles to failure, C_1 and C_2 are constants. Some authors [25, 26] use this empirical equation with the plastic strain deformation. The majority of them [10, 13, 27, 28, 68–70] replace the plastic strain by the accumulated creep strain using associated creep models. The Coffin-Manson equation is written as follow in such cases.

$$N_f = C_3 (\varepsilon_{cr,acc})^{C_4} \quad (2.66)$$

where the accumulated creep strain $\varepsilon_{cr,acc}$ is the sum of all computed creep strain of a cycle:

$$\varepsilon_{cr,acc} = \sum |\Delta\varepsilon_{cr}(i)| \quad (2.67)$$

where $\Delta\varepsilon_{cr}(i)$ is the computed creep strain for each increment i . The difficulty of this method is clearly to clarify where the creep strain has to be measured (at node, elements, volume...). Some examples are presented by [27, 71, 72].

2.3.4 energy based methods

The energy based method has for hypothesis, that during a thermo-cycle, the dissipated energy is a good state variable to describe the lifetime [73].

$$N_f = C_1 [\Delta W_{cr,ave}]^{C_2} \quad (2.68)$$

[11, 74] use the average dissipated energy, which is given by

$$\Delta W_{cr,ave} = \frac{\sum \Delta W_{cr} \cdot V}{\sum V} \quad (2.69)$$

where V the volume of an element and ΔW_{cr} is the dissipated creep energy. This is calculated for an increment i by:

$$W_{cr}(i) = \Delta\sigma(i)\Delta\varepsilon_{cr}(i) \quad (2.70)$$

More than 1 element can be used. The lifetime is then given by

$$N_f = C_1(\Delta W_{cr,ave})^{C_2} \quad (2.71)$$

Such analysis are performed by [33, 75, 76]

2.3.5 crack propagation analysis

The solder alloys like SnPb and SnAgCu are very soft materials, i.e. are very ductile. Authors [77, 78] showed that it is possible to describe the crack development, by the crack growth rate pro cycle ($\frac{da}{dN}$) which could be dependant to a physical value. This crack growth rate is often described by an empirical equation [79]:

$$\frac{da}{dN} = K_1 (\Delta F)^{k_2} \quad (2.72)$$

where $\frac{da}{dN}$ is the crack growth rate pro cycle, K_1 and K_2 are parameters from experiments and ΔF a physical parameter. For solder alloys, some authors [80] use the stress intensity factor ΔK to characterize the crack propagation, some others [81–83] use the ΔJ integral concept which measures the energy at the surface in the crack forefront, some other the C^* integral concept [33, 78]. For all these models, it is necessary to know the form and the crack propagation direction before performing the analysis. To avoid this inconvenience, Darveaux et al. [10, 76] purposed a model based on the creep energy. This model is a mix between empirical models and damage models. He assumed that:

$$N_0 = C_1 \times (\Delta W_{ave})^{C_2} \quad (2.73)$$

$$\frac{da}{dN} = C_3 \times (\Delta W_{ave})^{C_4} \quad (2.74)$$

where N_0 is the number of cycles to crack initiation, C_1 , C_2 , C_3 and C_4 are parameters which have to be calculated from experimental data. $\frac{da}{dN}$ is the crack growth rate per cycle. ΔW_{ave} is the average creep energy (see equation 2.69). This energy is calculated in a volume where the crack which occurs. The crack length L can be calculated at N cycle:

$$L = (N - N_0) \times \frac{da}{dN} \quad (2.75)$$

Chapter 3

Creep test sample

The following chapter deals with the different opportunities to perform a creep test. The choice of the test specimen was the first step of the work. It was thought using two different test specimens. Indeed, two analysis will be performed. The first was to study the creep behavior of different solder alloys. The second one was the study of the crack propagation caused by thermo-mechanical damage. For the first test, a specimen test, which might be loaded by a tensile or torsion machine might be used. For the second test, a test specimen that could be different from the first one will be led in a cycling temperature environment. Using a frame, which will have different thermal behavior (coefficient of thermal expansion), the solder joint will be thermo-mechanical loaded. It is expected to see the crack initiation and the crack propagation in the solder joint with Scanning Acoustic Microscope (SAM). These alloys were the well known tin-lead (SnPb), and other lead-free tin-based alloys. The tin-lead was used as reference case, but the goal of the study is to characterize the Pb-free SnAgCu solder alloy. All solders are used above 0,4 of their melting point temperature, that means that the creep will probably dominate the deformation process. The majority of models that are used to calculate the lifetime of solder joint try to represent the steady-state creep, which is also called the secondary creep (see section 2.1.4). Those models are used to perform the first analysis. It is necessary to pay attention in the choice of specimen, because it will condition all the results.

3.1 An overview of different creep test specimens

It is to keep in mind that the creep tests has two objectives. The first is to verify that primary creep reoccurs under reversible load conditions. The second one is to develop creep models including eventually both primary and secondary creep for FE-Simulation. The typical damage mode of solder joints is due to the mismatch of the different material CTE (coefficient of thermal expansion). The deformation mechanism of solder joints during their lifetime is the creep. Because of the planar geometry of the chip's solder joint the principle damage will be caused by shear stress. It is of course possible to perform tensile test of solder alloys but it would not be representative of the study case. In the literature it is easy to find authors which use standard geometry like Dog's bone shape bulk. It was shown in comparing some literature data, that the behavior of real solders could be very

different from that of bulk solder [3, 7]. To have good results with the creep test, the solder joint of the test specimen has to be representative of solder joints that are available in production. That means that the volume of the solder joint must not be too large and the microstructure of the test specimen solder joint comparable to the real solder joints (the bulk also called dog bone test specimen was excluded of this study, because it is not representative of the solder joints of the production and it can be loaded under reversible conditions because of the buckling in compression). For those reasons, the test specimens that are soldered and loaded by shear stress/strain were chosen. To have good results, a multi-axial loading might be avoided, i.e. a pure shear-stress was chosen. It is not easy to realize it, and it is why the choice of the test specimen is very important. The folk-shape test, the ring-and plug test, the single lap test the double lap test, and the grooved-lap test will be successively presented. Two other characteristics of the test specimen must be particularly observed: The first one the homogeneity (constant stress through the solder joint) and the second one the pureness (only shear stress) of the shear stress.

3.1.1 The folk-shape specimen test

The folk-shape specimen was developed to be used with a rheometer test machine. This is really practical to use such a machine to perform creep behavior test. Indeed, this machine will measure direct the torque and the angle versus time, it is so easy to have the stress and strain history. This special form of geometry (folk-shape) is used at the IZM institute to characterize solder joint behavior. It is really easy to mount this test sample on rheometer, and this geometry was developed for this reason. In Figure 3.1, the form of this specimen test.

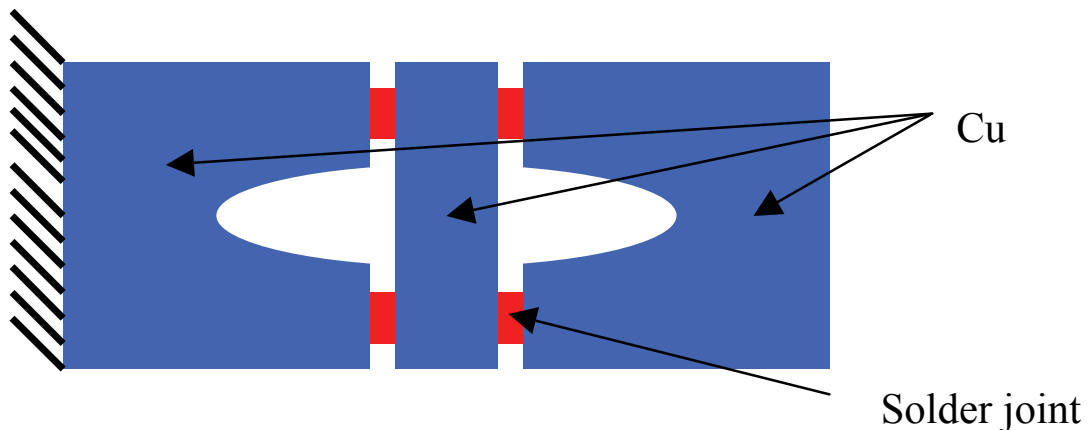


Figure 3.1. *the folk-shape test specimen. the right side is fixed in the torsion machine and moment is applied to the other side*

Some analysis at IZM have shown that the stress that are produced by a rotation of one of the part is not homogeneous, i.e. a pure shear stress is not occurring, because of the two large deformation of the copper piece [84]. The other problem is that there are 4 solder

joints, and these 4 solder joints have to be identical. It would be very difficult to have 4 comparable solder joints using the standard soldering processes. In other case, the stress and the strain level will not be the same for all solder joints. For those reasons, such a test piece was not used.

3.1.2 The ring-and-plug test specimen

Presentation of the test specimen

The ring-and plug test specimen is normally used with a torsion machine [85,86]. The test specimen is composed by two elements that are soldered together. The first element is a cylinder called "plug", the second is a "ring" (see also Figure 3.2). In the majority of

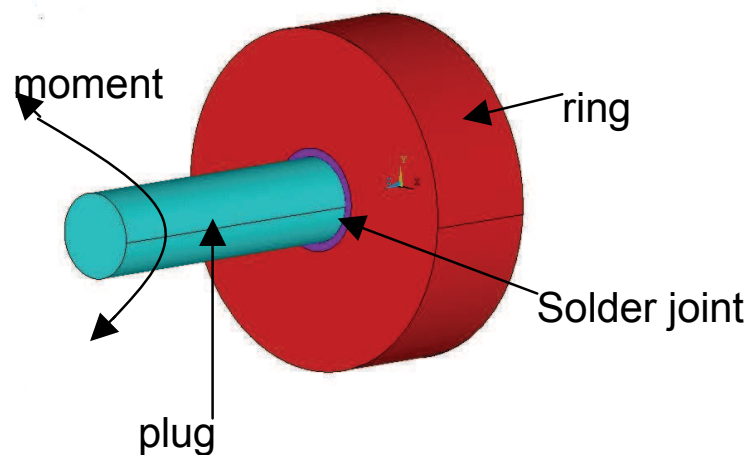


Figure 3.2. *the ring an plug geometry. the plug has to solder in the middle of the ring. The difficulty in this operation is to center this plug to have a constant solder joint thickness*

cases, the ring is fixed on the machine and the plug is rotated. The ring and the plug can be done with Cu, Al, Steel, or ceramic. All solder alloys which are available can be used to solder the two pieces. The ring and the plug are really easy to be built, but to solder these two piece together, it could be problematic. Indeed, the plug has to be really in the center of the ring, and the solder joint must have a constant thickness. A montage help should be imagined to maintain the 2 components in the right position. To have a good material behavior, the micro structures of the solder alloy are expected to be constant though the solder joint. The ring and plug specimen test are massive and heavy, and we have to pay attention on the fact, that the temperature will not be homogeneous in the solder core. The metallography analysis has to be probably performed, to check that.

Ring-and-Plug and Rheometer

The Ring-and-Plug test specimen has the advantage to be loaded symmetrically in two directions. It could be a very good solution to perform creep test under reversal conditions. The other benefits of this ring and Plug test specimen, in comparison with the other traditional "tensile" test specimen, is that it could be used with the rheometer, which would make easier the measurements. The geometry has to be worked, to be correctly fixed to the rheometer, that is available at IZM. Indeed, the fixing system is composed by two jaws (disk geometry), where a 2 mm large mortise takes place.(figure 3.3). The ring

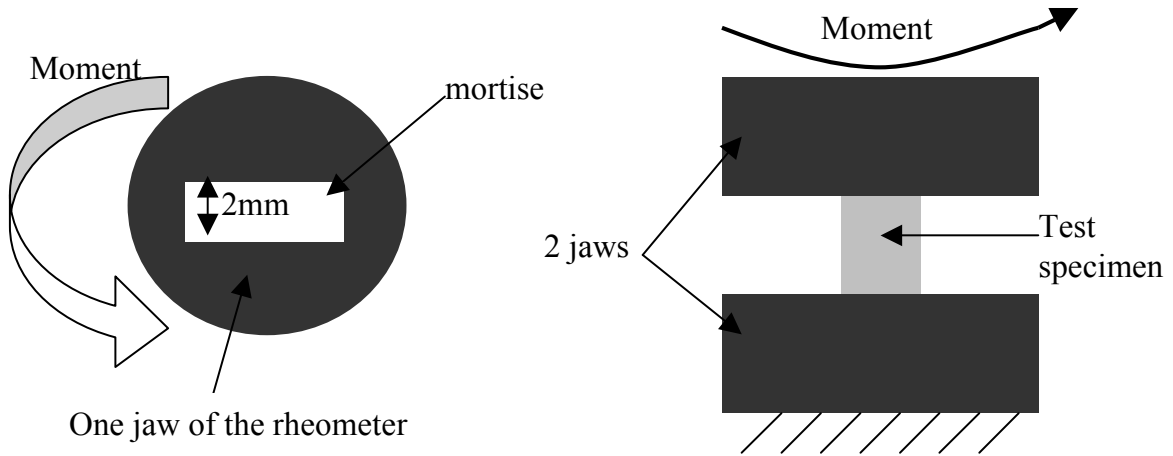


Figure 3.3. *the rheometer jaws: on the left the top view, on the right the front view*

and plug such it was presented could not be fixed directly in the jaws of the rheometer. To have a good interfacing between the rheometer and the Ring and Plug test specimen, this last one has to be modified. The figure 3.4 shows the geometry which has been imagined. The rheometer available at the IZM is a Physica MCR 300. The specifications [87] show that the maximal torque is 150 mNm. With the hypotheses that the ring and Plug are Rigid unworkable bodies, it is expecting to have an homogeneous shear stress, that could be calculated as follow:

$$\sigma_{r\theta} = \frac{M}{d} \times \frac{1}{S} = \frac{M}{d} \times \frac{1}{\pi dh} \quad (3.1)$$

where M is the torque, d the mean diameter of the solder joint, h is the high of the solder joint. For the ring and plug models designed in the figure 3.4 the torque is:

$$\sigma_{r\theta} = \frac{150}{\frac{3,2}{2} \times 3,2 \times 2 \times \pi} = 4,66 MPa \quad (3.2)$$

This value seems to be too small, to have efficient creep behavior of the solder joint. To have a bigger stress value, the solder joint surface has to be reduced, it can not naturally be reduced indefinitely. The creep tests are performed at different stress levels and up to 50 MPa. That means that the test specimen has to be reduced drastically of a factor 10, because it is not possible to change the machine. The new test specimen would be

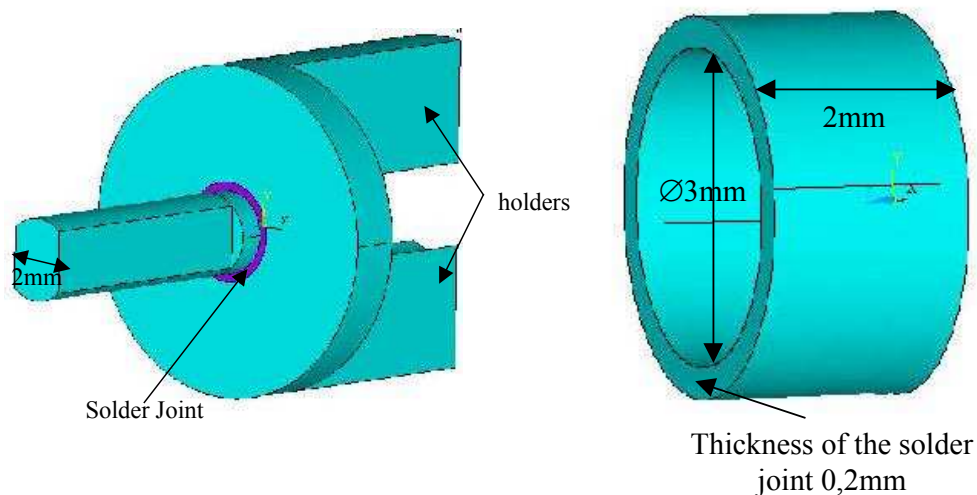


Figure 3.4. *The modified Ring-and-Plug test specimen. The "plug" has to be milled to facilitate its montage on the Rheometer. Holders are added to the "ring". On the left, the solder joint dimensions are shown. (N.B: It will be not easy to reduce these dimensions)*

impossible to machine, that why, the Ring-and-Plug test specimen is not useable with the rheometer.

FEM Analysis

It was demonstrated that the Ring-and-Plug test specimen can not be used with a rheometer to perform creep tests. The other possibility is to use this kind of test specimen with a standard torsion test machine, like the Zwick 1446 machine that is available at IZM. Nevertheless to verify the capability of this test specimen (homogeneous pure shear stress), a FEM analysis was performed. This calculation was performed with Ansys 7.0. The solder joint was the first part to be meshed. The hex20nodes (solid186) elements were used. The mesh was done with the sweep command. The mesh of the two holders was performed also as described previously. The tet10nodes (tet187) elements were used for the other parts, with the automatic Ansys mesher. The faces that are in contact with the Rheometer's jaw are fixed (Boundary conditions: displacement equal to zero). The torque is transmitted by the planar faces of the Plug, which are in contact with the other jaw. A MPC 184 [88] (for Multi Point Constraint) and it is a rigid beam (bar) Element (the mesh can be seen on the Figure 3.5). For the first approach a non-linear calculation was performed in order to verify that an homogeneous shear stress in the solder joint is present as expected. The secondary creep models of Grivas-Hacke [49, 89] was used to model the creep behavior of the SnPb solder joint. The moment 150 mNm was applied at the room temperature during 500 seconds to have the stabilization of the stress in solder joint. The results of the performance are shown in figure 3.6.

The first establishment is that the stress is not homogenous as expected ($\sigma_{r\theta, min} = -27.8MPa$ and $\sigma_{r\theta, max} = -0.62MPa$) but is nevertheless pure shear strain. To verify this affirmation,

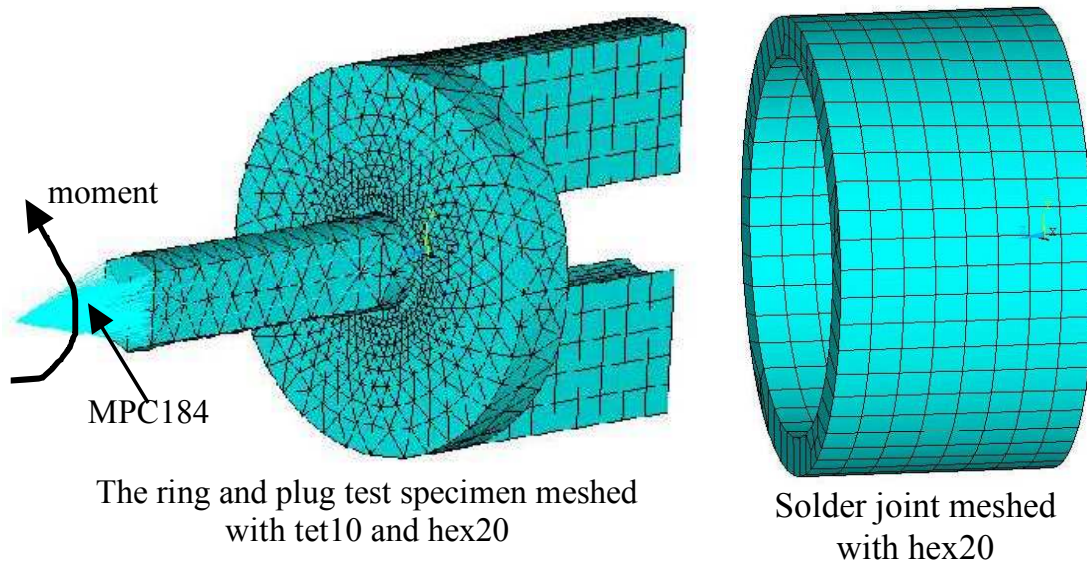


Figure 3.5. Mesh of the Ring and Plug test specimen

the ratio $r_\varepsilon = \frac{\varepsilon_I}{\varepsilon_{III}}$ [90] (where ε_I and ε_{III} are the first and the third principle stress) was calculated and was for each node very closed to -1, that means that $\varepsilon_I = -\varepsilon_{III}$ and that the shear stress is pure. The second establishment is that a stress concentration due probably to the geometry definition is observed. The third establishment is that the calculated mean shear stress on the solder joint is 4,61 MPa. This value is very closed to the analytical value 4,66 (see equation 3.2). The rheometer is definitively not the machine adapted to perform creep tests with the ring and Plug test specimen, but a bigger stress level using the torsion machine can be obtained. During the postprocessing an eventual influence of the holders was detected (see figure 3.6 right). To verify that the inhomogeneity of the stress in solder joint was not due to this holders, the calculation was newly performed but the holders were deleted. Of course the same boundaries conditions were applied to the plug. The results of this analysis are presented in figure 3.7

It is clearly shown that the local stress inhomogeneity disappears without the holders (to compare the two pictures, the same color scale was used in the representation (figure 3.5 right and figure 3.6 right)). Unfortunately, the stress repartition is strength inhomogeneous, and is not due to the holders. A another Ring and Plug test specimen was calculated by the IZM, [91] with a 2D Model using the symmetric axis boundaries conditions and found the same inhomogeneity. It is was decided not to use this kind of test specimen for the creep test, because it could be very difficult to determine the stress-strain conditions in correlation with the moment and the angle measured.

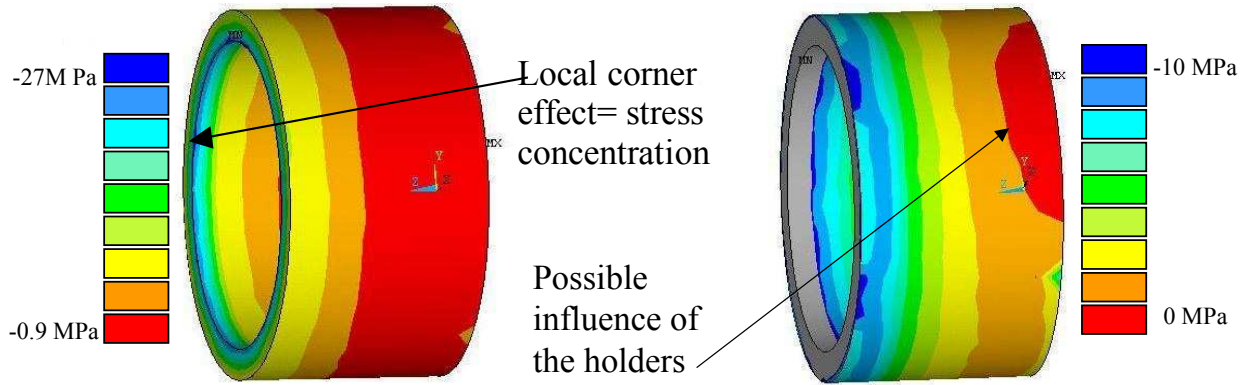


Figure 3.6. results of the static elastic-creep analysis, with a torque of 150 mNm, The Ring and Plug test specimen in pure Copper, and an eutectic SnPb as solder joint alloy. The shear stress in a cylindrical coordinate system is shown. On the left the original scale given by Ansys, on the right, a modified scale(-10MPa 0Mpa) to bring to the fore the possible holders influence

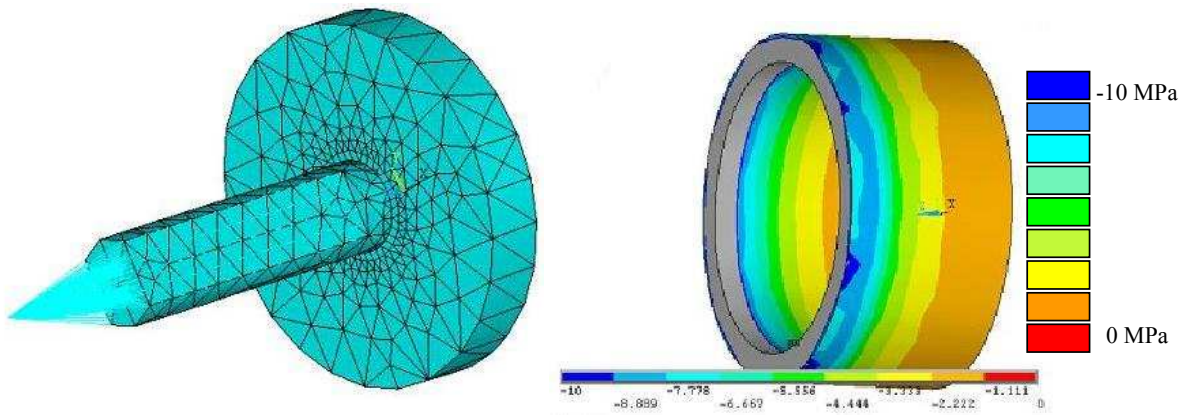


Figure 3.7. New performance for the ring and plug test specimen without holders. On the left the meshed Geometry, on the right the cylindrical shear stress results with the scale -10 MPa 0 Mpa

3.1.3 The single lap test specimen

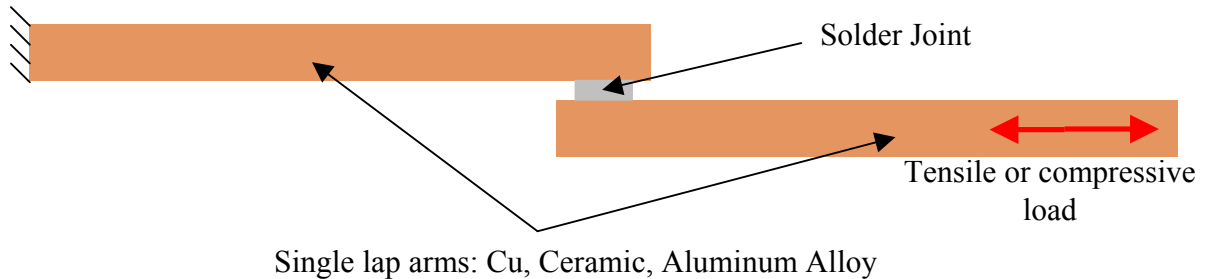


Figure 3.8. *the single lap test specimen*

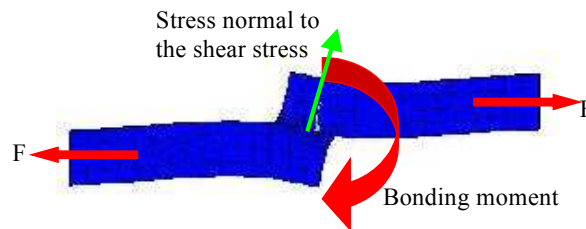


Figure 3.9. *the single lap test specimen*

The single lap test specimen (figure 3.8) is often used for the fatigue test [92] and is probably the most common solder joint shear test sample. This geometry is normally easy to construct, however the user has to pay attention in the fact that the two arms should be parallel, in order to keep a constant thickness between the two arms. The single lap test is easy to set up, but due to its geometry, bonding mounts and constraints could appear and will provide stress normal to the shear direction. [93]. Figure 3.9 illustrates these comments. To avoid such disagreements, the double-lap test is often used. (see section 3.1.4)

3.1.4 The double lap test specimen

In literature, authors use this test specimen (double lap), but the solder joints used are often a lot of bumps (see [94]). In comparison with the Darveaux [51] geometry, the Double lap arms are extended, to offer the possibility to fix this Geometry on tensile machine. The main difficulty is to keep the force equality, and the parallelism of the force. It is difficult because of the geometry of the chuck jaws. To have the best results, it would be maybe interesting to create a fixing help (see figure 3.10)

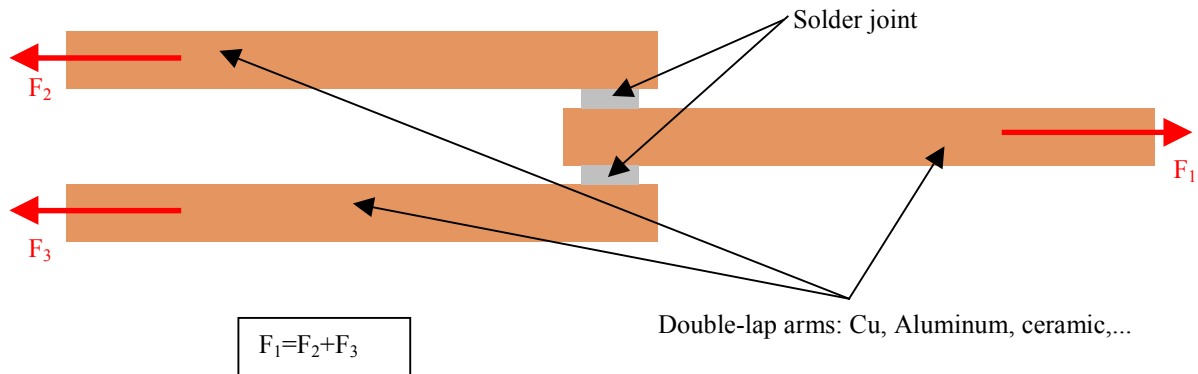


Figure 3.10. *The double lap test specimen*

3.1.5 The grooved-lap test specimen

The grooved-lap test specimen is a geometry which is extrapolated from the work of Iosipescu [95,96]. The Iosipescu geometry (see Figure 3.11) was firstly developed, to test general properties of materials, in the typical shear state.

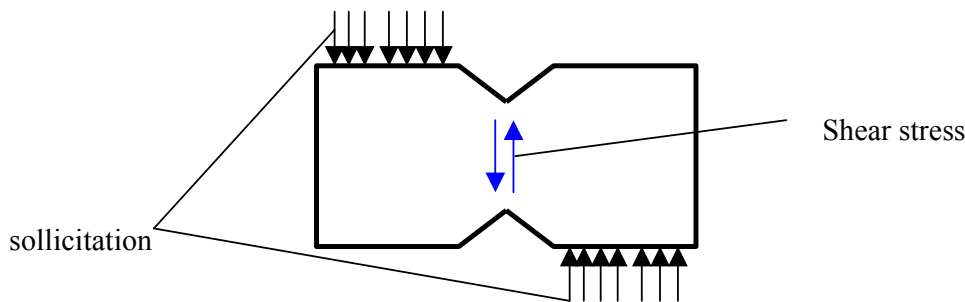


Figure 3.11. *The original Iosipescu geometry. A special montage is necessary to fix this test specimen on standard tensile machine, because of non collinearity of the two surfaces, where the load must be applied*

Reinikainen et al. [97,98] has developed the concept of the grooved-lap geometry applied to the test of solder joints. The solder joint is tested in shear and it could be a good alternative to the standard tensile test. In his work, Reinikainen has compared 8 test specimen geometries. For that he first used the FEM Software ANSYS to perform analysis. The 8 test specimens were loaded by a uni-axial tensile force. He showed that the best pureness of the shear deformation and stress was found for the grooved-lap geometry and defined it as follow (see Figure 3.12). He also verify the homogeneity of the stress (difference between the maximum stress and the minimum stress level) and the pureness of the shear stress. According to Reinikainen the shims have been used to maintain parallel the two parts of the specimen. Those two shims are not fixed or glued with the copper (or steel) arms to let the translation of their free in order to perform the creep test. The difference

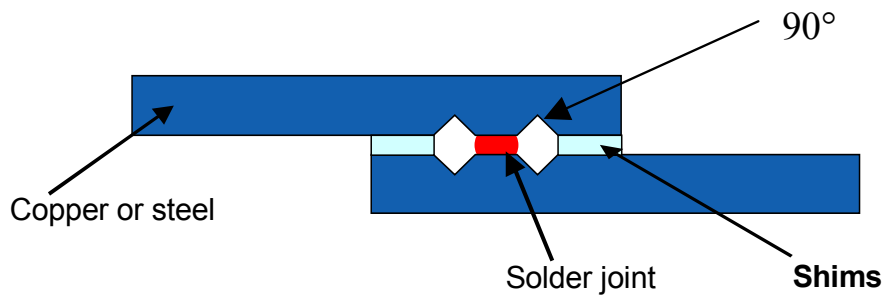


Figure 3.12. *The "Reinikainen" grooved-lap test specimen*

of this new test specimen in comparison to the single lap (figure 3.8) on the both side of the solder joint, a corner is machined in the arms with an angle of 90° . The consequence is to report the stress concentration in this corner and not in the solder joint anymore. The stress repartition in the solder joint was calculated for this grooved lap test specimen and was compared to the other in the next paragraph (3.2)

3.2 comparison between the different test specimens

3.2.1 mechanical load

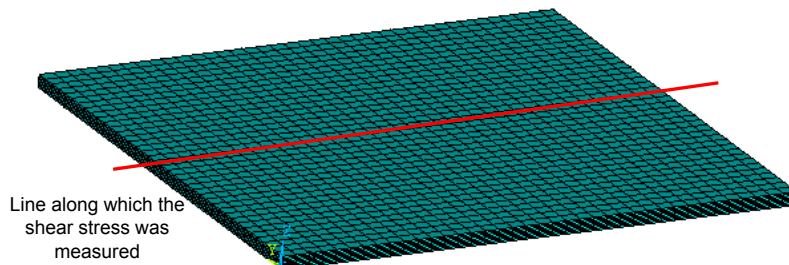


Figure 3.13. *mesh of the solder joints for the simulation of the single lap double lap and grooved lap test specimen*

To verify the relevance of the grooved lap geometry, a creep test was simulated with this geometry and was compared with the results of the others (single lap, double lap, ring-and-plug). For all models (excluding the ring-and-plug), the solder joint(s) were meshed with the same elements and mesh density (figure 3.13). The materials chosen for this simulation was the SnPb solder alloy, and the copper for the other pieces of the test specimen. The test is a standard creep test under a constant stress of 10 MPa. The simulation was performed at the room temperature and the force was applied during 1000 seconds. To characterize the homogeneity of the stress repartition the postprocessing consisted in calculating the

stress level along a virtual line in the solder joints (The shear stress at the corner was not compared, because the corner influences the results due to local singularity). This line is represented in figure 3.13, and is parallel to the two interfaces between the solder joint and the metal, and is in the middle of the solder joint. The measurements along this virtual line has been represented in the figure 3.14. It is interesting to see that the maximum stress always appears at the boundary (boundaries effects and stress concentration). As criterium to determine the best repartition, it is interesting to look at the ratio:

$$r = \sigma_{shear,max} - \sigma_{shear,min} \quad (3.3)$$

it is possible to visualize this ratio in figure 3.14. The smaller ratio can be seen for the

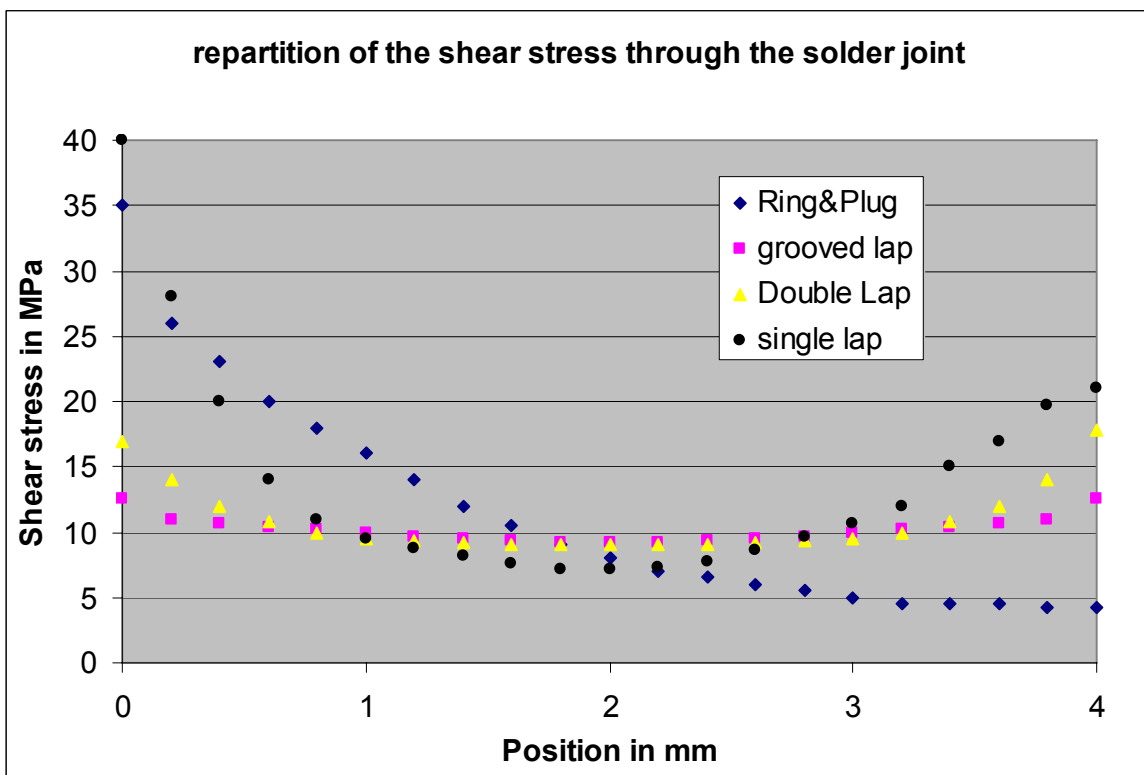


Figure 3.14. mesh of the solder joints for the simulation of the single lap double lap and grooved lap test specimen

double lap and for the grooved lap test specimen. It is clearly demonstrated, that the two best test specimens are the double lap and the grooved lap geometry. For the double lap this affirmation has to be nuanced. Indeed the simulation was realized with two perfect solder joint geometries. In real cases, it would be very difficult to produce two solder joints completely comparable. If a solder joint is smaller than the other one, it will create a local torque and a discrepancy. These simulation has shown that the grooved lap geometry has the best capabilities to occur an homogeneous shear stress repartition.

3.2.2 thermal load

The other application of the test sample is to evaluate the resistance of solder joint to fatigue creep. The idea is to fix the test specimen on a frame that has a different CTE. It will be put in a cycling oven for temperature cycle. A temperature shock tests will be performed. Because of the change of temperatures and the difference between the expansion of the frame and the test specimen, the solder joint should be loaded thermo-mechanically. The Objective of this test is to check the resistance of the solder joint, reproducing what is happened in real case for solder joints that are loaded in shear stress during temperature cycling tests. With different frames, it is expected to obtain different stress strain levels in solder joints. A model for the lifetime prediction of planar solder joint could be developed with such tests. To simulate the reaction of solder joint, it was decided to simulate an ideal case: it was considered that the material of the frame does not have any thermal expansion ($\alpha = 0$ ppm). It simplifies the boundary conditions. Indeed the both sides of the test specimen has been fixed, and the frame for this case has not to be designed. This ideal case was only used to verify the capabilities of the shear test specimen under this kind of thermal load. A typical temperature shock was simulated (-40C +125C, holding time 30 minutes). Three cycles were simulated, and the postprocessing was only done for the last one. The shear stress was also measured as it was shown in the paragraph 3.2.1. In this case it was not possible to represent the curves for each time of the cycle, only the ratio r (equation(3.3)). This ratio was represented as a function of the time (see figure 3.15). The ratio was calculated for the single lap and the grooved lap. It was observed during the phase that the grooved lap test specimen has a better stress repartition than the single lap.

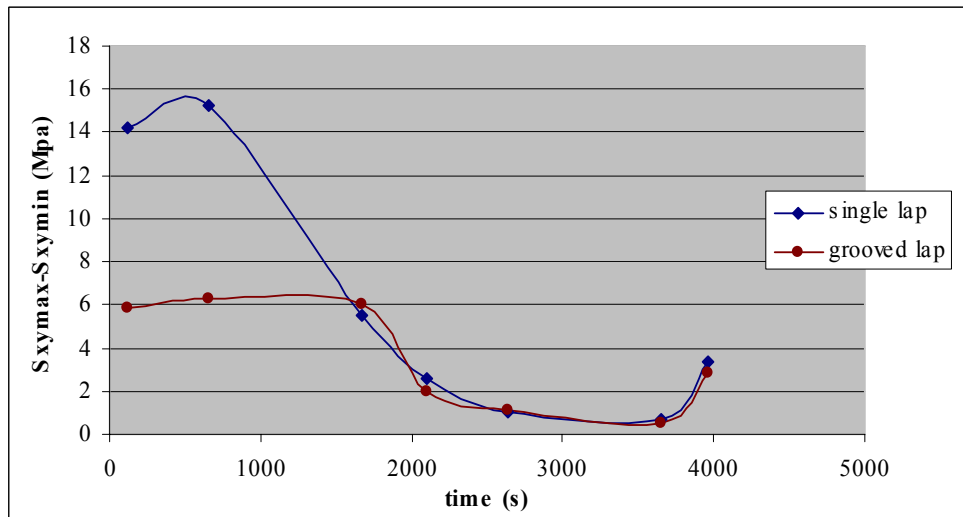


Figure 3.15. *characterization of the homogeneity of the stress for a typical temperature cycle. The first part of the curves is corresponding to the cooling and the second part to the warming*

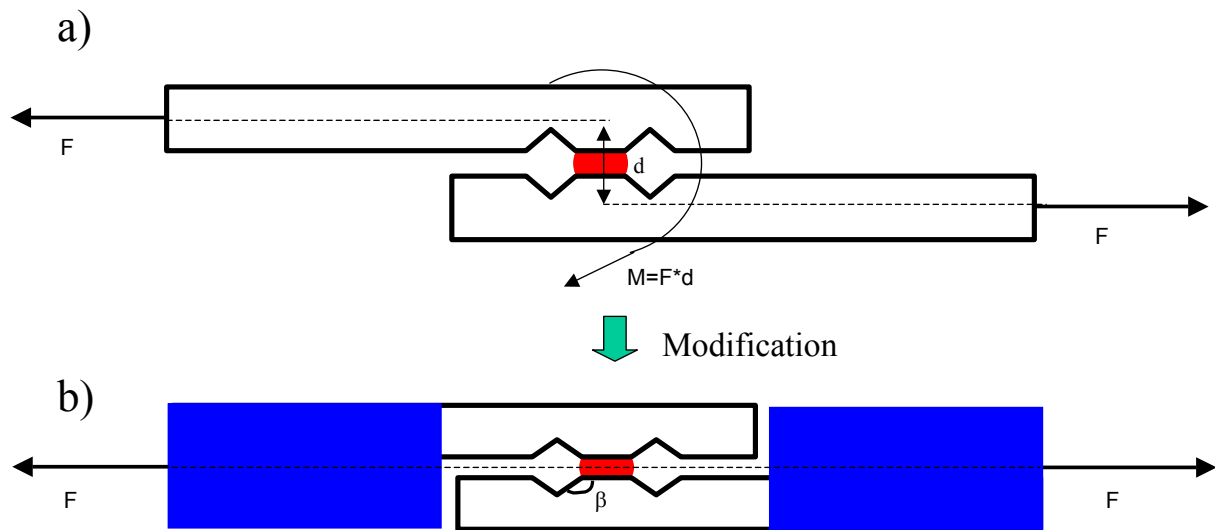


Figure 3.16. a) grooved lap geometry without any modification. The unwanted torque is represented. b) the first modification of the test specimen. The torque disappears

3.3 improvement of the test specimen

3.3.1 new kind of test sample

It will be shown in this section how the test specimen can be improved in order to have a better homogeneity of the stress repartition. The first important point is that due to the non collinearity of the two copper pieces, when a force is applied to the test specimen performing the shear test, a torque will automatically appear in the solder joint. It will cause other stress components (no pure shear stress) in the solder joint. the part of the copper pieces that are fixed in the tensile machine were modified to avoid this torque as shown in figure 3.16.

The second modification has two objectives:

- to minimize mechanical boundaries effect due to the corner (stress concentration)
- to avoid the acoustic boundaries effects using a SAM (scanning acoustic microscope). This SAM is used to investigate the solder joint, to check the eventual cracks and voids after soldering or performing temperature cycling test with the test specimen (see also in section 3.2.2).

Indeed when an ultrasound has to be focused on the boundary of the solder joint half the ultrasound goes through water and half through the test specimen (see figure 3.17a). The impedance mismatch between the two medium causes a boundary effect which leads to image disturbances. To avoid these, a chamfer has been machined, to create a pyramid geometry at the solder surface. (see figure 3.17b). The increase of the angle α from 90° to 135° should also reduce the stress concentration due the corner boundaries effect. Two test specimens were calculated; one without chamfer (figure 3.18 case a) as described before this section, and the other with a chamfer (figure 3.18 case b).

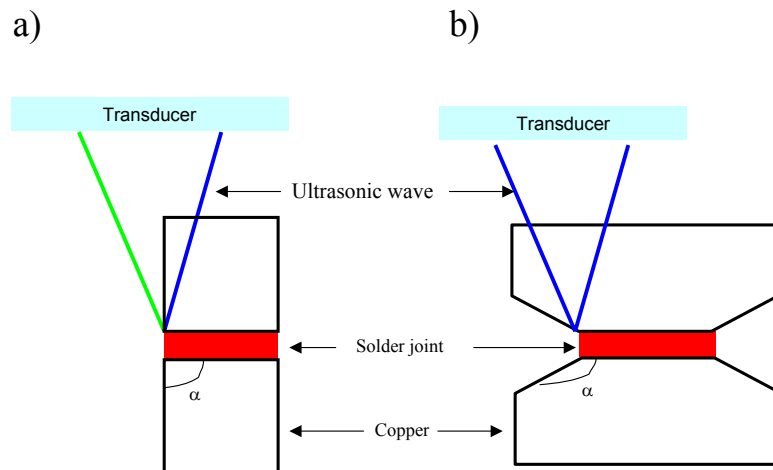


Figure 3.17. *The two figures represent a section of the test specimen whom the solder joint is scanned by a SAM: a) the grooved lap test specimen without chamfer. the propagation speed of the green and blue acoustic signal will not be the same because of different acoustic impedances of the two mediums. b) the test specimen with a chamfer. both solder joints were meshed with the same density*

The FEM analysis was performed for both geometries. Two analysis types were performed; the first was an elastic performance and the second an elasto-plastic performance (using the Grivas Hacke creep laws [49, 89]). In the two cases, the mesh of the solder joint, the boundaries conditions, and the material characteristics were identical. The test specimen was supposed to be in Cu One part of the test specimen was fixed, and the other part was pushed or pulled with a constant force. The forces were chosen to have a shear stress at the solder joint lying between 2 and 60 MPa. In all cases, the homogeneity and the stress pureness were identical or better for our own test specimen (as an example see the next figure 3.18) compared to the standard grooved lap geometry.

The angles α and β of the figures 3.17 and 3.16 were defined by default to be equal to 135° because of the machining capabilities (paragraph 3.3.2). According to Iosipescu [95, 96], to have the best homogeneity of the stress the best angle is 145° . It was verified for our test sample after FE-analysis using the parametrical capabilities of Ansys that the best angle is 150° (The geometries were calculated with an angle from 125° to 160° with a increment of 5°).

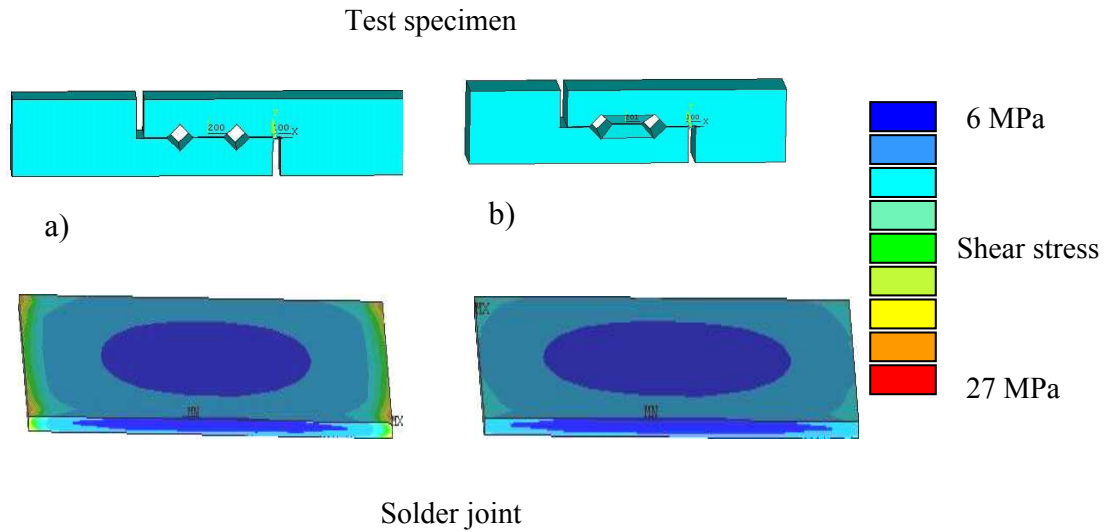


Figure 3.18. *FE model and stress repartition at the solder joint of two kind of test specimens. The calculation was performed to have a mean shear stress of 10 MPa at Room temperature a)grooved lap without chamfer. Stress concentration is clearly seen.b)modified grooved lap. the stress concentration is reduced*

3.3.2 fabrication and investigation of the test sample

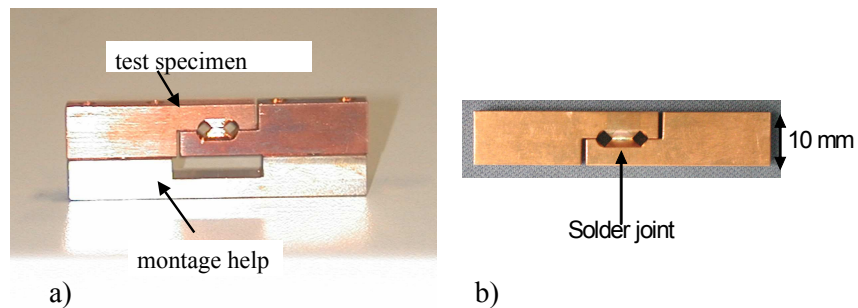


Figure 3.19. *a) the montage help with the 2 copper pieces b) the test specimen soldered*

The test specimen used for the experiment were machined and honed in a pure oxygen free copper (SE Cu F30 DIN 1787). This copper was chosen for two reasons: the SE-Coppers are the copper that are currently being used by the electronic industry. In this family of coppers, the copper with the largest hardness was used to make the machination easier. The two parts were machined with a 5 axis metal milling machine. The parts were honed at the solder joint place to have a low rugosity and to have a good planarity and better tolerances. The Cu parts of the test specimen were controlled with light microscopy, to verify and to measure the size of the solder joint face in order to calculate the shear stress of each test specimen as a function of the applied force. Just before soldering, the copper face of the test specimen was also cleaned with isopropanol, to remove the oil rest, and only

the solder face was cleaned with an acid to remove the oxidation and to have at this place a good wettability. A montage help was also machined in order to maintain the two copper pieces together during the soldering. This montage help was also milled and honed in the same copper for avoid CTE mismatch during soldering, which could load the solder joint. The goal of this montage help (see figure 3.19) was also to maintain a constant thickness of the solder joint.

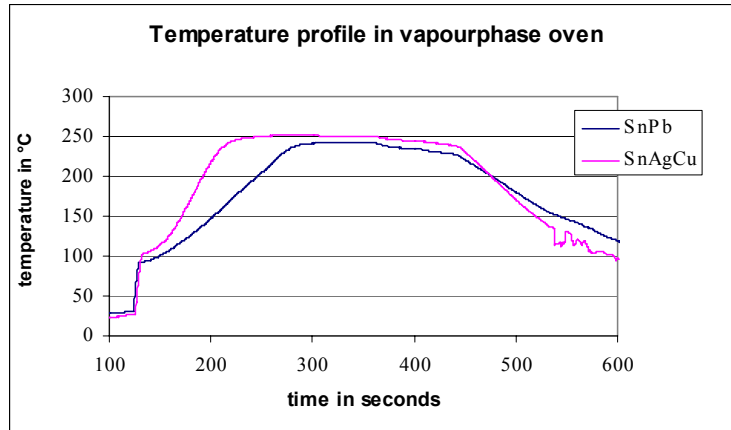


Figure 3.20. *Temperature profile of a thermo couple which was glue at the solder place on the copper*

A solder paste was used, including a flux that is relatively aggressive to avoid the oxidation of Copper during soldering. This paste was applied with a dispenser. Due to the high heat specified capacity of copper and the relatively big size of the the specimen on the help montage, the specimens are soldered in a vapour phase oven at a temperature of 260°C for the SnAgCu, and 240 °C for the SnPb, and before cooling, the specimens are put into vacuum, in order to avoid voids in the solder joints. The temperature profiles are given by figure 3.20. To verify that the test specimen could be used to perform creep tests, the solder joint was checked to measure the thickness and to check the solder joint (see figure 3.21). As already shown by Wiese et al. [4] the microstructure depending on the solder joint geometry and the cooling rate during soldering of the alloy influences the creep behaviour of the alloy. The microstructure of our test specimens was also investigated (see figure 3.22 and 3.23). The SnPb structure looks like expected, i.e. Pb globules (dark grey) in Sn matrix (pale grey). The sizes of these elements are comparable with standard SnPb microstructure [99,100]. With optic microscopy as shown in figure 3.22 a and b is difficult to investigate the microstructure. To be able able to see the grain boundaries, the test sample was etched and investigated with REM. figure 3.23. The grains seem to be very large, probably, because of the small cooling rate after soldering (figure 3.20), and because the solder joint is already large.

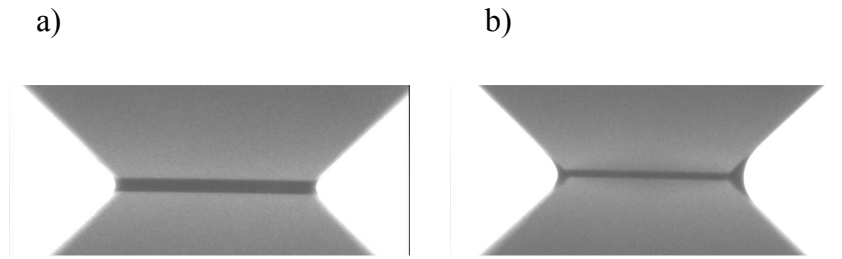


Figure 3.21. a) x ray picture of a good solder joint b) X-ray picture of a bad solder joint

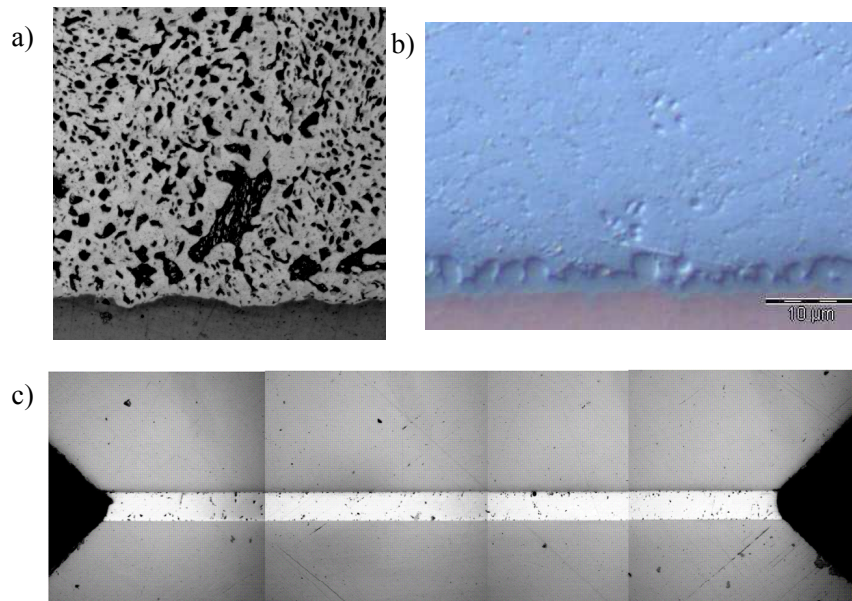


Figure 3.22. optical microscopy: a) the SnPb microstructure b) SnAgCu microstructure c) the full solder joint geometry investigation

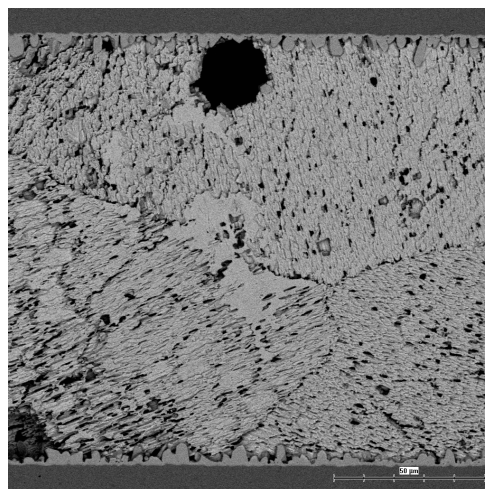


Figure 3.23. SnAgCu after chemical etching. REM picture. The grain are relatively big and oriented

Chapter 4

Development of new creep constitutive equations

The time and temperature dependant creep deformation of solder alloys has to be studied to describe material characteristics and failure behaviour in order to use it for lifetime evaluation by FE-simulation. The objective of this chapter is to show how the creep test were performed and how the constitutive equations were developed. The grooved lap test sample as it was described in the precedent chapter was used for this creep test. The main objective of this creep test was to observe both primary and secondary creep and to verify if the primary creep reoccurs under cycling load conditions. Indeed it is often found in the literature that material behavior for eutectic SnPb and lead-free such as SnAgCu solders is described considering only secondary creep. They justify it considering that primary creep occurs only during the first cycle: that is not the fact, and it is now important to investigate primary creep. So, it is necessary to develop a new kind of constitutive equations combining these two creep modes. Here the solder alloys SnPb eutectic and SnAg4.0Cu0.5 are investigated.

4.1 creep tests

In chapter 2, different creep models were presented. The methods that were used is the method which describes the creep rate as a function of the time, the stress and the temperature. Indeed, the Anand or Chaboche's model do not have significant advantages. Then, to develop such kind of constitutive equations, the creep tests has to be performed at constant stress and temperature state. Of course different combinations of stress and temperature were adjusted.

The other important point, that has to be reminded, is the tensile machine which was chosen to perform the creep tests. At IZM three machine are capable to perform such tests. The first one is a Zwick machine, an electro-hydraulic machine, the second one the instron and the third one the MTS. The MTS was relatively quickly removed from the precedent list, because its maximal force was to low. The creep tests were performed till a stress of 32 MPa, i.e. a force of 512 N. The first tests were performed with both instron and Zwick tensile machines. It was observed till 500 N a better force and displacement accuracy

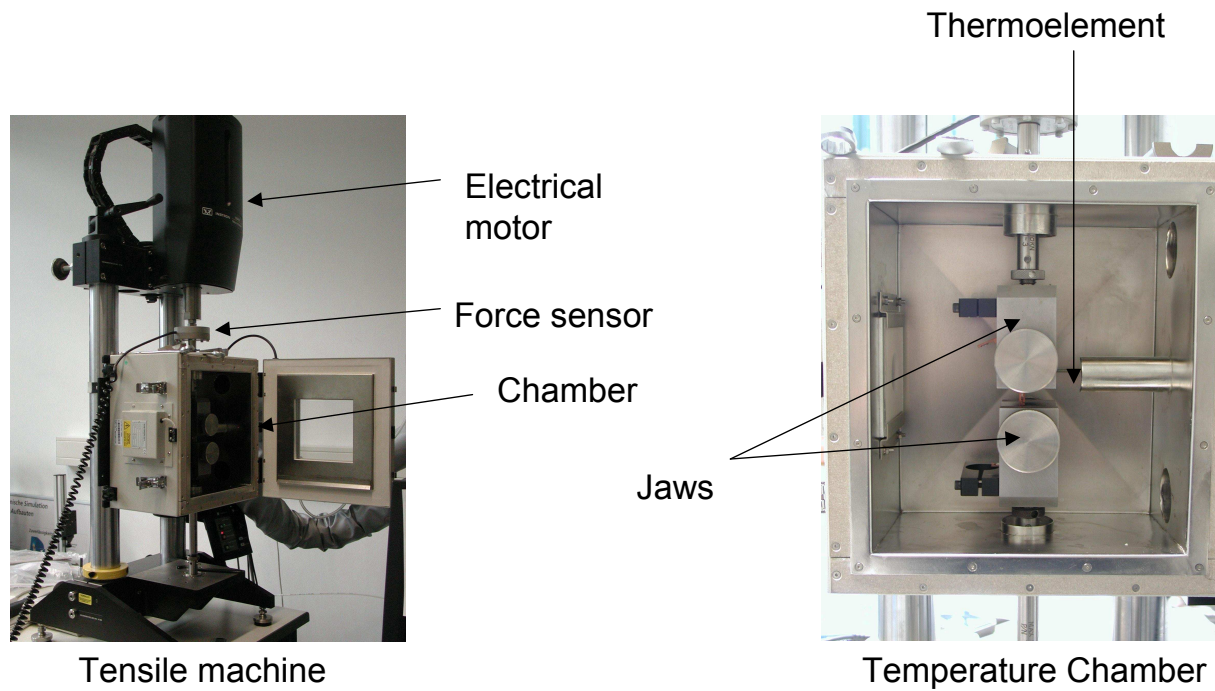


Figure 4.1. *Instron tensile machine*

and a better temperature maintaining for the Instron. The temperature amplitude was 10 K for the Zwick (when 2K was measured with the instron), and with such amplitude the creep curves are not useable. The creep test were carried out on a Instron Microtester 5848. The temperature chamber was capable of maintaining a temperature within $\pm 1\text{K}$, the tensile machine was also capable of maintaining a stress level within $\pm 0.05\text{ MPa}$. The machine is presented in figure 4.1.

| shear stress | -20°C | 22°C | 70°C | 110°C | 150°C |
|--------------|-----------------------|----------------------|----------------------|-----------------------|-----------------------|
| 2MPa | no | no | yes | yes | yes |
| 4MPa | no | yes | yes | yes | yes |
| 7MPa | no | yes | yes | yes | yes |
| 10MPa | no | yes | yes | yes | yes |
| 12MPa | yes | yes | yes | yes | no |
| 15MPa | yes | yes | yes | yes | no |
| 20MPa | yes | yes | yes | no | no |
| 32MPa | yes | yes | no | no | no |

Table 4.1: combinations of stress and temperature for the creep tests

Those creep tests were performed at different temperatures (-20°C , 22°C , 70°C , 110°C , 150°C) and for different stress levels. All combinations were not used because for low temperature or stress the creep was not always observable, and for some test samples at high temperature and high stress level the fracture of the solder joint came very fast (only tertiary creep). In those cases, it was impossible to measure a real creep curve. The

combinations used are reported in table 4.1.

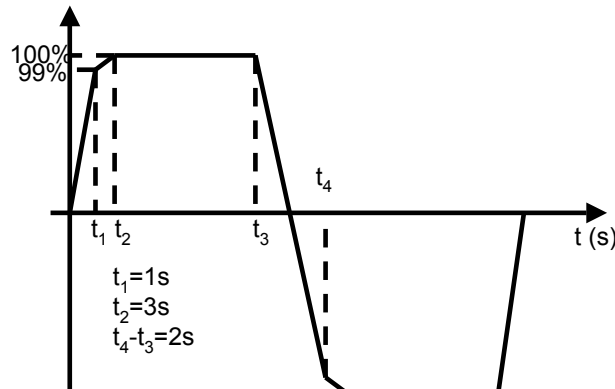


Figure 4.2. *The load cycle: The double ramp is used against overshoot*

To have a good statistic, 4 creep tests were performed for each combinations. However, some data were not used to build the model, because the results were not accurate or realistic. During the tests, the force was controlled. The test specimen was cyclically loaded to see if the observation of the primary creep was reversible or not. To have a good view of the primary creep, it is important to obtain quickly the creep load. However the speed to obtain the creep load was limited by the apparition of an overshoot. To get the best compromise between the speed and the precision, it was decided to use a double ramp: 99% of the load was obtained in 1s, the last 1% in 2s (see figure 4.2). It was the best compromise between the speed and the precision.

The other important point is the position of test samples on the tensile machine. Before every measurement, the position of jaws were adjusted to keep the same distance between them. The test sample was placed in the middle between the two jaws, taking care about its verticality. The jaws was closed so that the measured force was equal to 0 ± 2 N. When the temperature was not the room temperature, the test sample was put in the oven, the force adjusted to 0 N, the test program was started to maintain the force closed to 0 N, the oven was switched on, and we waited till the real temperature was obtained. The temperature was controlled with the help of a thermoelement and the thermal expansion was measured by the machine (displacement of the jaws maintaining a force closed to 0 N). When the temperature was stable and the thermal expansion did not occur anymore, the measurement was started.

The shear stress was obtained by dividing the force (given by the tensile machine) by the solder joint surface. The surface of the solder joint was systematically controlled with an optical microscope. The strain was calculated as division of the deformation by the high of the solder joint. This height was revealed by X-ray before the test performance (for more information, see also section 3.3.2). During the loading phase, the elastic deformation of the Copper pieces and of the machine is also measured and observed. The elastic and inelastic deformations of the solder alloy were also observable. During this short time, the primary creep has probably begun. It would be very difficult to quantify this creep strain,

because it is a creep by non constant stress. So, the deformation after the loading phase has been used for the evaluation of the creep deformation (see Figure 4.3).

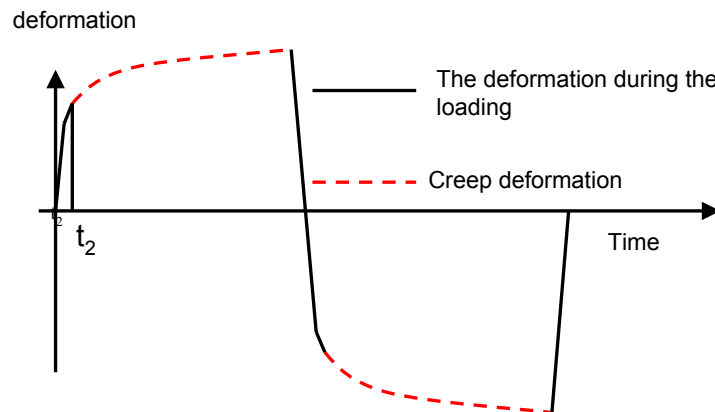


Figure 4.3. *The load cycle: The double ramp is used against overshoot*

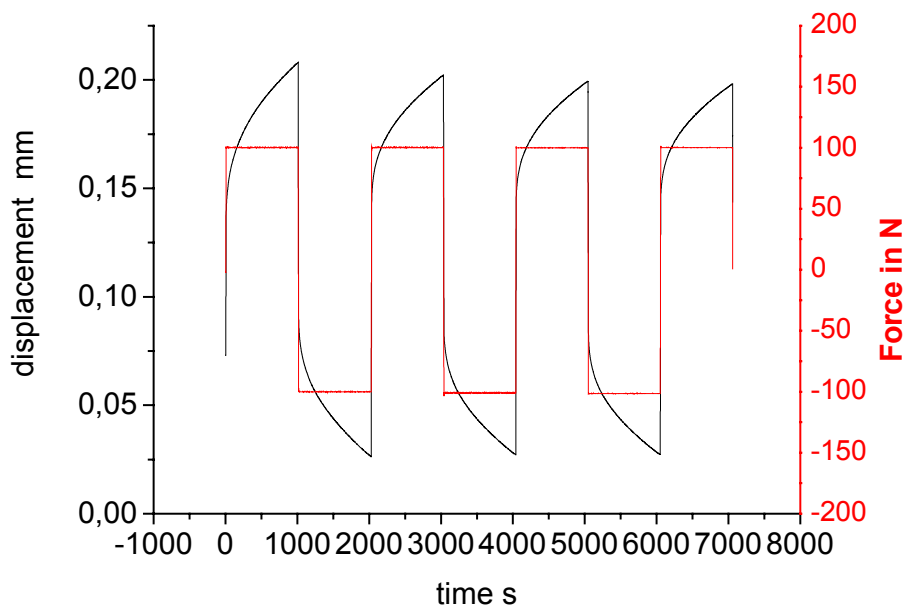


Figure 4.4. *results of 4 cycles. The force and the deformation as function of the time are represented*

This cycle was performed several times. In this case, and it is the most important result of this thesis, an alternation of primary and secondary creep is occurring. It means, that the primary creep is not a transient phenomena under cycling conditions (See figure 4.4). After 120 cycles, the primary creep was still observable (see figure 4.5). After 50 cycles, the creep strain is equal to the creep strain of the first cycle. After 120 cycles, just before the solder joint fails, an acceleration of the creep is seen. It is probably due to the damage

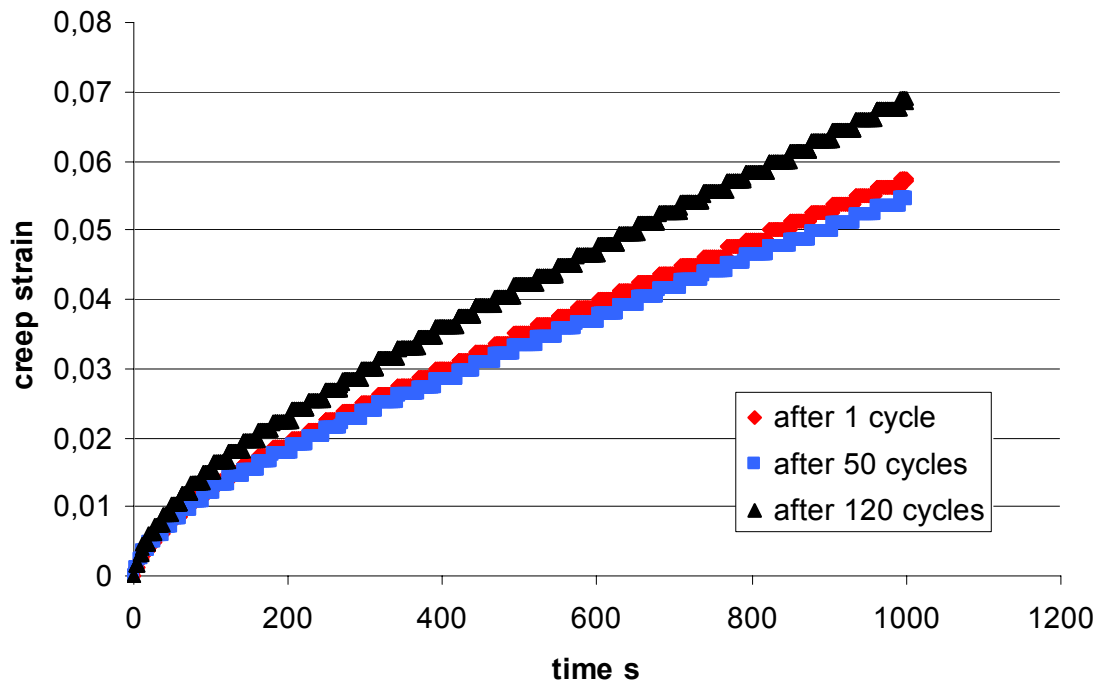


Figure 4.5. *shear strain creep of SnPb solder joint at room temperature, under 10 MPa*

of the solder joint where the shear stress is locally higher. An another interesting observation is that during the 2 or 3 first cycles a softening of a hardening could happen, but after these 3 cycles the cycles are regularly and symmetric. No explanation for this behavior was found, but for the model building, only the results from the 5th cycle, after the stabilization were used. The results were stored as ASCII file; the force, the displacement of jaws, the temperature and of course the time were saved every 0.1 seconds. Unfortunately the measurement at -20°C were not workable. Indeed the displacement measured due to the thermal expansion was really larger than the displacement due to the creep. The oven was cold down by liquid nitrogen but this system was not capable of maintaining a constant temperature. Moreover, the creep rate at low temperature is also very low. Hence, the primary creep is present for each time where the stress level and/or sign is changed. Therefore, neglecting of the primary creep leads to a systematic error in the description of the creep behavior of solder joint. This has been shown under isothermal load and is also expected for thermomechanical load, where the stress level is continuously changing during the cycling time. To see the relevance of this effect quantitatively, the primary and secondary creep law has been accurately measured. The results are shown in section 4.2 and 4.3.

4.2 steady-state creep

4.2.1 SnPb

In section 2.1.4, different creep mechanisms were presented. For the Sn-based alloys like SnAgCu and SnPb, the creep rate vs. the applied stress is divided in two regions. Grivas et al. [49] investigated these two regions. They assumed at low stress the superplasticity or grain boundary sliding process occurs. It is the region II. The other region (III) is governed by the matrix creep due to dislocation climb and glide. They also assumed that the contributions of the two mechanisms to the total shear creep rate were additive so that:

$$\frac{d\gamma_s}{dt} = \frac{A_{II}}{T} \tau^{n_{II}} \exp\left(\frac{-\Delta H_{II}}{RT}\right) + \frac{A_{III}}{T} \tau^{n_{III}} \exp\left(\frac{-\Delta H_{III}}{RT}\right) \quad (4.1)$$

where T is the temperature in Kelvin, A and n are constants from experiment, ΔH is the activation enthalpy, R the gas constant ($8,314 \text{ J.mol}^{-1}.\text{K}^{-1}$) The steady state creep rate

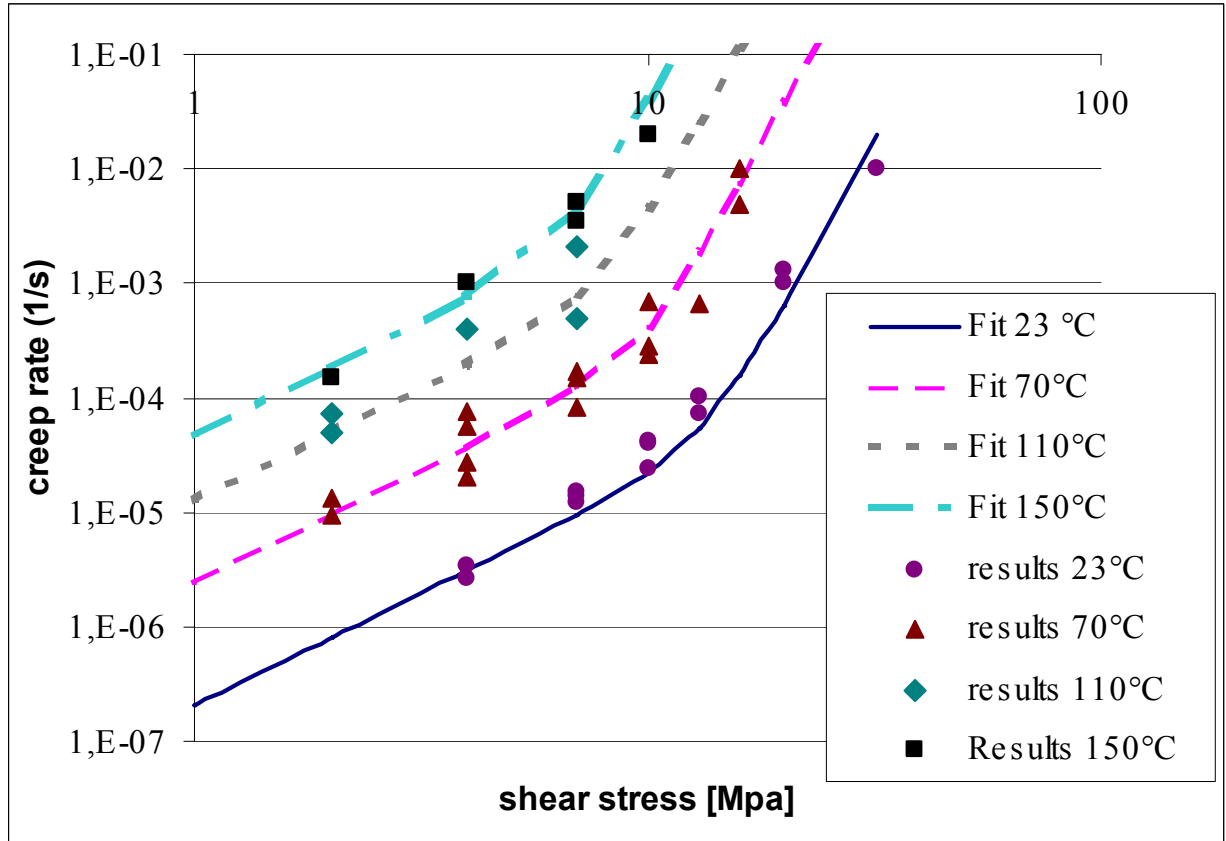


Figure 4.6. steady state creep behavior of eutectic SnPb. the points are results from experiment, and the curves the model with fitted parameters

is calculated in the linear region of the extracted creep curve. For each temperature and stress combination 3 or 4 values of this creep rate were found and reported in figure 4.6

for SnPb and in figure 4.7 for SnAgCu. For SnPb the parameters of the equation 4.1 were determined using non linear regression. The started values were the data given by Hacke. The parameters are reported in table 4.2

| Region | A(K/s^{-1}) | n | ΔH (kJ/mol) |
|--------|-----------------|------|---------------------|
| I | 18140 | 1,97 | 48 |
| II | 2380 | 7,51 | 79 |

Table 4.2: SnPb parameters for equation 4.1 determined from experiments

The figure 4.6 shows that there is not a large distortion or discrepancy between the values from experiments and the model. Our own results are in good agreement with the Grivas Hacke law. For the region II of the creep, the results are similar. For the region III, our creep rate is higher than the creep rate of the Grivas Hacke law: we noticed a difference of the stress exponent, but the activation energies are still equivalent. The parameter from hacke [31] are reported in table 4.3.

| Region | A(K/s^{-1}) | n | ΔH (kJ/mol) |
|--------|-----------------|------|---------------------|
| I | 18140 | 1,96 | 48 |
| II | 2380 | 7,10 | 81 |

Table 4.3: SnPb parameters for equation 4.1 determined from hacke

Some electronic packages like the PBGA (see section 5.4.3), flip-chips (see section 5.4.2) or resistance were calculated with equation 4.1 using alternatively the parameters given by Hacke and our experiments. The difference calculated from the accumulated creep strain was irrelevant. Performing creep test with a different geometry but the same microstructure gives same results for SnPb! However Wiese [48] showed in his PhD the high dependance of the creep rate on the microstructure (i.e. the cooling rate and the solder joint geometry).

4.2.2 SnAgCu

Same methods and same work were done for the SnAgCu. Unfortunately, the well-known sinus-hyperbolic-function given by equation 4.2 was not able to describe the experiment data.

$$\frac{d\gamma_s}{dt} = C \times [\sinh(\alpha\tau)]^n \exp\left(\frac{-\Delta H}{RT}\right) \quad (4.2)$$

Based on equation 4.1, Wiese et al. [4] purposed the following equation:

$$\frac{d\gamma_s}{dt} = A_{II}\tau^{n_{II}} \exp\left(\frac{-\Delta H_{II}}{RT}\right) + A_{III}\tau^{n_{III}} \exp\left(\frac{-\Delta H_{III}}{RT}\right) \quad (4.3)$$

where T is the temperature in Kelvin, A and n are constants from experiment, ΔH is the activation enthalpy, R the gas constant ($8,314 \text{ J.mol}^{-1}.\text{K}^{-1}$)

From our experiment, the parameters given in table 4.4 were calculated with non linear regression method; the started values were the value of Wiese for joint see ??:

| Region | $A(K/s^{-1})$ | n | $\Delta H(kJ/mol)$ |
|--------|---------------|------|--------------------|
| I | 1,33E-5 | 3,2 | 23 |
| II | 3,18E-10 | 11,5 | 62 |

Table 4.4: SnAgCu parameters for equation 4.3 determined from experiments

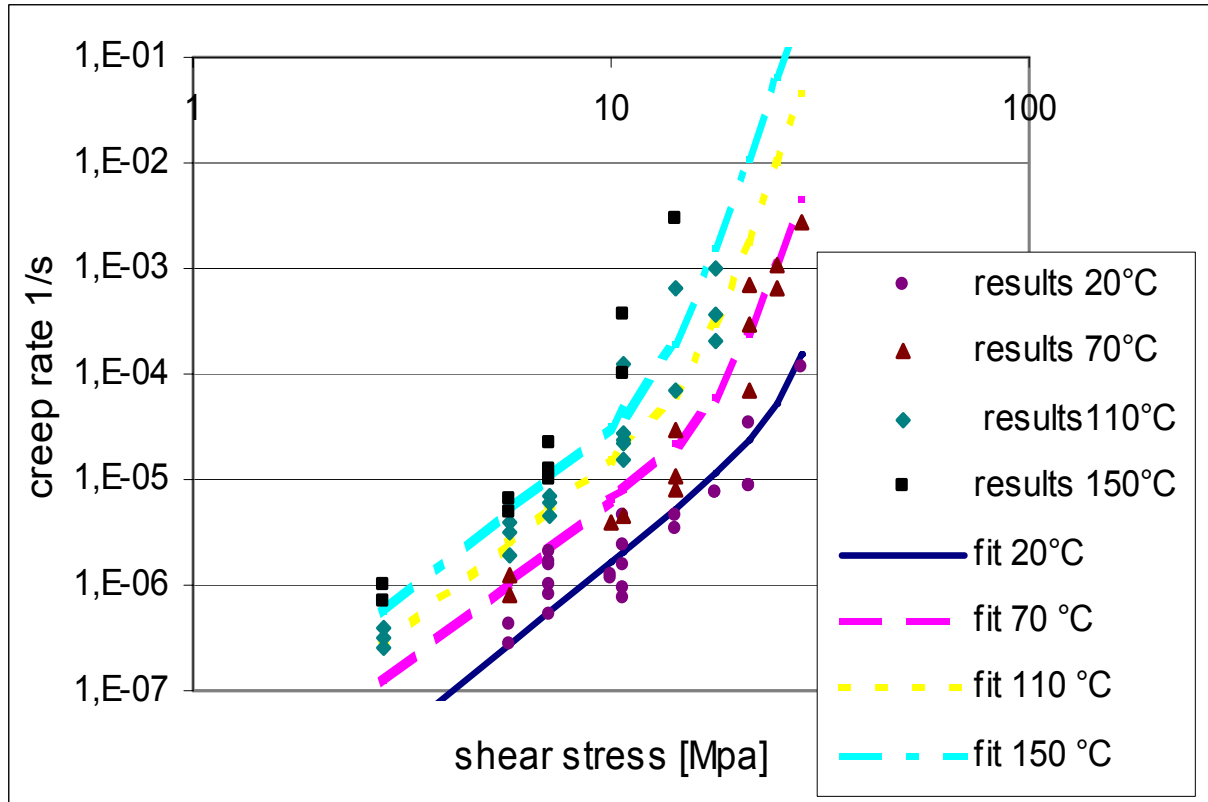


Figure 4.7. steady state creep behavior of eutectic SnAgCu. the points are results from experiment, and the curves the model with fitted parameters

Experimental data and model are represented in figure 4.7:

Two regions (superplasticity, and grain boundary sliding) of the secondary creep were clearly observable, which is a sinus hyperbolic function which is generally used to describe the behaviour of lead free alloys was not used (see [7]). Indeed, because of the two different deformation mechanisms, the two regions have different inclinations. Figure 4.8 compares three SnAgCu models (Wiese et al. [4], Schubert et al. [7] and our own model [101]). The three authors agree for a stress level above 10 MPa but the largest difference can be observed below this value. The difference between the Wiese model (joint) and our model is less relevant than the difference between our model and the model of Schubert et al. particularly for low stresses, in order to predict the end of life of solder joints. The difference are observed because of the microstructure influence. Schubert et al. used a lot of data from the literature to constitute their models. It explains why their models differs from our model and from their experimental data. Indeed, the majority of the data are

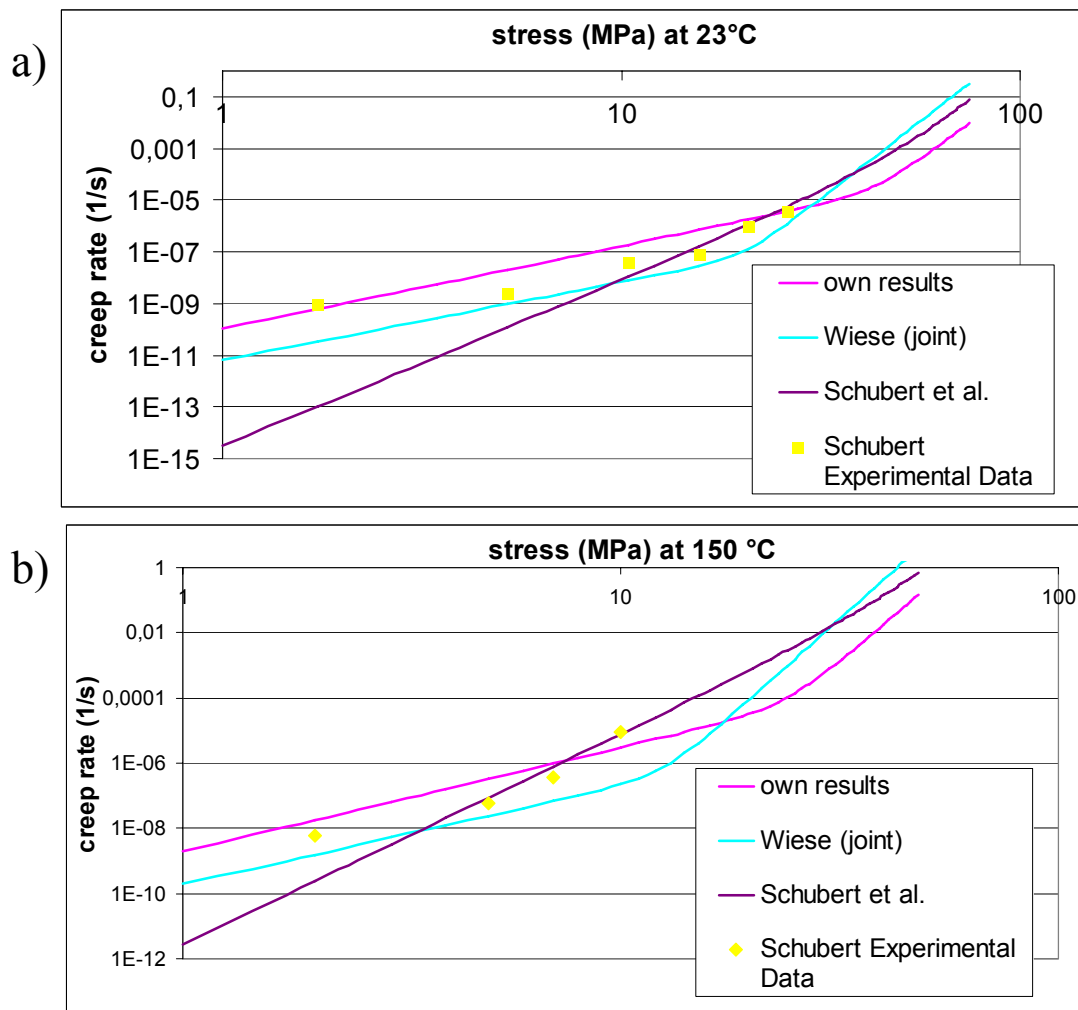


Figure 4.8. *different models describing the secondary creep at room temperature (figure a) or at 150 °C (figure b)*

at high stress (above 10 MPa), and the curve was extrapolated at low stress. Calculating with our model or with the Wiese’s Model could give a difference of 10%, but up to 25% with the Schubert’s model (calculated accumulated creep strain).

4.3 primary creep

The primary creep was investigated, it was tried to use the existing primary creep laws that was found in literature [43, 54, 102, 103], but no one was capable to describe the primary creep that was observed at all temperatures and for all stress levels, because of its high dependance on the temperature and the stress (fit with all curves). There was no convergence when all the curves with the same model have to be fitted. However, it was possible to describe the primary creep law with a lot of creep at constant temperature. For

solders, we found in the literature (see [7]) a creep law combining primary and secondary creep, so that:

$$\gamma_{creep} = \gamma_p + \gamma_s \quad (4.4)$$

where γ_p is the primary creep and γ_s is the secondary creep. The creep composed of a primary and secondary part at constant stress and temperature can be described by the following equation:

$$\gamma_{cr} = \gamma_{sat} \left[1 - \exp \left(-K \left(t \times \frac{d\gamma_s}{dt} \right)^n \right) \right] + \frac{d\gamma_s}{dt} \times t \quad (4.5)$$

Where K et n are constants. $\frac{d\gamma_s}{dt}$ is the steady-state creep rate. γ_{sat} is the saturated transient creep strain. It is obtained by extrapolating the steady state creep line back to the starting point (see figure 4.9).

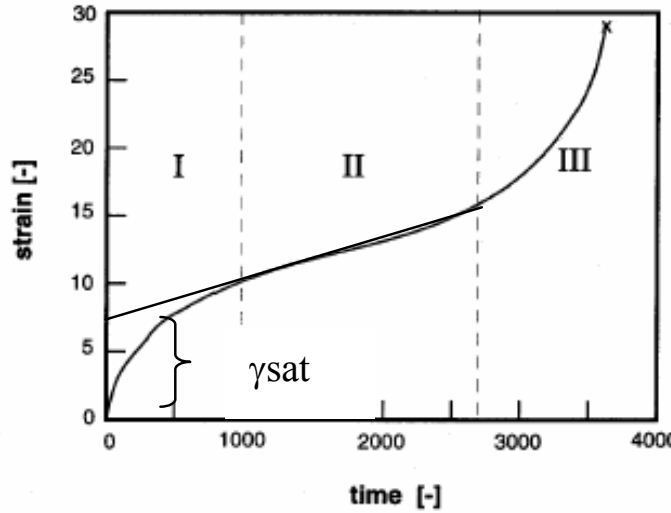


Figure 4.9. Creep curve: for this creep curve, the primary saturated creep is about 7%

Authors [7, 104] have given the saturated transient creep strain as a constant approximately equal to 0,5%. This is not possible in our case. It is clear that, bigger the temperature or the stress is, bigger the saturated transient creep strain is. A relationship between the saturated transient creep strain and the steady-state creep strain was developed:

$$\gamma_{sat} = \left(a \times \frac{d\gamma_s}{dt} \right)^b \quad (4.6)$$

where a and b are constants. The parameters were fitted as follow (table 4.3) with a non linear regression method.

The figure 4.10 corresponding to the precedent equation and the measured data are designed. In this figure the saturated transient creep cannot be considered as being constant.

| | a[s] | b |
|--------|-------|-------|
| SnPb | 1.613 | 0.467 |
| SnAgCu | 1.71 | 0.40 |

Table 4.5: coefficient values determining the saturated transient creep

Combining equations 4.5 and 4.6, the creep scan be described as:

$$\gamma_{cr} = \left(a \times \frac{d\gamma_s}{dt} \right) \left[1 - \exp \left(-K \left(t \times \frac{d\gamma_s}{dt} \right)^n \right) \right] + \frac{d\gamma_s}{dt} \times t \quad (4.7)$$

with a,b,K and n constants. The coefficients of equation 4.7 were fitted to experimental results. The started values for K and n were the values of Schubert et al. [7]. a and b were still adjusted. The table 4.3 shows the results achieved hence.

| | a[s] | b | K | n |
|--------|-------|-------|-----|------|
| SnPb | 1.613 | 0.467 | 111 | 0.79 |
| SnAgCu | 1.71 | 0.40 | 109 | 0.6 |

Table 4.6: equation for equation 4.7 resulting from our own results

The steady-state creep rate depending on the temperature and on the shear stress, the total creep depends explicitly on the time, the temperature and the stress. In general, if the stress or the temperature is increased, the saturated transient creep is also increased, but the secondary creep stage is reached earlier.

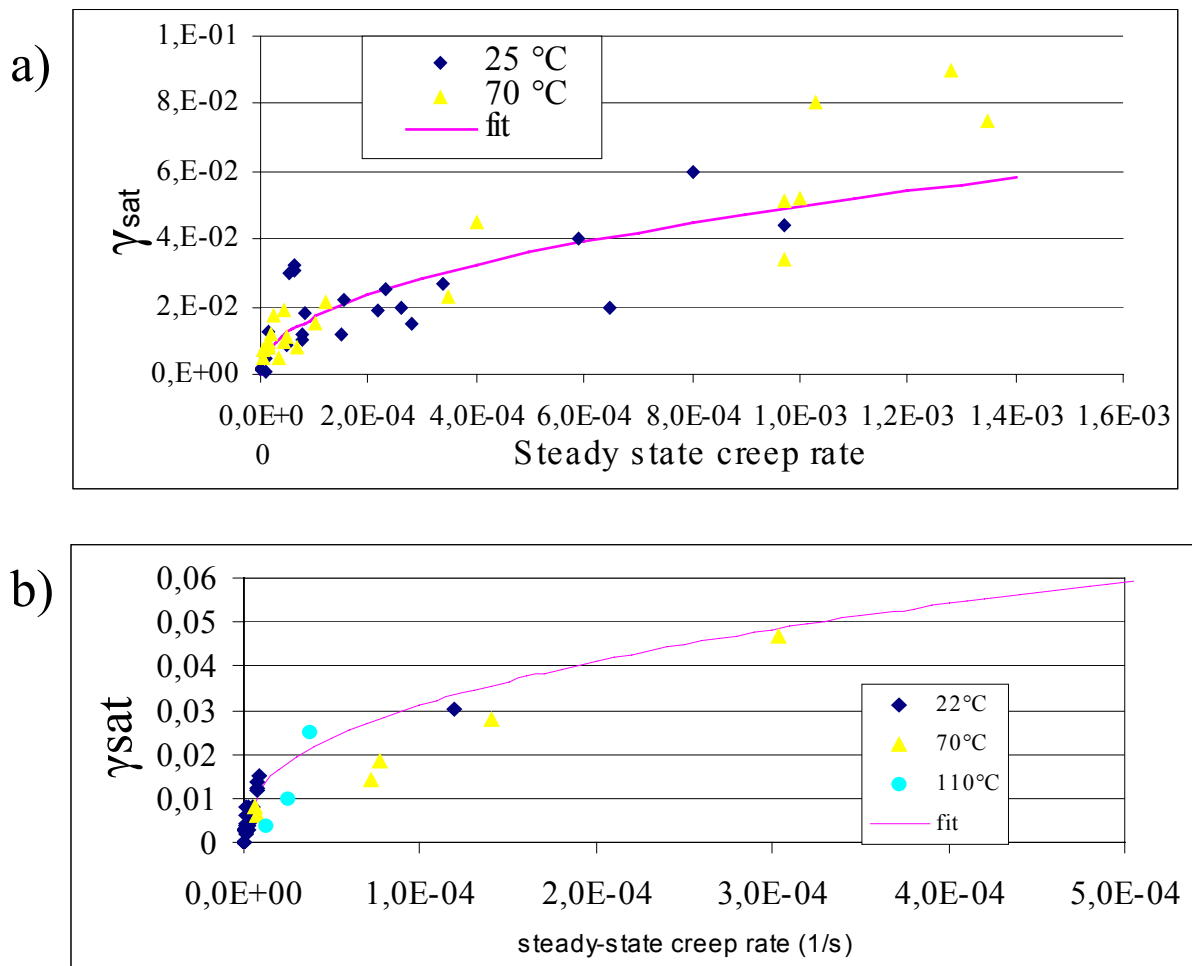


Figure 4.10. diagram representing the saturated transient creep in function of the steady-state rate. the experimental data at different temperatures and stress levels and the model are represented: a) SnPb b) SnAgCu

Chapter 5

Implementation of the creep laws in FE-codes

In this chapter, it will be shown how to implement the constitutive equations which were developed for the solder alloys. A large variety of equations are already implemented in the software Ansys, but no one was capable to describe the behavior of the solder alloys under different temperatures and stress level. This chapter purposes to show that it is not accurate to implement the creep law only as a relationship between the creep rate, the temperature and stress. It is also necessary to write some routine which can describe the change of stress level, and to detect a stress direction change. Some verification tests were performed and compared with experimentations to verify the validity of this implementation. At the end of this chapter the influence of primary creep on the temperature cycling test simulation will be presented. Different types of electronic packagings were simulated with and without primary creep, and a large variety of results are compared.

5.1 Fortran subroutine

5.1.1 different kind of subroutines

Ansys offers the possibility to be customized. Indeed, some routines exist and can be used to describe physical behavior, that are not already contained in Ansys. These routines are Ansys user-programmable features. As example, a new kind of elements can be developed, new material constitutive equations can be implemented. In Ansys three possibilities to program the creep behavior are available.

The first one is the routine called *usermat.f*. It is the routine with the best flexibility and possibilities. However the full material has to be described with this routine (elasticity, thermal expansion, plasticity ...). This routine was not chosen to implement the creep behavior, because the already existing constitutive equation from Ansys describing the isotropic elasticity and the thermal expansion are convenient for the description of solder joints. If this routine would have been used, the computation would have been much more difficult in comparison with the solution which was chosen.

The second one is routine called *usercr.f* is a routine which compute the creep strain with a implicit time integration schema.

The third one is a routine called *usercreep.f*, has the same capabilities but uses a explicit time integration schema and was selected to implement the constitutive equations.

5.1.2 Computation of the creep strain

The *usercreep.f* is a Fortran subroutine and has to be compiled in order to create a new ansys executive file. This routine can be called by Ansys, when necessary for each calculation increment. This routine calculate for each increment the creep rate $\dot{\epsilon}_{cr}$. Here there is a work distribution between the FE-kern and the subroutine. The FE-software calculates the temperature and the time and the creep strain and the equivalent stress (von-Mises). The routine can be called to calculate a creep rate using, the pre-cited computed data. For each increment the creep will be calculate by the FE-code extracting the creep rate from the subroutine:

$$\epsilon_{cr,n} = \dot{\epsilon}_{cr,n} \times dt_n \quad (5.1)$$

where dt_n is the duration of the increment in seconds, $\dot{\epsilon}_{cr,n}$ the equivalent creep rate, and $\epsilon_{cr,n}$ the computed equivalent creep strain ¹.

As the equivalent stress is depending on creep strain and reciprocally, an iterative computation is performed until the stabilization of the strain and the stress. This step is already integrated in the FE-kern. For this step the subroutine has to deliver the derivation of the creep strain from the equivalent stress.

$$\frac{d\dot{\epsilon}_{cr}}{d\sigma_v} \quad (5.2)$$

and also the derivation of the creep strain from the equivalent creep strain

$$\frac{d\dot{\epsilon}_{cr}}{d\epsilon} \quad (5.3)$$

ANSYS employs the "Newton-Raphson" approach to solve nonlinear problems. This algorithm uses this two terms for convergence. [102]

5.1.3 from an equivalent stress and strain to a stress and strain tensor

As shown in the precedent subsection (see 5.1.2) the creep routine is able to estimate for each increment the equivalent creep strain. This is an uniaxial approach. The kern of Ansys is also capable to generate stress and strain tensors. This section will show how Ansys computes this stress and strain tensor using a subroutine. We assume for a 3D state

¹the model and the correlated implementation is only able to describe and isotropic creep strain

using the notations developed in the section 2.1.2 that the small strains can be decompose so:

$$\varepsilon_{ij}^{tot}(t) = \varepsilon_{ij}^{el}(t) + \varepsilon_{ij}^{pl}(t) + \varepsilon_{ij}^{th}(t) + \varepsilon_{ij}^{cr}(t) \quad (5.4)$$

where the total strain depending on the time evolution $\varepsilon_{ij}^{tot}(t)$ is composed by an elastic strain tensor $\varepsilon_{ij}^{el}(t)$, a plastic rate independent strain tensor $\varepsilon_{ij}^{pl}(t)$, a thermal strain tensor $\varepsilon_{ij}^{th}(t)$, and creep strain tensor $\varepsilon_{ij}^{cr}(t)$. For the solder joint with our model the rate independent plasticity is neglected because already included in the creep law. The thermal and elastic strain are computed using the equation developed in section 2.2. It was already shown in the Chapter 4, that the creep was only tested in a uniaxial direction. However The FE-code is capable to compute a multiaxial creep strain using the method that will be presented. It will be shown, how the creep routine is capable to calculate the creep strain, (a scalar) and to translate it as a strain tensor, to describe the 3D state. The equation that was developed to describe the creep gives the shear creep strain as a function of the shear stress in a multiaxial state. Since the von Mises stress is used in the routine, the constitutive equation has to be written in an equivalent tensile strain and strain relationship. It is possible using the convention of Von Mises. Shear strain γ_{cr} and shear stress τ are converted to tensile quantities by:

$$\sigma = \tau\sqrt{3} \quad (5.5)$$

$$\varepsilon = \frac{1}{\sqrt{3}}\gamma \quad (5.6)$$

For the increment n, the routine calculates first the equivalent stress as scalar, from the equivalent total strain, the thermal strain calculated during this increment, and the creep strain calculated during the last increment:

$$\sigma_{eq,n} = E(\varepsilon_{tot,eq,n} - \varepsilon_{th,eq,n} - \varepsilon_{cr,eq,n-1}) \quad (5.7)$$

The *Fortran* Subroutine calculates now the equivalent creep strain for the increment n by:

$$\Delta\varepsilon_{cr,eq,n} = \int_{t_n}^{n+1} \dot{\varepsilon}_{cr,eq,n} dt = \dot{\varepsilon}_{cr,eq,n} \Delta t_n \quad (5.8)$$

with the scalar which is the creep strain that has to be defined by the programmer in the subroutine:

$$\dot{\varepsilon}_{cr,eq,n} = f(\sigma_{eq,n}, T, t) \quad (5.9)$$

The variable $\sigma_{eq,n}$, the temperature T and the time t are called from the solver into the subroutine. After calculating the creep strain, and its derivative with respect to stress and its derivative with respect to strain. Since the solder joints are considered as isotropic materials, it flows in the direction of the stress deviator. The creep strain increment in three dimensions is obtained by:

$$\Delta\varepsilon_{ij,n}^{cr} = \frac{3}{2} \frac{\varepsilon_{cr,eq,n}}{\sigma_{eq,n}} s_{ij,n} \quad (5.10)$$

Where $\sigma_{eq,n}$ is the von Mises stress and $s_{ij,n}$ is the stress deviator. This routine will be run for each integration point and for each increment of the calculation.

Finally the sum over the individual increments gives the accumulated creep strain, which is used for the lifetime prediction:

$$\varepsilon_{cr,acc,n} = \sum_{k=0}^n |\Delta\varepsilon_{cr,eq,k}| \quad (5.11)$$

In the *Fortran* subroutine, the programmer has to define the creep strain rate over the time as a function of the temperature and the equivalent stress. It will be shown in the next paragraph, that we don't use the absolute time in the definition of the creep strain rate.

5.2 New algorithm

The constitutive equation for primary creep that was developed for solder alloy was:

$$\varepsilon_{pr} = \varepsilon_{sat} \left[1 - \exp \left(-K \left(t * \frac{d\varepsilon_s}{dt} \right) \right)^n \right] \quad (5.12)$$

where K, n are constants, t is the absolute time and the saturated primary creep is :

$$\varepsilon_{sat} = \left(a * \frac{d\varepsilon_s}{dt} \right)^b \quad (5.13)$$

a and b are constants and $\frac{d\varepsilon_s}{dt}$ is a function of the von Mises stress and temperature and does not depend on the time. Those constitutive equations are only developed on the basis of experiments performed at constant stress and temperature levels. The delivered equations are also not able to describe the behavior of solder joints in case of change of loading direction. In this section the algorithm describing the creep rate in case of change of stress level such as an algorithm detecting the change of stress direction will be presented.

5.2.1 stepwise creep test and implementation in the subroutine

This paragraph does not deal with the implementation of the secondary creep rate, because it is not dependant on time, but only on stress level and temperature. It will be demonstrated here that the primary creep rate is not only dependant on time, stress and temperature but depends also on the creep strain. The problem is that the constitutive equations were written for a constant stress level. The thermo-mechanical simulation is a continuous process, which means that the system does not work at a constant stress level, as during our experiments. In fact, the FE-code is working step by step, increment by increment, and a new stress level is calculated for each increment. The figure 5.1 shows how the FE-code calculates the creep strain in case of change of stress level. In case of stepwise simulation, under different stress σ_1 , σ_2 and σ_3 , the 3 corresponding creep curve

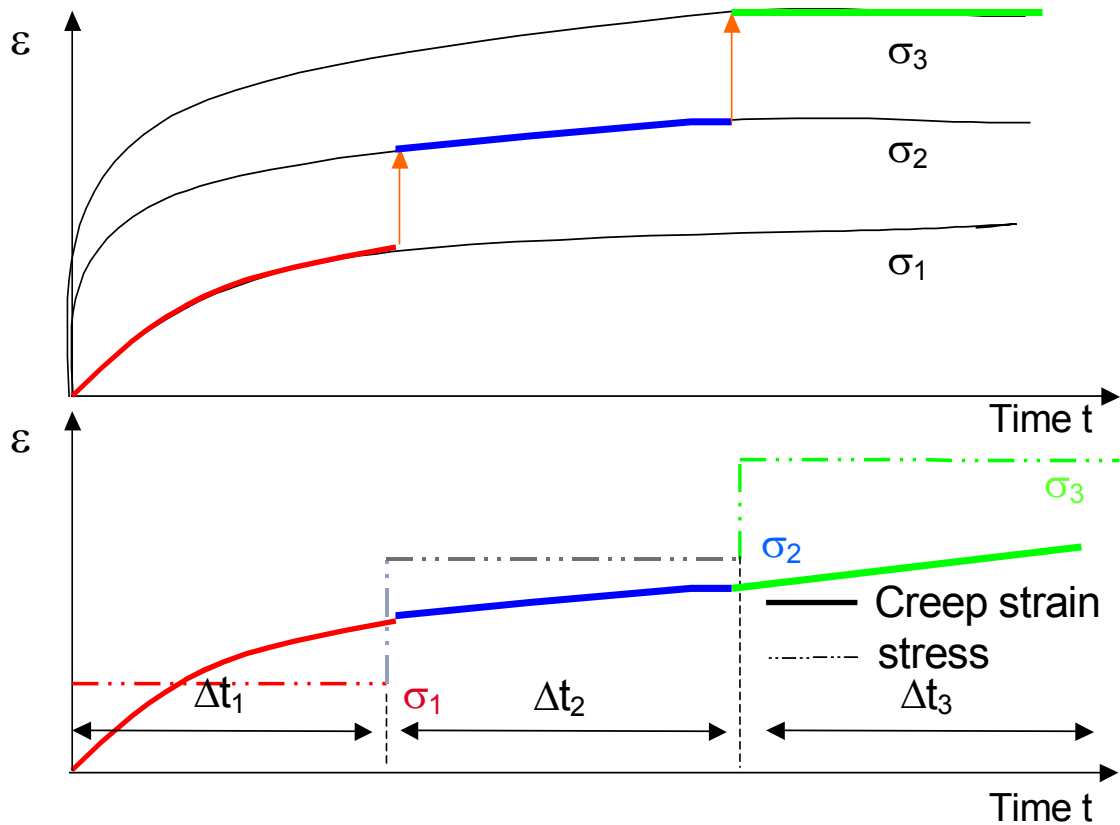


Figure 5.1. *standard implementation of primary creep using the absolute time. Only primary creep is represented*

pieces (red, blue and green) will be used to calculate the creep strain. Since the subroutine uses the absolute time to calculate the creep strain by change of the stress level k to $k+1$, it will spring vertically from a curve k to the curve $k+1$ (orange arrow). This model takes into account the primary creep only at the beginning of the simulation. It will be shown above that is not the reality. Using of the absolute time, the primary creep will not be taken into account in case of change of the stress direction and level. The experimental data showed that primary creep in such cases reoccurs.

New experiments were performed. There were creep tests with a stepwise load. The loads 5 MPa, 10 MPa, 15 MPa and 20 MPa were successively applied in a step loading with the shear test specimen. The results of the experiments are reported in figure 5.2.

In case of change of the stress level, primary creep reoccurs. It is sensibly logical: For each stress level corresponds a saturated primary creep. The saturated primary creep is the maximal primary creep obtainable at the stress level. In case of increasing of this stress level, the saturated primary creep also increases. In the presented results, for the stress level σ_1 the creep curve show a primary part $\varepsilon_{pr,1}$ and a secondary part. By a spring to the stress σ_2 , the strain springs also because of the elastic deformation of the solder joints. The

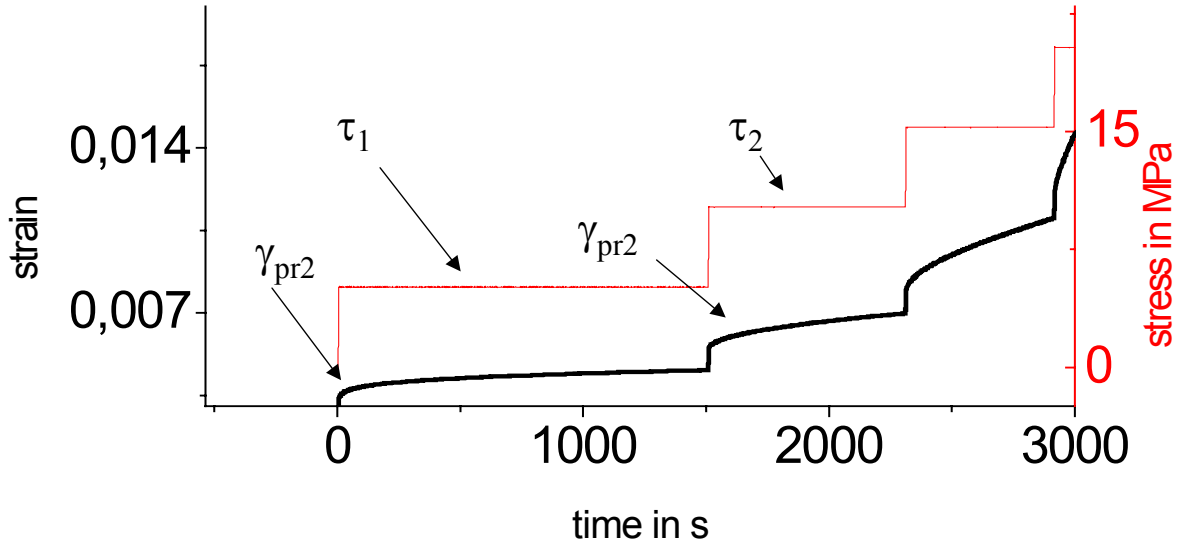


Figure 5.2. Stepwise load and strain for SnPb solder alloy as a function of time, experimental data.

primary creep reoccurs $\varepsilon_{pr,2}$ till the secondary creep. The sum of $\varepsilon_{pr,1}$ and $\varepsilon_{pr,2}$ depends on the saturated primary creep $\varepsilon_{sat,2}$:

$$\varepsilon_{sat,2} = \varepsilon_{pr,1} + \varepsilon_{pr,2} \quad (5.14)$$

If $\sigma_{n+1} > \sigma_n$ then $\varepsilon_{sat,n+1} > \varepsilon_{sat,n}$ and primary creep reoccurs.

To understand what happens, the creep curves at different stress levels are represented above (see figure 5.3).

The figure 5.3 describes how the FE-program must compute the creep strain. In contrary to figure 5.1 the FE-program springs horizontally from a creep curve to the other by increasing of the stress. In this case the creep strain is dependant on temperature, stress, time and hitherto primary creep (accumulated) strain. Since this hitherto primary creep is not defined as variable in the constitutive equations, a the concept of pseudo time t'_k is introduced.

This pseudo-time is calculated for each increment. It is necessary to know the hitherto primary creep. For that a state variable is also defined. This variable is the accumulated primary creep and is defined by:

$$\varepsilon_{pr,acc,n} = \sum_{k=1}^n \Delta\varepsilon_{pr,k} \quad (5.15)$$

where $\Delta\varepsilon_{pr,k}$ is also an introduced state variable and represents the computed primary strain for the increment k. The accumulated primary creep strain has 2 functions in the

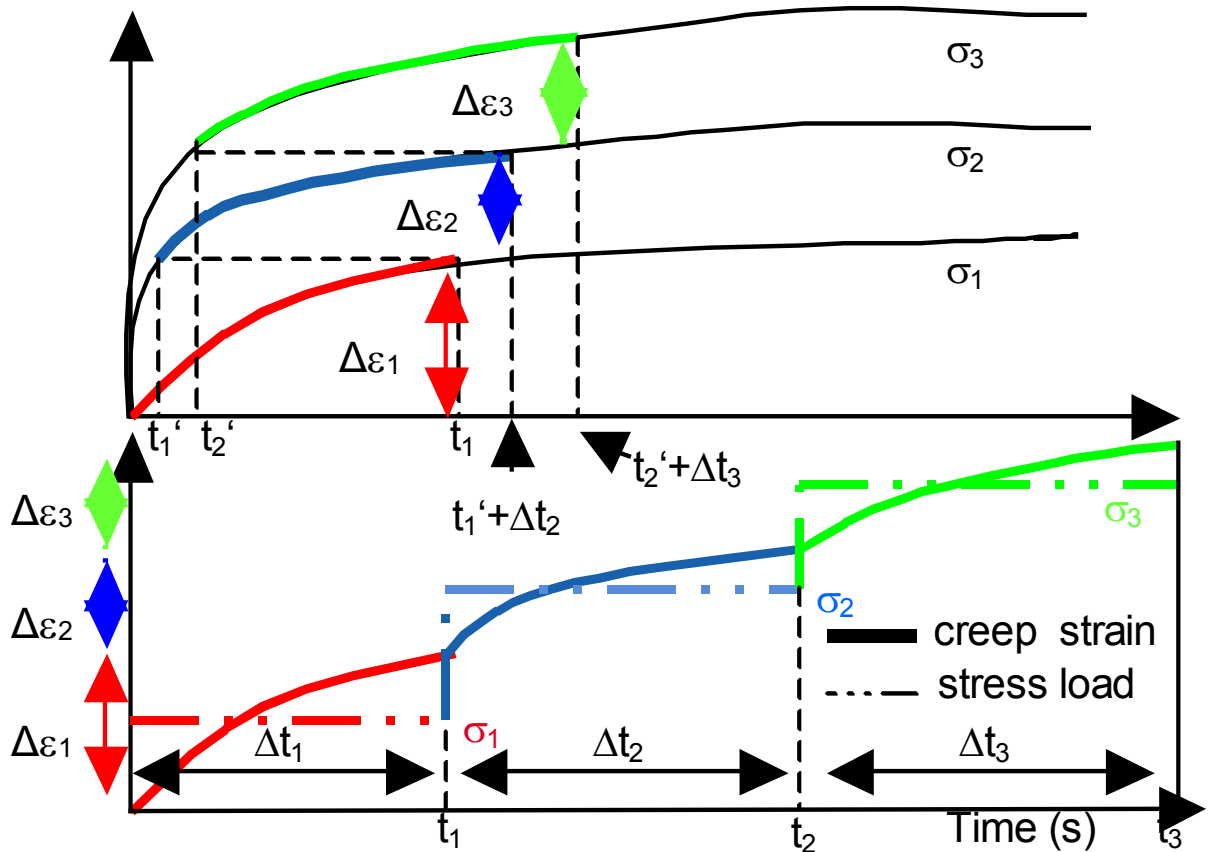


Figure 5.3. Representation of the creep behavior under stepwise load. Above, we see how to switch from one creep curve to another, below, the stepwise load and the corresponding creep curve in an absolute time scale

subroutine. The first is to determine if primary creep occurs, and the second to calculate the pseudo time t_n at increment n . 2 cases are differentiated:

- if at increment n $\varepsilon_{sat,n} < \varepsilon_{pr,acc,n-1}$ then no primary creep occurs ². In this case the subroutine only computed the steady-state creep rate which does not depend on the time.
- if at increment n $\varepsilon_{sat,n} > \varepsilon_{pr,acc,n-1}$ then primary creep occurs and the equation 5.12 has to be calculated.

It is necessary in this case to calculate the pseudo time corresponding to the $\varepsilon_{pr,acc,n-1}$. The equation 5.12 uses the time as parameter. To calculate the corresponding pseudo-time t'_n for the increment n , the equation 5.12 has to be inverted:

$$t'_n = \frac{\ln \left(1 - \frac{\varepsilon_{pr,acc,n-1}}{\left(a * \frac{d\varepsilon_s}{dt} \right)^b} \right)^{1/n}}{-K * \frac{d\varepsilon_s}{dt}} \quad (5.16)$$

² $\varepsilon_{sat,n}$ is calculated from the von mises stress and the temperatur. See Chapter III

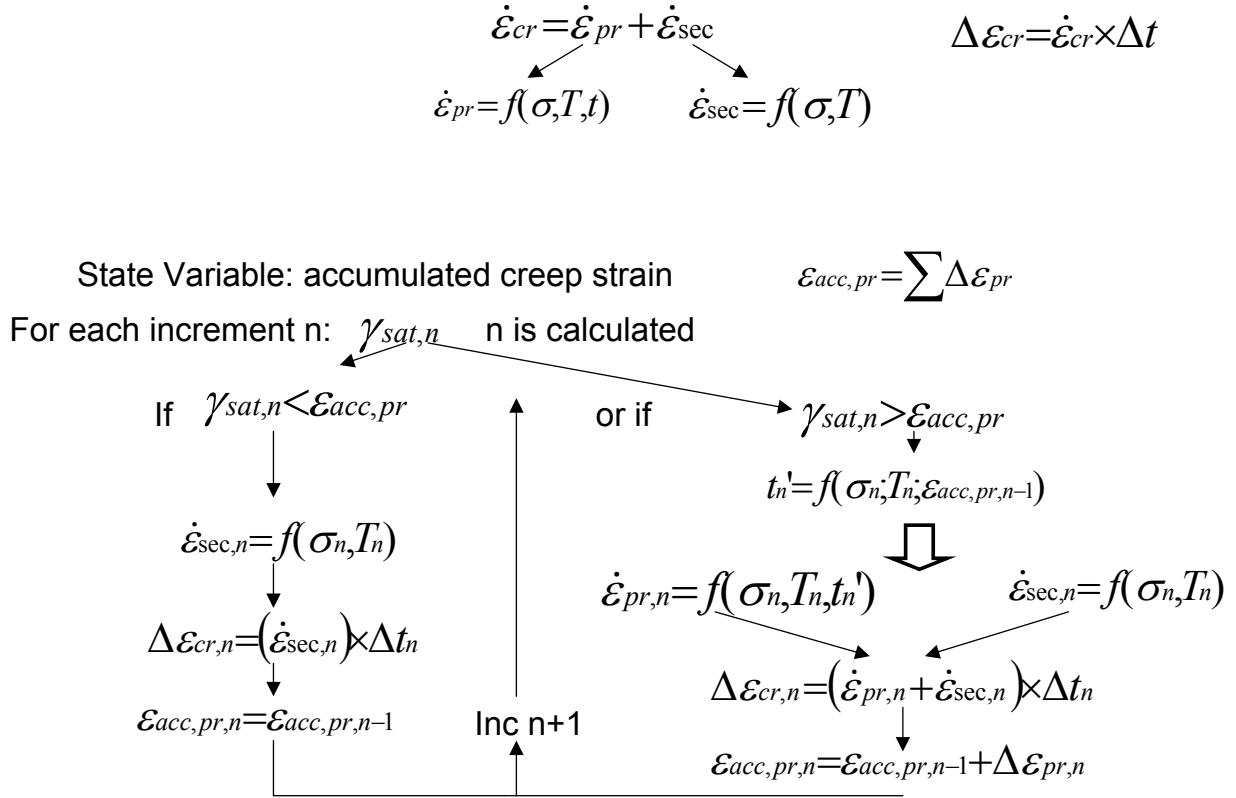


Figure 5.4. algorithm of the computation of creep strain in case of stepwise load

with $\frac{d\epsilon_s}{dt} = f(\sigma_{eq, n}, T_n)$ (see equation 5.12). The primary creep strain can be calculated with the pseudo time using the equation 5.12:

$$\epsilon_{pr} = \epsilon_{sat} \left[1 - \exp \left(-K \left((t'_n + \Delta t_n) \times \frac{d\epsilon_s}{dt} \right) \right)^n \right] \quad (5.17)$$

Where Δt_n is the duration or time of the increment. The increment of the primary creep is obtained by:

$$\Delta \epsilon_{pr, n} = \epsilon_{pr, n} - \epsilon_{pr, acc, n-1} \quad (5.18)$$

With the primary creep strain and the steady-state creep rate, the increment of the creep strain can be computed as follow:

$$\Delta \epsilon_{cr, n} = \Delta \epsilon_{pr, n} + \dot{\epsilon}_{sec, n} \times \Delta t_n \quad (5.19)$$

At the end of the subroutine the state variable accumulated primary creep strain has to be actualized, so:

$$\epsilon_{pr, acc, n} = \epsilon_{pr, acc, n-1} + \Delta \epsilon_{pr, n} \quad (5.20)$$

In case of detection of change of the stress direction at the beginning of the increment, the state variable, accumulated primary creep is reinitialised:

$$\varepsilon_{pr,acc,n} = 0 \quad (5.21)$$

The algorithm is summarized in figure 5.4. The difficulty of this routine is to calculate the derivation of the creep rate from the von Mises Stress $\frac{d\dot{\varepsilon}_{cr,n}}{d\sigma_{eq,n}}$ for the newton Raphson convergence algorithm. Indeed, the pseudo time depends on the von Mises stress. The other value necessitated for the convergence algorithm is the derivation of the creep rate from the creep strain. In our case:

$$\frac{d\dot{\varepsilon}_{cr,n}}{d\varepsilon_{cr,n}} = 0 \quad (5.22)$$

5.2.2 detection of the change of stress direction

The experimental data show that in the case of change of stress direction of the stress, the primary creep reoccurs and the accumulated primary creep has to be reinizialised:

$$\varepsilon_{pr,acc,n} = 0 \quad (5.23)$$

To restart the subroutine in case of change of direction, for example from a positive shearing to a negative one, a special algorithm was developed. The goal of this algorithm is to detect the change of stress direction in a 3D environment. The algorithm which was found is based on the comparison between the hitherto deformation $\underline{\underline{B}}$ and the incremental deformation $\underline{\underline{I}}$ ³. Since the deformation $\underline{\underline{B}}$ and the incremental deformation $\underline{\underline{I}}$ are deviator and since an angle can not be defined between two deviators, a method are developed to detect, if this two deviators are in the same direction. If yes, no change of direction are detected, if no the detection of direction is detected and accumulated primary creep reinitialised. The following steps are used:

1) the predominant direction of the hitherto deformation has to be known. As predominant direction, we mean the eigenvector corresponding to the biggest measurable eigenvalues of $\underline{\underline{B}}$. Since $\underline{\underline{B}}$ is a deviator, this vector is unique⁴. This vector will be called \vec{R}_1 .

2) It will be defined which deformation occurs in the direction of \vec{R}_1 . For this step, the incremental deformation $\underline{\underline{I}}$ must be decomposed into two parts:

- the intending deformation due to an extern force loading
- the other forced deformation, which is necessary for the conservation of the volume in case of inelastic deformation.

³The algorithm needs intern three strain tensors: The strain tensor $\underline{\underline{T}}_1$, which describes the position of the last cycle. The tensor $\underline{\underline{T}}_2$, which describes the hitherto deformation, and the tensor $\underline{\underline{T}}_3$ describes the current deformation. So: - $\underline{\underline{B}}$ is the hitherto deformation relative to the last cycle deformation: $\underline{\underline{B}} = \underline{\underline{T}}_2 - \underline{\underline{T}}_1$
- the incremental deformation is $\underline{\underline{I}} = \underline{\underline{T}}_3 - \underline{\underline{T}}_2$

⁴for the deviators, the sum of the three eigenvalues e_1 , e_2 and e_3 is 0. So the biggest calculable eigenvalues are unique (except for $e_1 = e_2 = e_3$). For this reason the corresponding eigenvector is also unique. The case $e_1 = e_2 = e_3$ occurs only when there is no deformation. In this case there is also no change of direction.

Mathematically the forced deformation is described by $\underline{\underline{1}} \cdot e_2(\underline{\underline{I}})$, where $e_2(\underline{\underline{I}})$ is the second eigenvalue of the deviator $\underline{\underline{I}}$.

Hereby the intending deformation could be described through the tensor $\underline{\underline{A}}$ as follow:

$$\underline{\underline{A}} = \underline{\underline{I}} - 1 \cdot e_2(\underline{\underline{I}}) \quad (5.24)$$

3) the distortion (or deformation) of the vector \vec{R}_1 through the intending incremental deformation is calculated by the following matrix product:

$$\vec{R}_2 = \underline{\underline{A}} \cdot \vec{R}_1 \quad (5.25)$$

4) An angle can be calculated between the two vectors \vec{R}_1 and \vec{R}_2 , calculating the scalar product.

5) The calculated angle can be compared with a defined value. In our case, when this angle was superior to 135° , the change of direction is detected. In fact a value of 90° is the real value between the two directions fields, but was not selected as the frontier, because in such cases numerical problems are occurring (instabilities of the routine).

In this description of the algorithm, the protection and the routine to improve the numerical stability were not described. For example the detection of the change of the stress direction is not possible, if no deformation occurs, and so the incremental deformation tensor $\underline{\underline{I}}$ equal to the tensor null.

An other algorithm is written to avoid the instability: only one detection is possible by half temperature cycle.

An other problem was that in the Ansys subroutine *usercreep.f* the strain and stress are only described by scalars (Von Mises stress and equivalent strain). Of course it is not possible to define a direction or a change of the direction. Through a status function it is possible to call the strain tensor of the last load case. Extra subroutines were used to calculated the eigenvalues and eigenvectors (see [105]).

5.3 verification of the subroutine

5.3.1 verification of the algorithm

To verify the algorithm a lot of test files were written. The following load cases were tested:

- tension at different stress level and temperatures (verification of the computation of the creep rate)
- tensile and compression load (detection of change of direction)
- positive and negative shear load (detection of the change of direction)
- tension with positive shear load and compression with negative shear load (detection of the change of direction).
- stepwise load and unload (shear and tension/compression)

- simulation of the real electronic packagings like flip-chips, chip on board and PBGA. The goal of this simulations were to verify the stability of the subroutines, and if the detection of the change of stress direction is coherent.⁵

5.3.2 comparison between analytical and FE-calculation

The shear test as it was described in chapter IV was simulated (FE-analysis) and also analytically calculated for both alloys and at different temperatures and stress levels. The objective was not to verify the creep constitutive equation, but only to verify that the same results were found from the simulative side or from the analytical side. In all case there was a good correlation between the FE-results and the analytical results. Here the different relevant results for SnPb solder alloy are presented. A shear test at 10 MPa

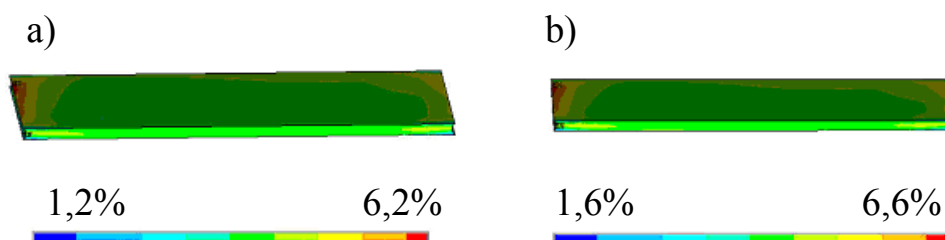


Figure 5.5. accumulated creep strain of solder joint. Only half of the model was calculated using the symmetry conditions. a) only sec. creep is taken care of b) both prim. and sec. creep are taken care of.

at room temperature, during 3600 seconds were calculated. Two cases were simulated: one taking care of the secondary creep, and the other taking care of both primary and secondary creep. In both cases the stress distribution were identical. However as expected, the accumulated creep strain was higher simulating the primary creep and secondary creep. The results are summarized in table 5.1.

| | Prim+sec. | Sec. Only |
|-------------|-----------|-----------|
| FEM results | 4,71% | 4,36% |
| analytic | 4,69% | 4,33% |

Table 5.1: comparison between the FE-results and the analytical solution

The small discrepancy between simulated and theoretical values is attributed to small numerical rounding errors and remaining torque in the model, not accounted for the simulation.

⁵during those tests, it was observed that the change of stress directions occurs from one to 3 increments after the change of the temperature (decreasing or increasing). For the calculation of temperature cycles, it is also possible to use the temperature as parameter for the detection of change of stress direction, because this two phenomenons are dependant. During the work, a routine using the temperature as criterium was also developed and tested. For the electronics packages that were simulated, the results were comparable to the results given by the other subroutine (1 or 2% for the accumulated creep strain).

Another important point revealed by this simulation is that the stress distribution in solder joints were homogenous. It verified the hypothesis formulated in Chapter III (Indeed, the calculation of the stress in solder joint were performed using a constitutive creep equations which did not take care about primary creep). The stress distribution is presented in figure 5.5

5.3.3 verification through a tensile test

In the two precedent sections, it was verified that the algorithm functioned correctly. Here a test that was capable to verify the accuracy of the model and the algorithm was imagined. Indeed the creep test was performed in shear and stress controlled. What is happening under other load conditions? Another creep test using IZM test conditions was performed. It was a tensile test (no compression) using Dog bone test sample and strain controlled. Those creep test were performed at room temperature and at 150°C for both alloys. A good correlation were found between the experimental curve and the simulated curves only when the primary creep was also taken care of. The figure 5.6 shows the results of this work at room temperature for a strain rate of $1,2 \cdot 10^{-5} s^{-1}$.

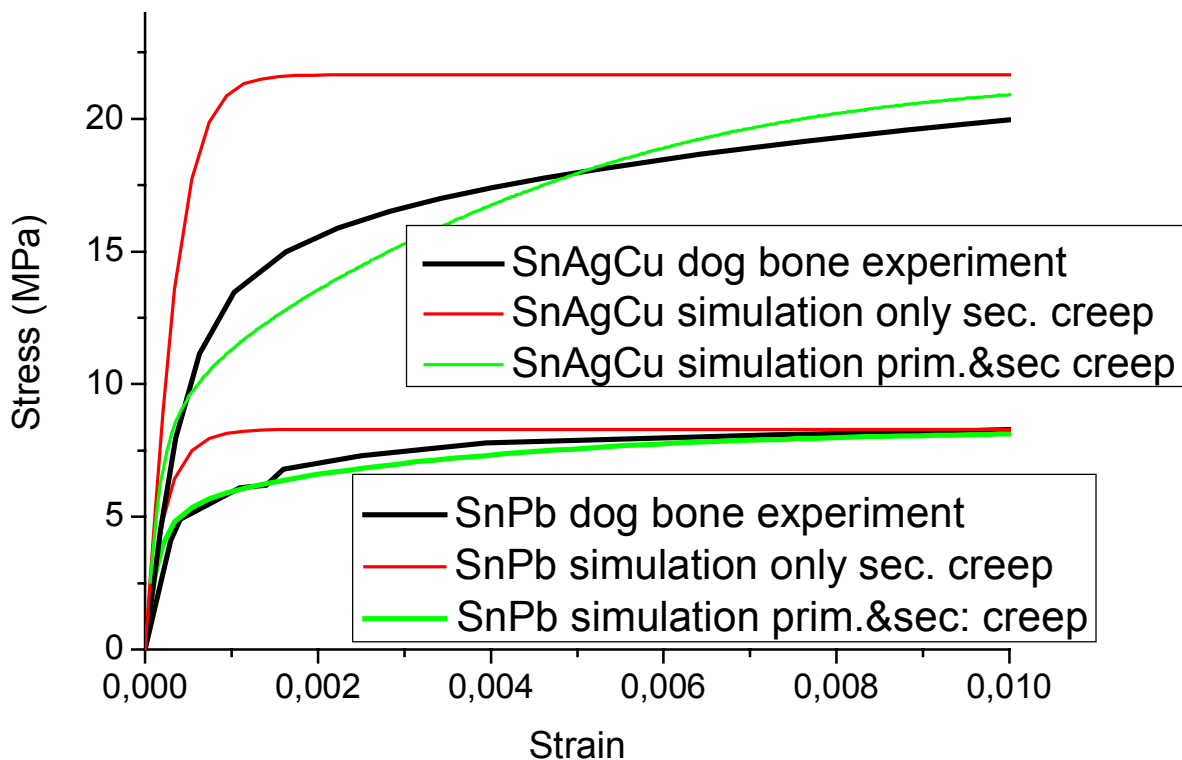


Figure 5.6. creep curve of SnPb and SnAgCu at room temperature under constant strain rate. the creep curve was also simulated with and without primary creep

Three conclusions are deduced from the analysis of this curve:

- the calculated creep curves with primary creep are more realistic in comparison to the experimental curves.
- The constitutive equation developed for shear load can also be used for tensile load case, and also for multiaxial load. That means that the hypothesis formulated by Von Mises and used to convert the shear into tensile stress by a factor $\sqrt{3}$ is good for solder alloys, i.e the alloy creeps isotropous
- creep test can be developed from a stress controlled tests and are capable to describe a strain controlled test.

It can be also expected that the creep law can describe a multiaxial temperature controlled load condition like a temperature cycle.

5.4 influence of the primary creep

It will be shown in this section the results difference resulting from primary creep. Two cases are always calculated:

- only the steady state creep or secondary creep are modeled.
- both primary and secondary creep are modeled.

5.4.1 shear test

The simulation described in section 5.3.2 (shear test at constant temperature) were also performed for 2 new different cases. In case I a shear stress of 1 MPa at 125 °C was used. In case II a shear stress of 40 MPa at -40 °C was used. This two cases can occur during temperature cycles. Indeed, a high temperature, the creep rate is high and the relaxation occurs rapidly so that the stress level decreases, in the contrary, the relaxation at -40 °C is neglected and the stress level is high. for both cases, the simulation duration was 1000 seconds, closed to the holding time of a temperature cycle. The results are reported in table 5.2

| case | Prim+sec. | Sec. Only |
|------|-----------|-----------|
| I | 1,26% | 1,84% |
| II | 0,22% | 0,45% |

Table 5.2: accumulated creep strain computed for case I and II

The portion of primary creep on the total of creep is 32% and 52% in case I and II respectively. So, depending on the loading case, for isothermal creep experiments, the primary creep can be a relevant part of the total creep value.

5.4.2 flip-chips

A thermo-mechanical simulation of different thermal cycles was performed for a flip chip package. The flip-chip used and its referred model was developed by Wunderle (for more

information about the model, the accumulated creep measurement, etc... see [68]). All simulations were performed with and without primary creep. the different cases were:

- Case 1: flip chip Bump with underfill (SnAgCu solder joint)
- Case 2: flip chip bump with underfill (SnPb solder joint)
- case 3: flip chip bump without underfill (SnAgCu).

The results of case 2 are presented in figure 5.7.

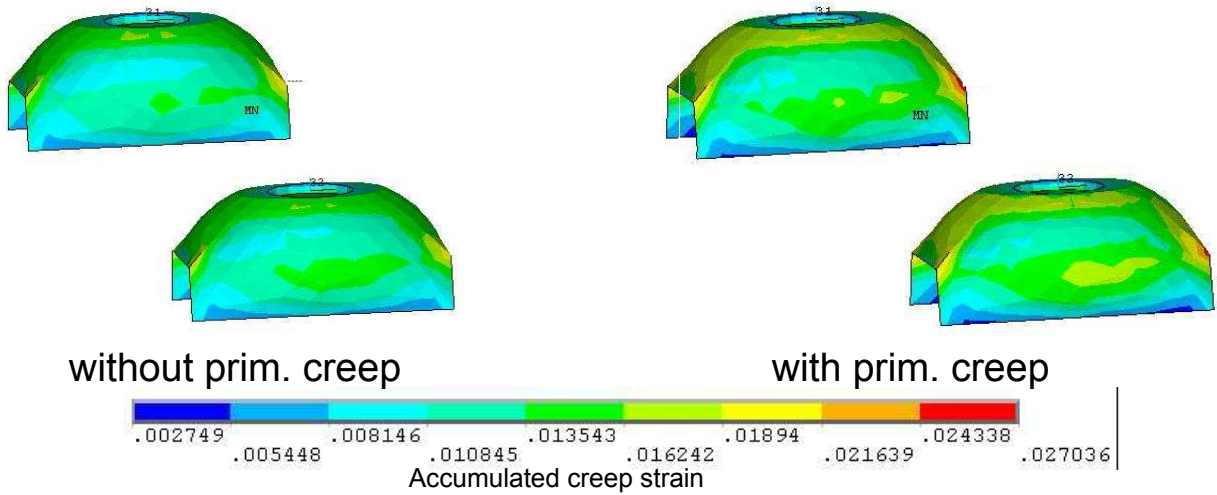


Figure 5.7. Flip-Chip with Underfill, Temperature cycle: $-40^{\circ}\text{C}/+85^{\circ}\text{C}$ holding time 25 min, Ramp 5 min. The accumulated creep strain of two bumps are presented. the accumulated creep strain repartition is not the same taking into account of the primary creep or not

| case | $T_{min}^{\circ}\text{C}$ | $T_{max}^{\circ}\text{C}$ | hold time (min) | with prim. creep | without prim. creep | Difference |
|------|---------------------------|---------------------------|-----------------|------------------|---------------------|------------|
| 1 | -40 | 125 | 25 | 2.67% | 2.87% | 8% |
| 1 | -40 | 85 | 25 | 1.85% | 2.29% | 24% |
| 2 | -40 | 125 | 25 | 1.40% | 1.46% | 4% |
| 2 | -40 | 85 | 25 | 1.06% | 1.21% | 14% |
| 3 | -40 | 85 | 25 | 3.89% | 3.92% | <1% |

Table 5.3: accumulated creep strain computed for different temperature cycles simulations.

A difference up to 24% in these calculation was found for the lead free alloy which is relevant for lifetime prediction. When the device is calculated without underfill or with a large temperature difference, the influence of primary creep decreases, which is logical: Indeed, in such cases the creep strain and the stress tends to be bigger, and the primary creep time is becoming less relevant in comparison to secondary creep.

5.4.3 PBGA

An another package was simulated with and without primary creep. This package is called Plastic Ball Grid Array (PBGA). The balls which are the critical positions of such packages ensure the mechanical and the electrical connection between the interposer and the PCB. Since those two entities have the same CTE, the balls are not extremely loaded like the flip chip bumps, and the accumulated creep strain is lower, for those reasons. It is expected that the primary creep has a bigger influence. For the elastic and viscoelastic behavior modeling, the models which are at IZM available for the glue (between the chip and the interposer), the FR4, the mold mass, and the Si were used. The model is represented in figure 5.8.

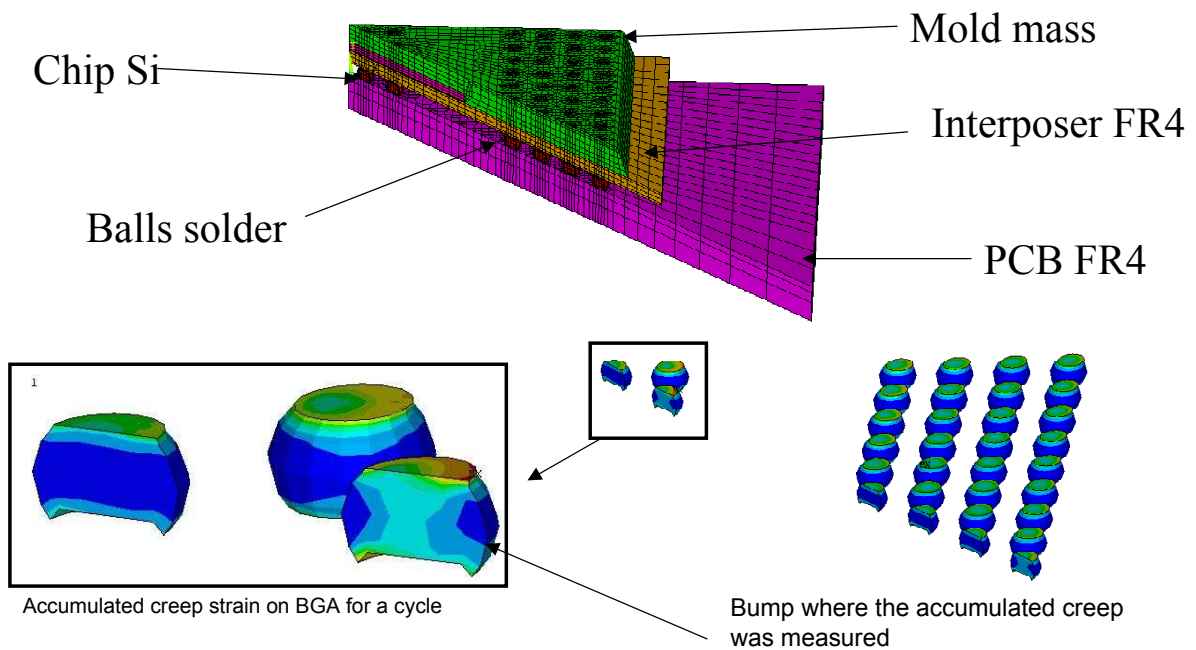


Figure 5.8. PBGA FE-model and results. The accumulated creep strain is represented.

The mean accumulated creep strain was measured through 12 elements at the top of the bump. This value is used to estimate the lifetime using a Coffin-Manson law (see equation 2.62). The mean accumulated creep strain are summarized in table 5.4.

| | accumulated creep strain with prim.creep | accumulated creep strain without prim.creep | relative difference |
|--------|---|--|---------------------|
| SnPb | 0,25% | 0,34% | 39% |
| SnAgCu | 0,20% | 0,26% | 32% |

Table 5.4: accumulated creep strain computed for the different solder alloys

The influence of primary creep is here clearly demonstrated for SnPb and SnAgCu. A difference of 39% was observed which is very relevant for lifetime prediction. However, the

quantitative influence on Coffin-Manson parameters was not investigated during this work, but will be presented elsewhere.

5.5 conclusion

After showing the existence of primary creep till the end of life of solder joints under load conditions and at different stress levels and temperatures in chapter III, the relevance of primary creep was demonstrated. Of course, at high stress level, the primary creep disappears so quick, that its influence can be neglected (case of flip chip without underfill) but for pure mechanical loaded solder joint or for thermo-mechanical simulation at low strain rate like PBGA the influence of primary creep can not be neglected. Now new lifetime prediction models have to be developed for this new kind of constitutive laws. In the next Chapter such a model will be presented for the die attaches.

Chapter 6

Lifetime Prediction of Die Attaches

The objective of this chapter is to show how to calculate the crack growth in Die attaches using the standard FE-methods. Speaking about Die attaches means in our case the solder joint of a Silicon Chip soldered on a bare copper board. This Chapter shows how to observe the crack growth in such kind of solder joints under thermal load conditions and how to calculate the damage after a known number of cycles using the equation given in Chapter 2. An another aspect of this Chapter is to present a method to test the thermal behavior of the test devices and to compare these experimental results with the simulation (Indeed it will be demonstrated that the thermal behavior of devices can be strongly influenced by the damage of the solder joint increasing its thermal resistance).

The chips that were studied are power transistors. They were soldered on Copper Substrate (NiAu metallization) with two different solder alloys (SnPb eutectic and SAC 305). The chip dimensions and the solder joint thickness have an influence on lifetime, so that two different chips with two different solder thicknesses were used as test specimens. These were thermally loaded, and the state of the solder joints was regularly checked. Three different kind of methods were used to characterize the damage of solder joints: the Scanning Acoustic Microscope (SAM) detects the crack initiation and growth; the cross section analysis can validate the results of the scanning acoustic microscope and can show the microstructure changes and the thermal resistance which is influenced by the damage of the solder joint was measured and correlated to damage. After presenting the results of these investigations, a general FE-method predicting the crack initiation and growth using the Paris-Erdogan Laws is presented.

6.1 Scanning Acoustic Microscopy (SAM), principe and application

The Scanning Acoustic Microscopy (SAM) [106–108] is a non-destructive method which is capable to investigate the damage, the failure and defects in electronic packages such as interfacial separation, delamination, die attach voiding, cracking etc in solder, at package interfaces. The principle of the SAM (see figure 6.1) consists of sending an ultrasound wave into the material which has to be tested. This method is a pulse echo method, that means,

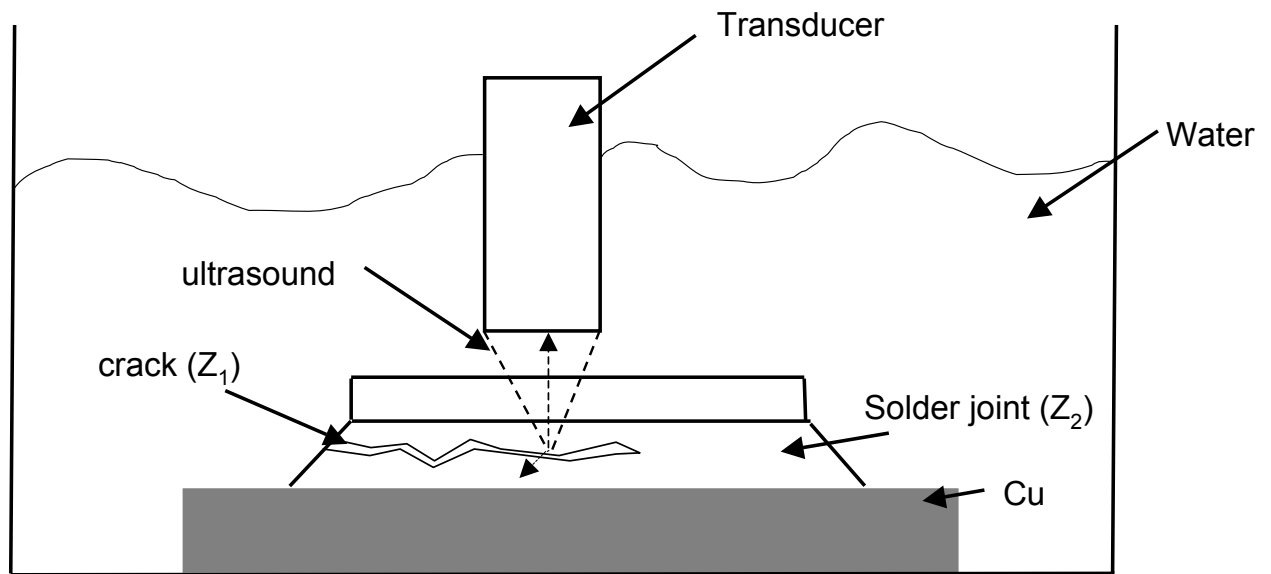


Figure 6.1. *principle of an scanning acoustic microscope*

the reflected wave will be also inspected. The ultrasound wave is generally generated by a transducer, which is composed by a piezoelectric crystal. The pulser will activate the crystal at a determined frequency. This crystal will generate the ultrasonic wave. Since the ultrasonic wave is a mechanical wave (and not electromagnetic) it can not travel through air at frequencies which are used. So a couplant has to be used to transport this wave, in our case it was demineralized water. This wave can travel through the package. The wave is focused from a transducer at the target object. There are at this point 3 possibilities: The wave is absorbed, transmitted or reflected. Typically, the waves are transmitted or reflected in electronic packages. For example if the wave is focused on a die attach, and no defects exist at this place, the wave will be transmitted. If a crack or void occurs, the wave will meet the interface between the solder alloys and the medium which fills the crack (water or air) will not have the same acoustic impedance than the solder alloy. The wave will be scattered or reflected. In case of crack in solder the acoustic impedance of the crack Z_1 (air or water) is really larger than the acoustic impedance of the solder Z_2 . In this case the wave will be reflected. The reflected or transmitted waves are gathered and measured. The reflected wave (echo) will also exited the piezoelectric crystal in the transducer, will generate a voltage, that will be amplified, digitalized and stored by a computer. Since the goal is to investigate a surface or a cross section, the transducer will be moved to scan the cross section. This method is called the B-scan mode. A B-scan is a cross-sectional display showing the ultrasonic reflection along a depth of the package (where the wave is focused). Ultrasound pictures are presented in figure 6.7. The color black corresponds to a transmitted wave and the color white to a reflected wave (voids or crack).

6.2 Test Vehicle

6.2.1 test devices, geometry and soldering

The test devices that were used are power transistors. The first variant is a Power-MOS transistor with a size of $3.6 * 3.9 \text{ mm}^2$. The thickness of the die is $380 \text{ }\mu\text{m}$. The second variant of the test device is a bipolar transistor with a size of $5.6 * 6.4 \text{ mm}^2$ and a thickness of $310 \text{ }\mu\text{m}$. The bottom side of this transistor was metallised with AlSn. Since the thickness of solder joints influences the lifetime of power devices, two different solder joint thicknesses are chosen ($50 \text{ }\mu\text{m}$ and $100 \text{ }\mu\text{m}$). The chips are soldered on bare copper. This substrate has two functions: the first is to be the source (MOS) or collector (bipolar) of the transistor, (this copper substrate could also be soldered on a PCB). The second function is to cool down the device. Its size is $1.6 * 0.9 \text{ mm}^2$, the thickness is 2 mm. The copper used to build the plate is an oxygen free copper (SE-Cu F30 DIN Norm). To solder the chips on the Cu boards it was not so easier as expected. Firstly, the standard method for soldering in SMT (surface mounting technology) was tested. It consists in printed a lot paste on the copper, to place the chip on the applied solder paste and to solder the sample in a reflow oven. It gave very bad results (no reproducibility, voids in the solder joint, very large tilt, bad wettability, and bad meniscus). To improve the wettability and the meniscus geometry, the bare copper is metallised with NiAu. A solder resist was also applied on the NiAu top side of the copper bare, and a rectangular hole was machined. (the size was $5.8 * 6.6 \text{ mm}^2$ for the bipolar transistor and $3.8 * 4.1 \text{ mm}^2$ for the power-MOS device). The solder resist is used to have a reproductive solder joint geometry and meniscus (see figure 6.2).

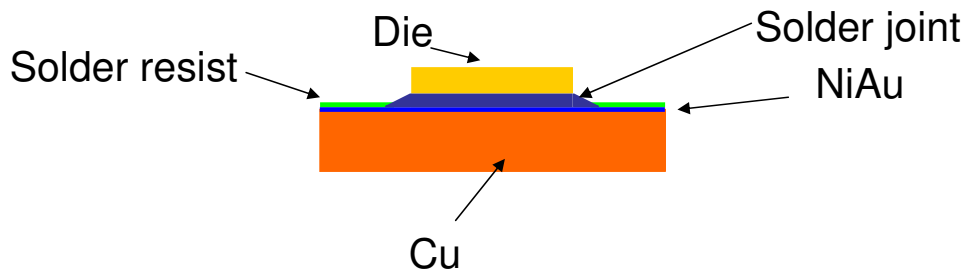


Figure 6.2. *Schematic: Chip on bare copper board.*

To improve reproducibility, preformed solder foils were preferred rather than solder paste. Both sides of these foils were impregnated with a flux. The solder foils are placed on the bare copper and the die is put on the solder foil with a fine-placer machine. Two solder alloys were used: the eutectic SnPb and the SnAgCu (SAC305). The specimens are soldered in a vapour phase oven at a temperature of 260°C for the SnAgCu, and 240°C for the SnPb, and before cooling, the specimens are put into a vacuum, in order to avoid voids in the solder joints. For each soldered test specimen, the tilt of the chip is checked using a laser profilometer. Only the chips with a tilt smaller than 20% of the thickness were selected for the thermal cycling test. The devices are also investigated with X-Rays and SAM to verify that the solder joint is free of voids (figure 6.3).

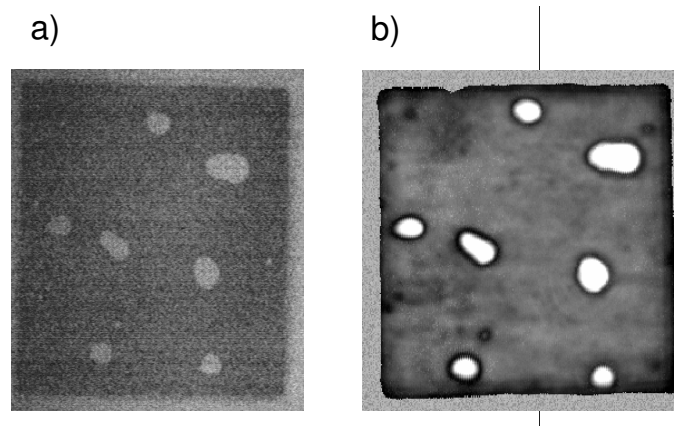


Figure 6.3. *a) an X-ray picture. b) an ultrasonic microscopy picture. In both cases the voids are observable. such devices were not used to build the model*

Figure (6.4) shows these devices.

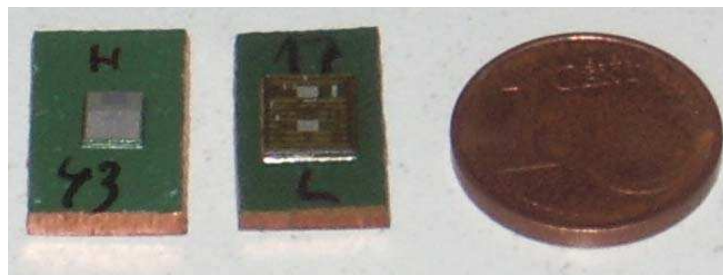


Figure 6.4. *Real chip on bare copper board*

To summarize, we have 2 different chip sizes, with 2 solder alloys and two different solder joints thicknesses, that means eight test device variants.

6.2.2 experimental procedure

For the thermal test, always 30 test specimens from each variant were tested together in order to achieve good statistical results. Two different test conditions were used for thermal cycling:

- for the SnPb and the SAC test specimen, a thermal shock with an upper temperature of 125°C and a lower temperature of -40°C and a holding time of 30 minutes was used. These thermal shocks were performed in a two chambers oven
- only for the SAC test sample a thermal cycling with an upper temperature of 150°C and a lower temperature of -40°C, and a ramp of about 5 K/minute was performed with a one chamber oven. The two cycles are represented in figure 6.5.

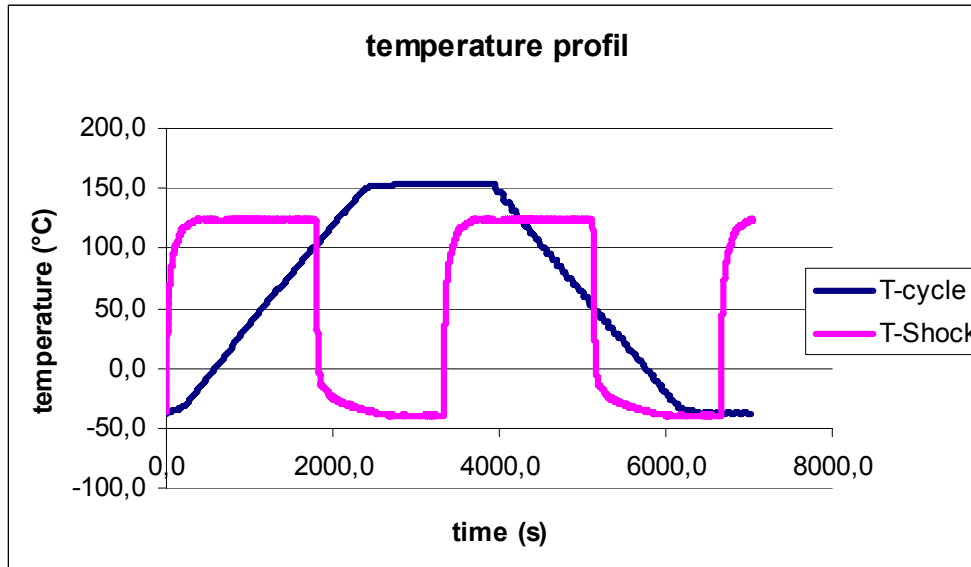


Figure 6.5. *two different temperature cycles. The temperatures were measured at different places of the oven; The maximum deviation was $\pm 2K$ and a mean value was calculated and hereby presented. This mean value was used for the simulation.*

Two different cycles were used to try to find a general model, which would not be dependent to the temperature load.

Depending on the crack growth evolution, the test sample were put out from the oven every 50 to 200 cycles and were checked using the scanning acoustic microscope . The map of reflected waves gives an idea of how impedance changes within our sample. In our case, a transducer with a frequency of 100 Mhz is used to perform the acoustic mapped. The transducer is focused in the solder joint (for more information about the procedure see also section 6.1). To verify that cracks and voids can be detected, some test samples are also prepared for a cross section and a metallography analysis. These cross sections are also used to verify the crack growth (no delamination at the interface of the solder joint with the bare copper or with the Si die (see figure 6.6). It is also possible with the cross section to observe where the crack occurs in the thickness z -direction. The SAM map is only a x - y direction 2D picture. Some examples of SAM maps are presented on figure 6.7. For the SnPb and the SnAgCu test specimens which are investigated, the temperature cycle and the electronic component (bipolar transistor) and the solder joint thickness ($100\mu\text{m}$) are the same. It is clearly demonstrated that the SnPb alloy has a better resistance to crack growth than the SnAgCu alloy.

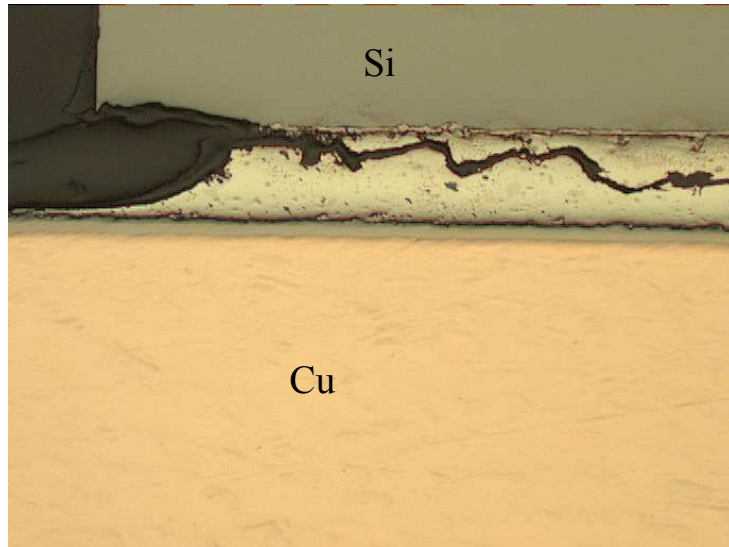


Figure 6.6. cross of a SnAgCu test sample after 300 cycles

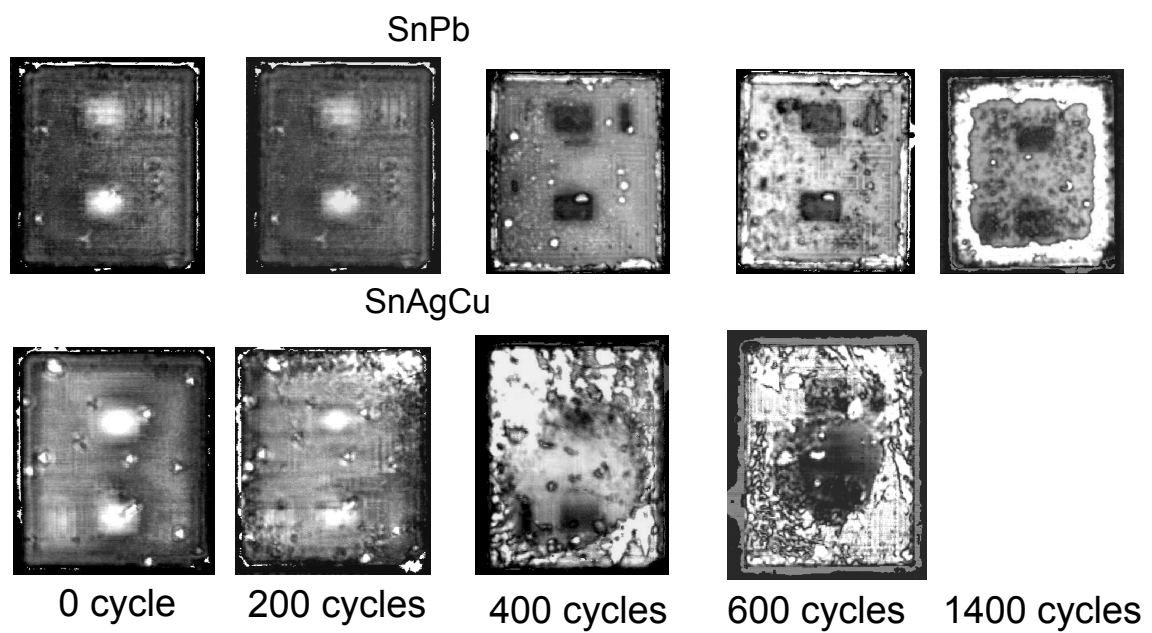


Figure 6.7. ultrasonic pictures at different times of the life of the test device

6.3 Thermal behavior

A reverse diode is often integrated in the MOS structure of power transistors, and so it is in the case of our power device. (See figure 6.8)

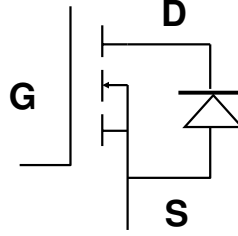


Figure 6.8. MOS Structure of the power MOS transistor: S for Source, D for Drain, G for Gate, the reversal diode is between the source and the drain

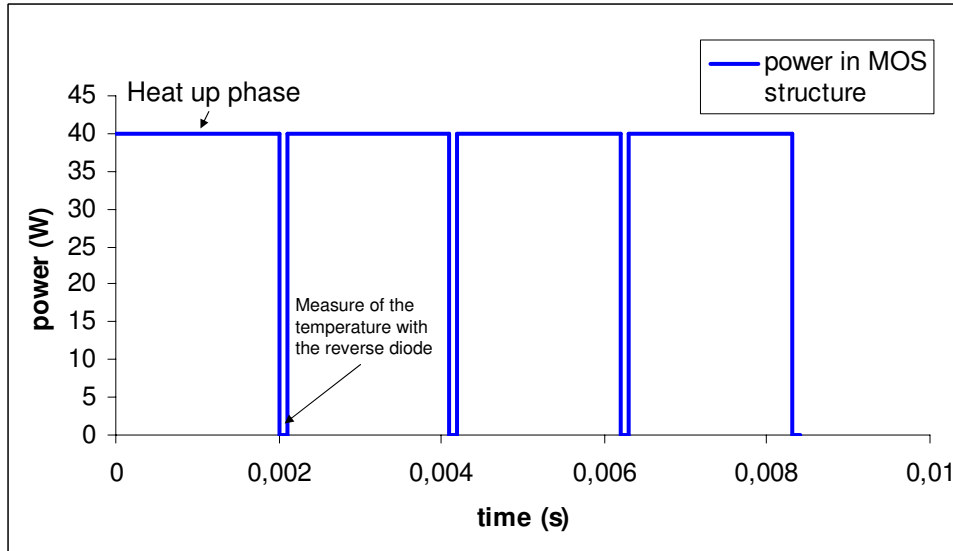


Figure 6.9. alternated power load and temperature measurements determining the thermal resistance of the power-devices

This reverse diode can be used to measure the junction temperature of the power device. Equation 6.1 describes the temperature depending on the physical effect of the forward voltage while having a constant forward current. In our case I_D was equal to 4 mA [109]

$$T \sim U_{F,Diode} = \frac{KT}{e} \ln\left(\frac{I_{F,Diode}}{I_S}\right) \quad (6.1)$$

$$\text{with } I_{F,Diode} = \text{const.} \quad (6.2)$$

where K is the Boltzmann constant ($1.38 \times 10^{-23} \frac{Ws}{K}$), e the elementary charge ($1.6 \times 10^{-9} A.s$), I_F is the forward current, and I_S the reverse saturation current. Using a linear

fit through four measured voltages at six different temperatures between 20°C and 150 °C, a numerical equation can be found to determine the junction temperature (equation 6.3).

$$U_{Diode,F} = A + B \times T \quad (6.3)$$

For each chip the parameters A and B were measured. To have a good precision, the voltage of the chip was measure at a constant intensity (2mA) at six temperatures (Room temperature, 50 °C, 80 °C, 100 °C, 120 °C and 150 °C). The parameters was fitted with the five points of the diode characteristic.

$$A \approx -600mV \text{ and } B \approx -2 \frac{mV}{K} \quad (6.4)$$

In expectation of a crack growth through thermo-mechanical fatigue, the thermal impedance of the solder joint will increase consistently. The thermal impedance can be calculated with the following equation 6.11:

$$Z_{th,jc}(t) = \frac{T_{j,maxC}(t) - T_{Cooler}}{U_{DS} \times I_D} \quad (6.5)$$

To measure the thermal impedance of the device the chip is put on an aluminium cooler. The temperature underneath the device in the cooler (T_{cooler}) is measured by Ni-Cr thermocouple. Therefore holes are drilled into the cooler close under the surface of the power device and the thermo-couple is assembled with heat conduction paste. The used thermo-couple has an accuracy of 0.5K. To heat up the transistor, the MOS structure is used and loaded under constant power (in our case 40 W), but during this phase the reverse diode is blocked. That means that we have to disable regularly the MOS structure to be able to measure the temperature (see figure 6.9). This Z_{th} measurement is done for a power of 40 W for 0.3 seconds. To calculate this thermal resistance, it is only necessary to measure the temperature of the cooler, because this experiment is done at constant power. The results that we will present are the results for 30 devices, before thermal cycling and after 500 cycles (the mean value of the thermal impedance from these 30 values was calculated). The ultrasonic microscopy shows that the equivalent damage surface after 500 thermal cycles represents about 32% of the full surface. The thermal behaviour of the chip is also simulated with Ansys. Using the symmetry condition, only one fourth of the model was built in the FE-Software. The material data that are used for the simulation are reported in table below (table 6.1).

| | density (kg/m^3) | specific heat capacity (J/(K*Kg)) | thermal conductivity (W/(m*K)) |
|--------|-------------------------|--------------------------------------|-----------------------------------|
| Si | 2330 | 710 | 148 |
| Cu | 8960 | 380 | 386 |
| SnAgCu | 7300 | 230 | 77.7 |

Table 6.1: Material datas used for the thermal simulation

Underneath the bare copper, a constant temperature is applied and it was the temperature measured by the thermal couple. The upper side of the chip was loaded with a power surface

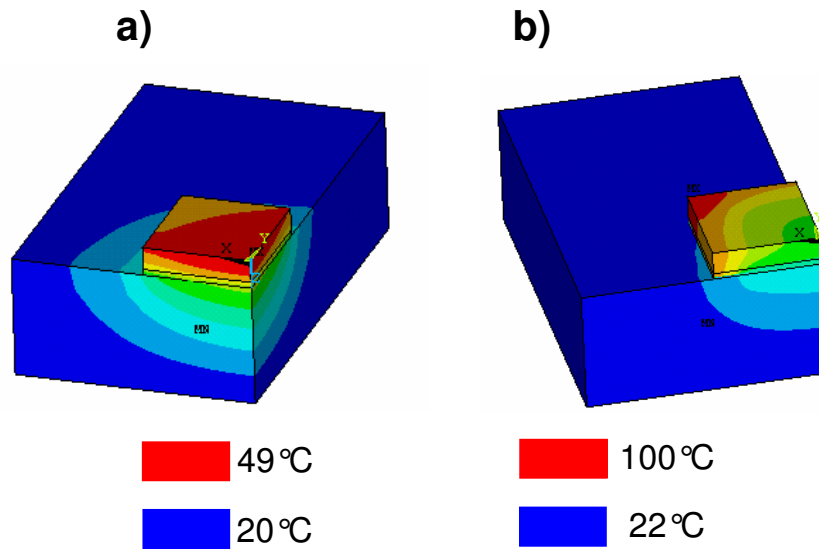


Figure 6.10. *results of the thermal simulation: temperature distribution after 0.3 seconds under 40 watts a) without damage b) with damage*

density in accordance with the experiment (see figure 6.9). To represent the crack in the solder joint, the corresponding elements are killed using the commando *ekill* of Ansys. The figure 6.10 represents the temperature of the device at the end of the electrical load under constant power. The temperature of the chip after thermal cycling is really higher than before thermal cycling. Another influence of the crack in the solder joint is that the temperature has not the same distribution through the Si-chip.

It has already been shown, that it is possible by the voltage of the reversal diode, to determine the maximal temperature of the junction. To calculate the simulative thermal impedance, it is necessary to calculate the maximal temperature of the junction, which does not occur at the same place for each increment of the simulation. The measured thermal impedance and the calculated thermal impedance are represented in next diagram (see figure 6.11).

The first logical observation is that the thermal impedance increases with the increase of the damage of the solder joint. The second observation is that it is possible to simulate the damage (deleting the elements corresponding to the cracks). The difference between the simulation and the experiment could be explained by the error of measurement during the calibration of the reversal diode, the errors during the measurement of the thermal impedance. These experiments show that it is very important to define the degree of damage of such device, because since this damage does not have a big influence on the electrical functions of the device, the damage of the solder joint could be lethal for the chip in case of high power load. The method of measuring the thermal impedance can be a good method to detect the cracks [110].

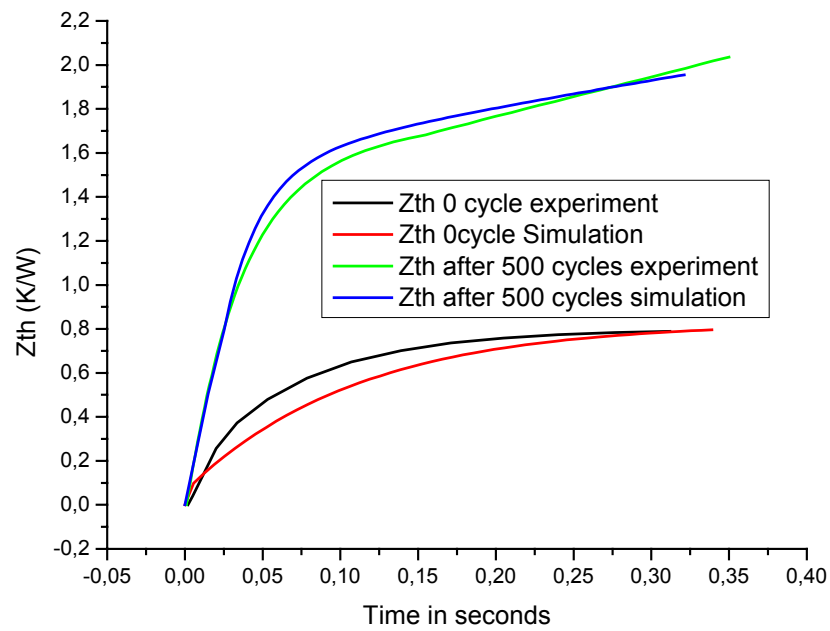


Figure 6.11. comparison between the measure of the thermal impedance and the simulation of this thermal impedance before thermo-cycling and after 500 cycles

6.4 crack growth

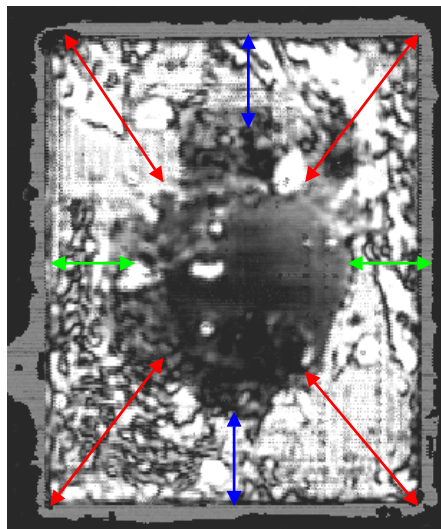


Figure 6.12. the 8 measure lines: The measurements along the red lines are called "along the diagonal", along the blue one "along the large side", and the green one along the small side. (see figure 6.13)

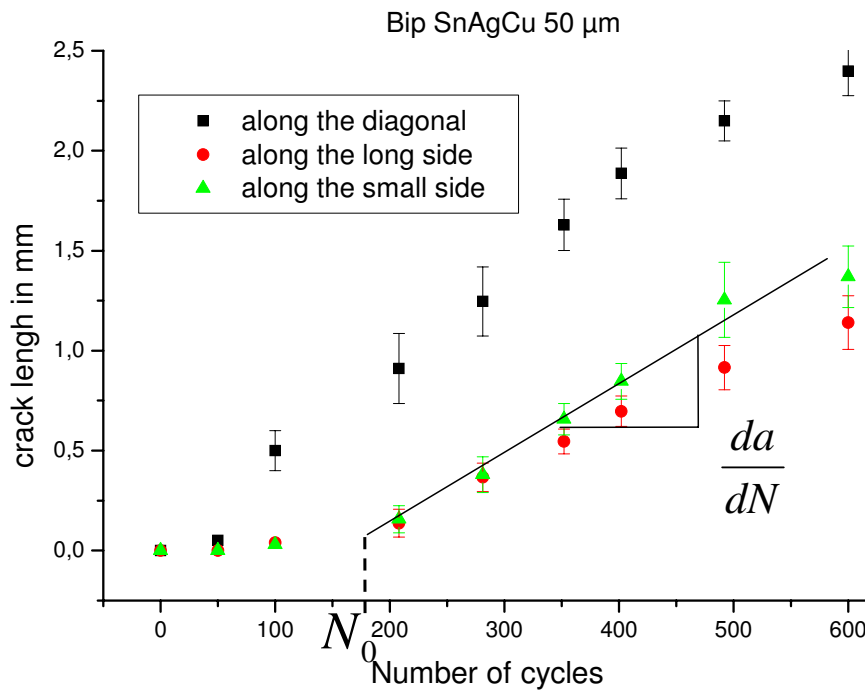


Figure 6.13. crack length as function of the number of cycles: only the mean values are represented with their standard deviation

For each ultrasonic picture, the crack length is measured at eight different places as shown in figure 6.12: 4 measures along the diagonal of the chip, two along the small side and 2 along the big side. The mean values of those results for the 30 devices per variant are reported and plotted.

The standard deviation is also calculated for each mean value and plotted. The figure 6.13 shows an example of the crack growth in the solder joint as a function of the number of cycles. It gives us an history of the crack growth. It is clear in this figure that during the first cycle, no crack is detectable (and no change of the thermal behaviour either). After the crack initiation, the crack growth seems to be linear ($da/dN = \text{constant}$). All variants of devices that were tested have the same behaviour. For each device, the number of cycles until crack initiation (N_0) and the crack growth rate (da/dN) are calculated using the fit function of the software Origin. All these value were used for the fitting of the function (see paragraph "results"), but are not represented by the next figures, because they are too many. Then, for each variant and measurement place, a mean value of N_0 and da/dN and their corresponding standard deviation can be calculated and their values are used in the next figures, that means 12 points per solder alloy and temperature cycle type.

6.5 FE-Model

For the computer simulation, the commercial FEM application ANSYS was used. A parametric model was created that allowed to perform all simulations from a common input

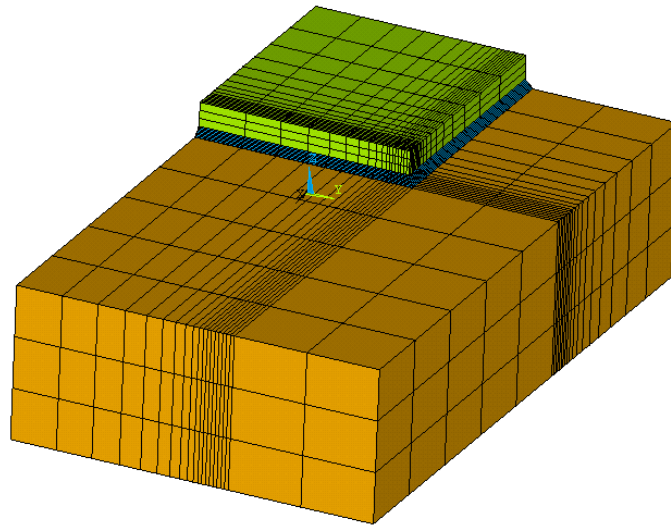


Figure 6.14. *FE Model of chip on bare copper*

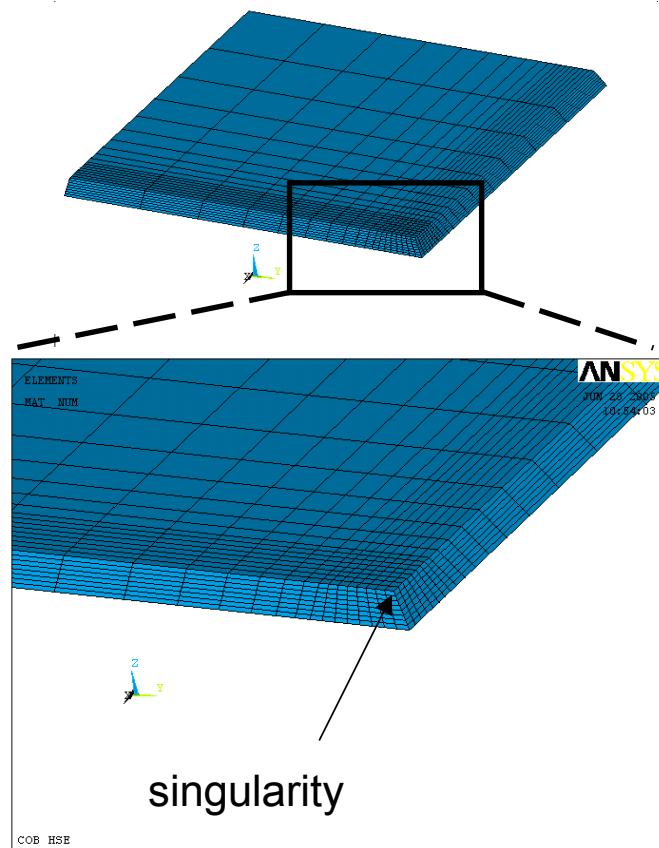


Figure 6.15. *detail of the solder joint meshing*

file. Due to symmetry only a quarter model is needed. Figure 6.14 shows this model: The colors correspond to the individual materials in the model.

The elements density is increased close to the singularity.(see figure 6.15). The mesh density influence will be investigated in the paragraph "results". For the Silicon and the bare copper, the E-module and the Poisson coefficient data were taken from literature. The coefficient of thermal expansion is measured with a thermal mechanical analysis (TMA) method, using directly both chips and the bare copper. The results of this measurement are given below.

Due to the high homologous temperature, creep must be included in the material description. We use the creep laws (equation 4.7), that we developed for SnPb and SnAgCu describing both primary and secondary creep (for more information see Chapter IV). The secondary creep rate can be described by the equation 4.1 for SnPb and by the equation 4.3 for the SnAgCu.

After performing the FE-simulation, a postprocessing routine was written to estimate the accumulated creep strain along three lines, corresponding to the three measures of the crack length (see section "crack growth").

As shown on figure 6.18, we chose a line which is at a distance of 1/8 of the thickness of the solder joint from the interface solder-chip, where the crack initiates. The accumulated creep strain was not extracted at the interface, because no delamination is observed with the metallography analysis, and to reduce the influence of the singularity. On figure 6.19, the absolute accumulated creep strain is represented, and is calculated with a linear interpolation (command *ppath* in Ansys). We represent the integrated accumulated creep strain from the meniscus to the center of the device (red curve for the diagonal is given as an example). For a point at a distance of w , this integrated accumulated creep strain is calculated as follows:

$$\varepsilon_{acc,int}(w) = \frac{1}{w} \int_0^w \varepsilon_{acc}(x) dx \quad (6.6)$$

$\varepsilon_{acc,int}(w)$ is then the mean value of the accumulated creep strain between $x=0$ and $x=w$. To simplify the rest of the study, we call method "u%" the method that uses the mean value $\varepsilon_{acc,int}(w)$ for $w = u\% \times L$. The influence of the mesh density was studied. Three different element sizes in the singularity zone see figure 6.15 are compared. The thickness of the element is always constant and equal to the thickness of the solder joint through 8. We also take the value at the singularity node. These results are reported in figure 6.20. This comparison revealed that it is impossible to use the result of the singularity to build a model, and this influence decreases with the increase of the value u (method u%) from $u=0$ to $u=5\%$ the error is relevant.

6.6 results

Inspired by methods developed by Darveaux [10,76], based on the work of Coffin et al. [29], Manson et al., and Paris et al. [111] the equations (6.9)(6.7) are used to describe the crack initiation and the crack growth.

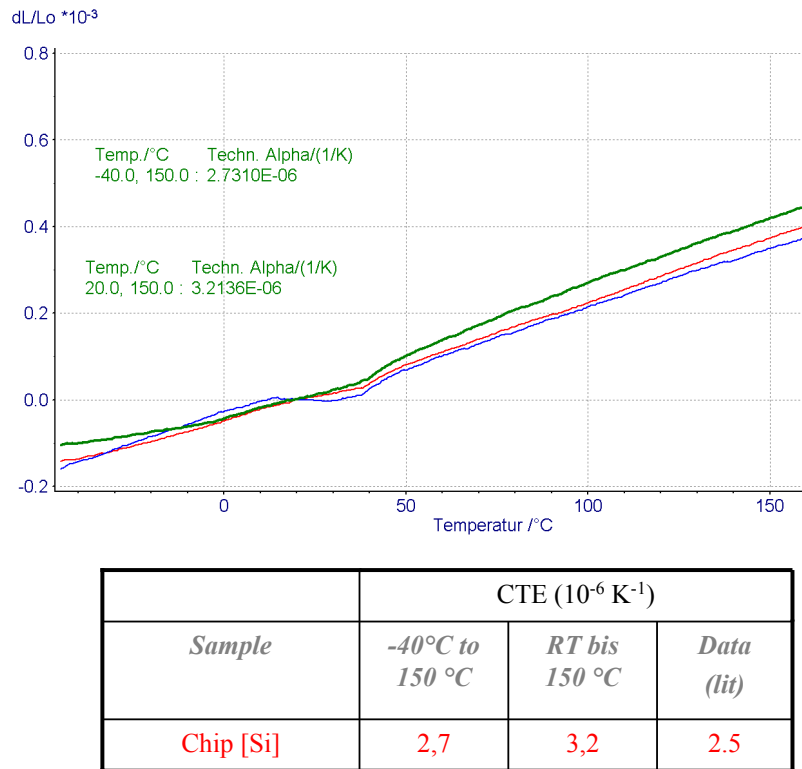


Figure 6.16. CTE measurement of the Silicon

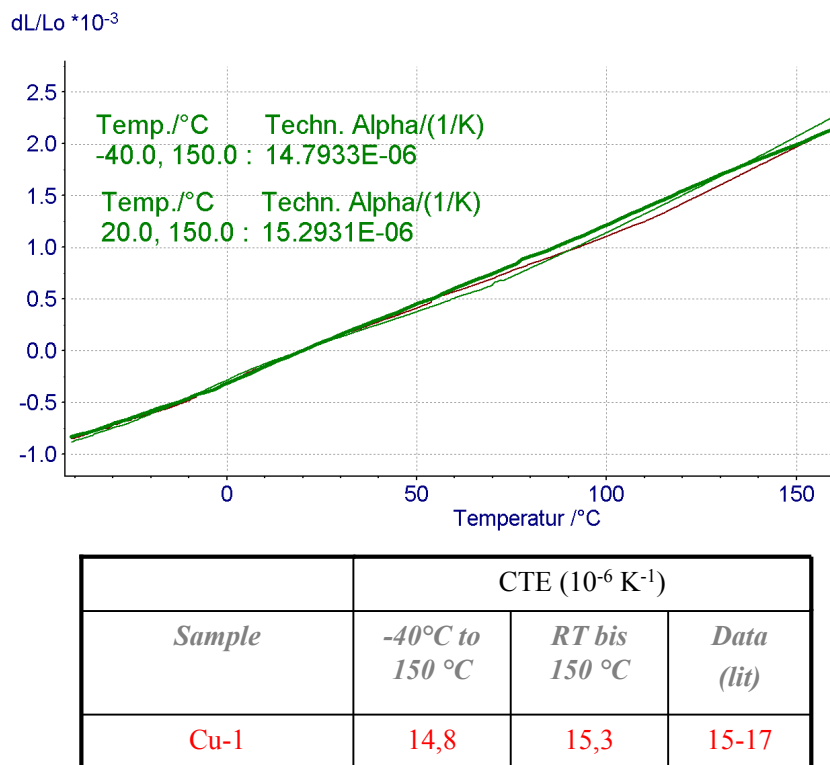


Figure 6.17. CTE measurement of the Copper

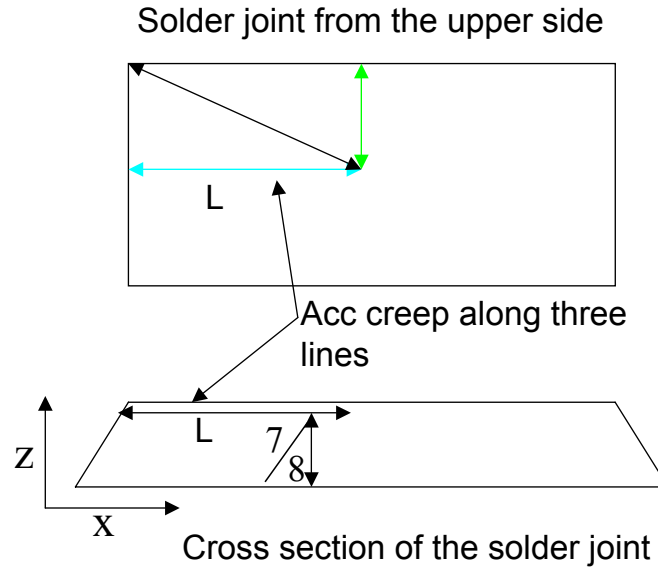


Figure 6.18. schematic representation of the solder joint and the analysis method; the colors correspond to the colors used in figure 6.19

$$N_0 = C_1 \times (\varepsilon_{acc,cr,int})^{C_2} \quad (6.7)$$

$$\frac{da}{dN} = C_3 \times (\varepsilon_{acc,cr,int})^{C_4} \quad (6.8)$$

where C_1, C_2, C_3 , and C_4 are coefficients, and $\varepsilon_{acc,cr,int}$ is the integrated accumulated strain along a line (different values of u for the method $u\%$ can be got). The crack length L can be calculated by:

$$L = \frac{da}{dN} \times (N - N_0) \quad (6.9)$$

Figures 6.21, 6.22 show the mean value of the crack growth rate as function of the integrated accumulated creep strain for the method 10%.

Figures 6.23, 6.24 show the same for the crack initiation.

The results were fitted with the pre-cited equations. The same work was done for SnAgCu (temperature cycle and T-shock). The crack growth rate and the number of cycles to crack initiation N_0 are also compared to the integrated creep strain from the method 5% to the method 50%. For all fit results, it is also possible to calculate the coefficient of determination R^2 . This coefficient gives the accuracy of the linear regression [112]. The quantity r is called the linear correlation coefficient is given by:

$$r = \frac{n \sum xy - (\sum x)(\sum y)}{\sqrt{n(\sum x^2) - (\sum x)^2} \sqrt{n(\sum y^2) - (\sum y)^2}} \quad (6.10)$$

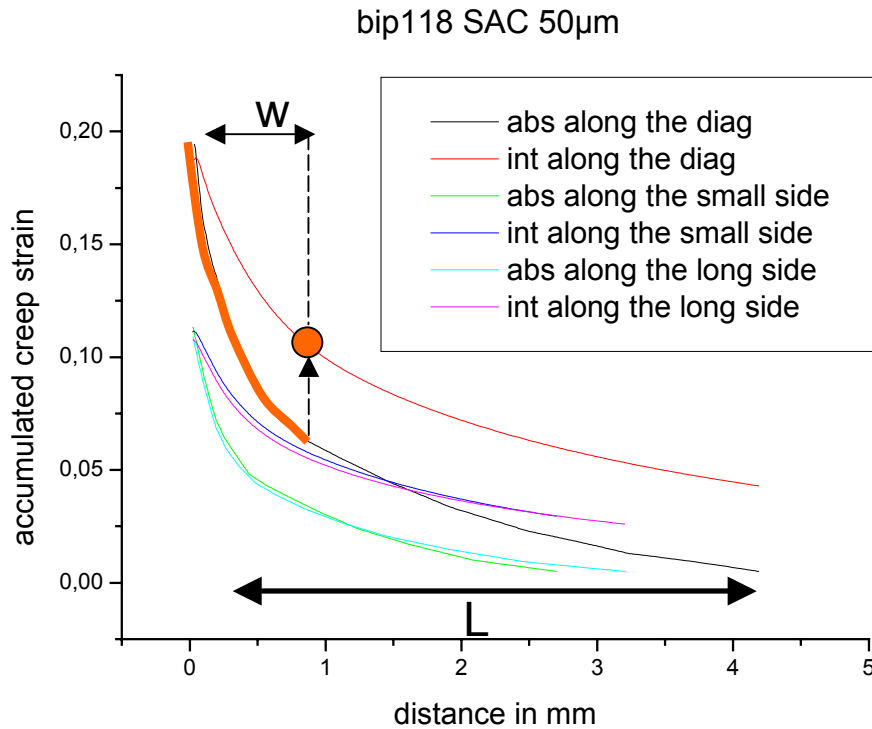


Figure 6.19. *results of the simulation*

where n is the number of pairs of data. The coefficient r^2 is called the coefficient of determination and is the square of r . It gives the variance of the predictable variable y (in our case N_0 or da/dN) from the other variable x (the accumulated creep strain). The coefficient of determination is a measure of how the regression line represents the data. For an ideal case, the regression line passes exactly through every point on the scatter plot, this value is 1. For a value between 0.7 and 1, the model can be considered as a good model to describe these physical phenomena. Figure 6.27 shows the coefficients of determination for each variant of test device, load and for different methods $u\%$.

So, for each variant the highest coefficient of determination is obtained for the method 10%. So this is the method that is chosen for the prediction of crack length. The parameters are given in table 6.2.

| | SnPb T-cycle | SnAgCu T cycle | SnAgCu T-Shock |
|----|--------------|----------------|----------------|
| C1 | 60,947 | 4,48 | 4,49 |
| C2 | -0,5391 | -1,2965 | -1,38 |
| C3 | 0,0057 | 0,021 | 0,0174 |
| C4 | 0,7376 | 0,681 | 0,6433 |

Table 6.2: parameters for the crack growth prediction using the equation (6.9) and (6.7)

The 4 parameters for SnAgCu are very close to each other, that means that the behaviour of

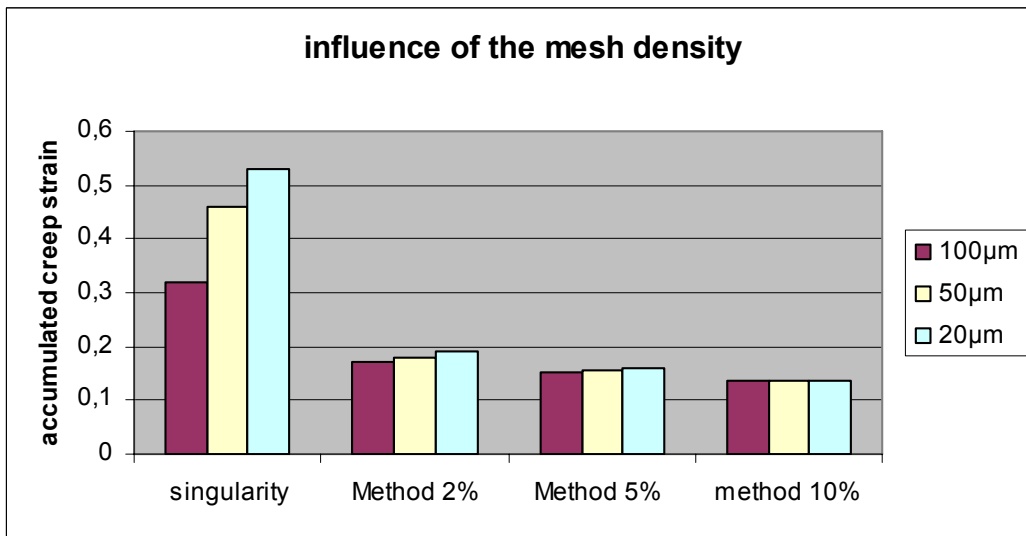


Figure 6.20. *influence of the mesh density: the result given at the singularity is the node value, for the method $u\%$ they are mean values, see above*

this alloy is the same for temperature shock and temperature cycles for our test conditions. The prediction intervals 90% were also calculated with the *fit help* module of the software Origin and are represented in figures 6.25 and 6.26.

This interval means that if the same experiment is done for a chip of a size between 13 mm^2 and 36 mm^2 and a solder joint thickness between $50 \mu\text{m}$ and $100 \mu\text{m}$, the statistical probability is 90% that the crack growth rate and the initiation number of cycles occurring in this prediction interval is also 90%.

These figures confirm the fact that the SnAgCu could be modeled using the same method. The accuracy for the prediction of the crack growth rate for the two temperature regimes is the same. The accuracy for the prediction of the number of cycle to crack initiation is better for the temperature cycle than for the temperature shock.

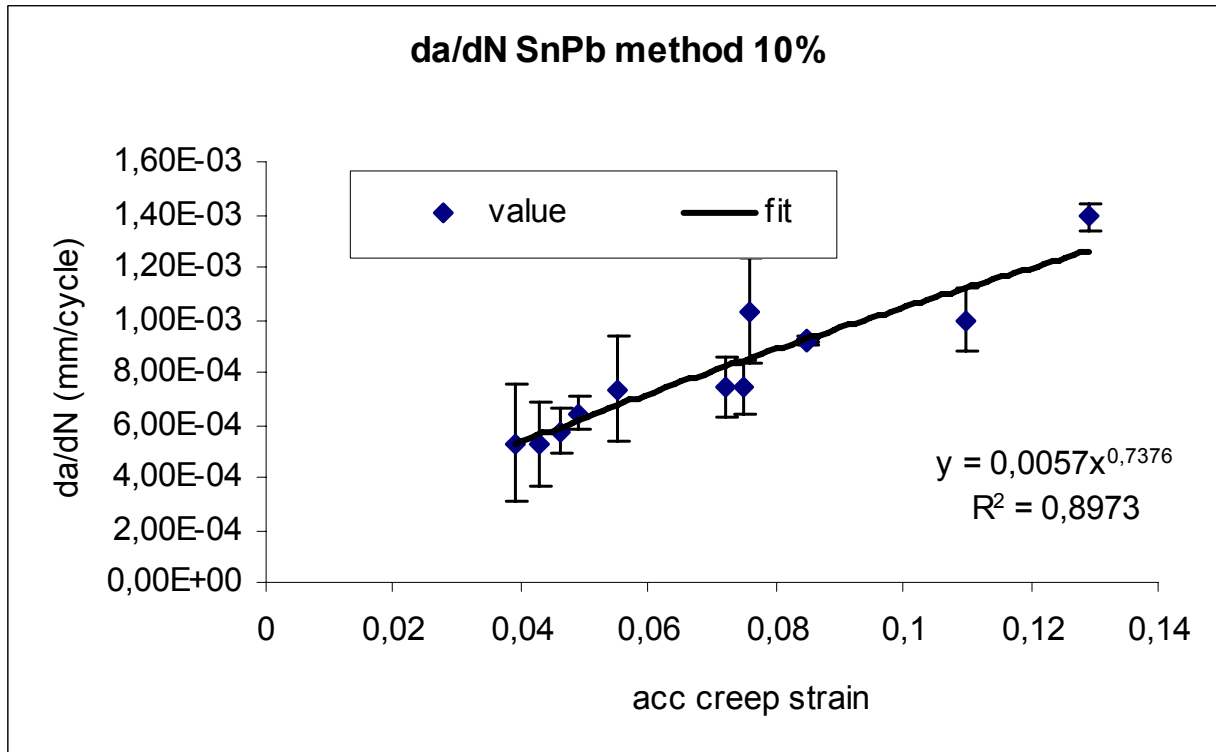


Figure 6.21. SnPb results: the crack growth rate VS the integrated accumulated creep strain calculated with the method 10%

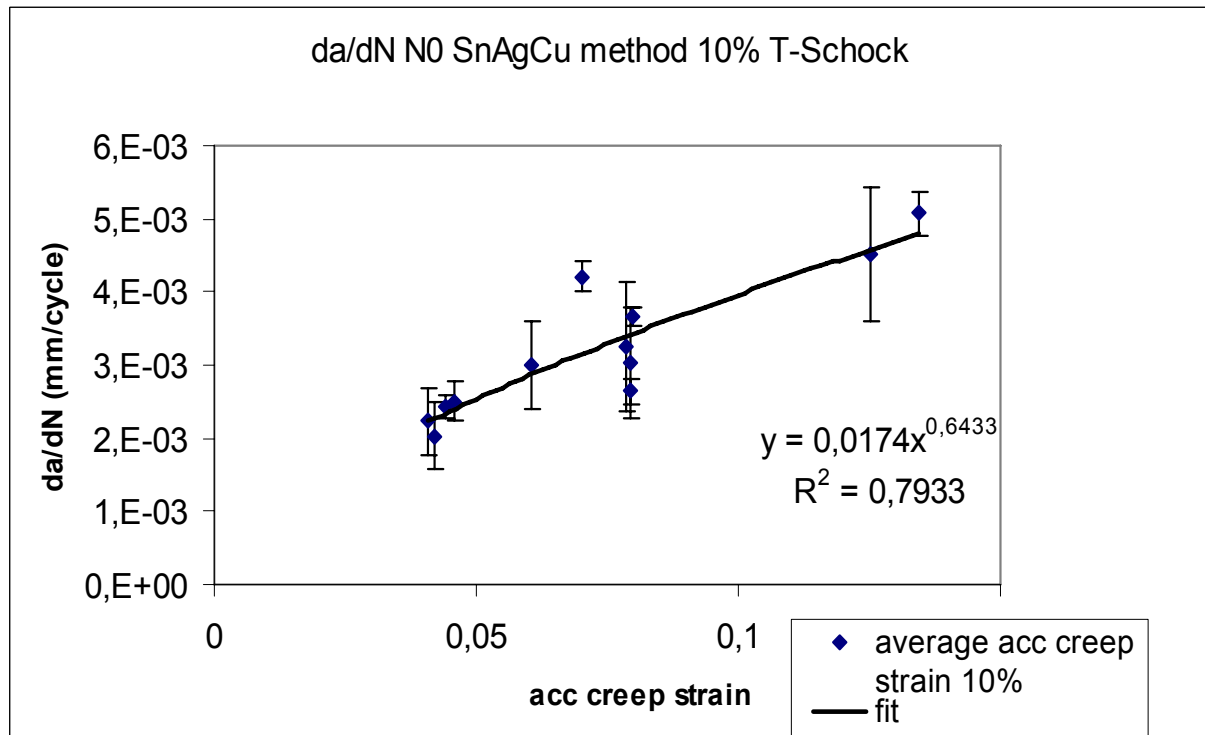


Figure 6.22. SnAgCu results T-shock: the crack growth rate VS the integrated accumulated creep strain calculated with the method 10%

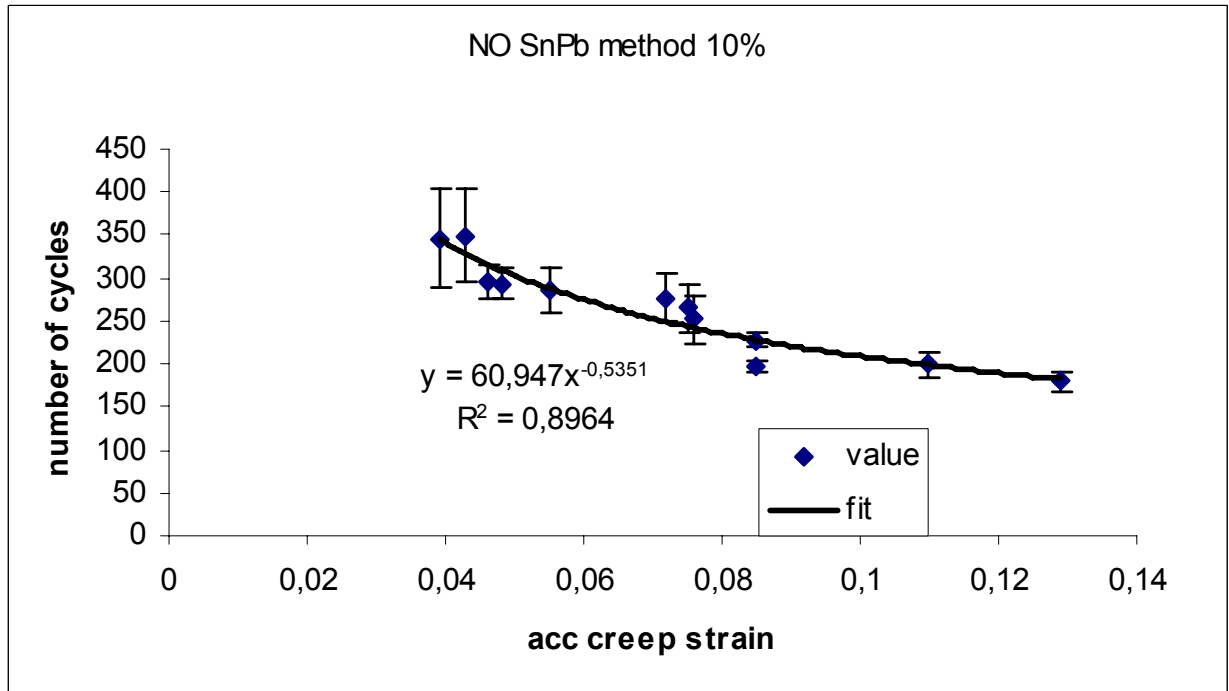


Figure 6.23. *SnPb results: Number of cycle N_0 VS the integrated accumulated creep strain calculated with the method 10%*

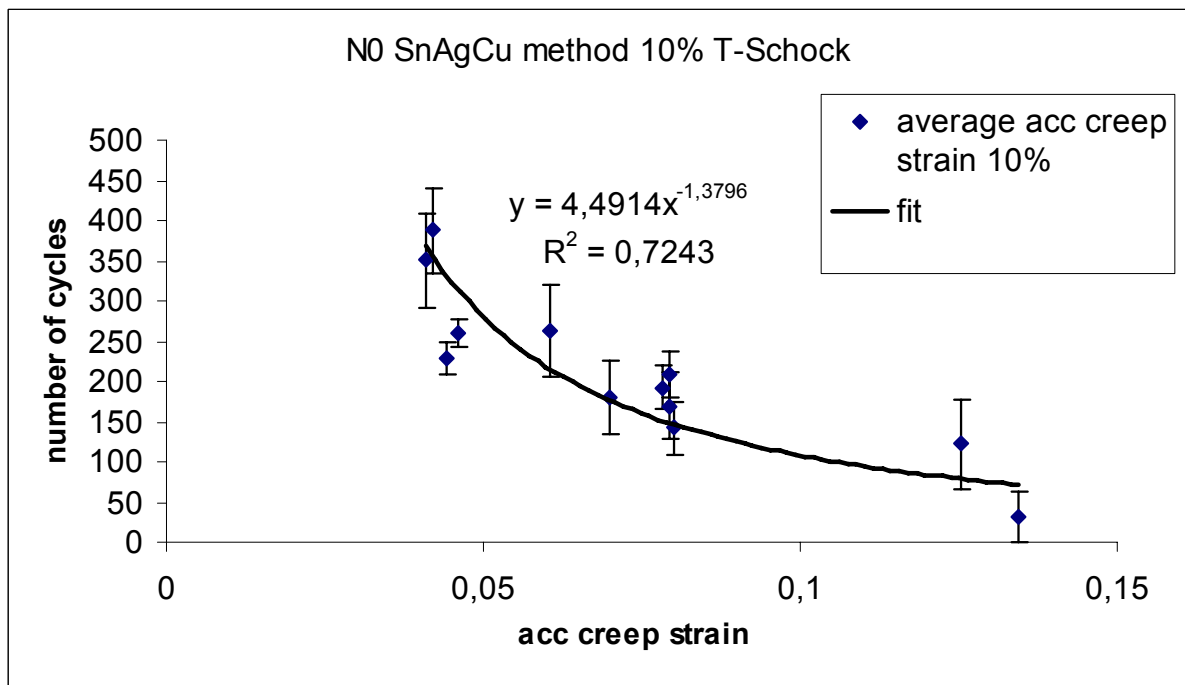


Figure 6.24. *SnAgCu results T-shock: Number of cycle N_0 VS the integrated accumulated creep strain calculated with the method 10%*

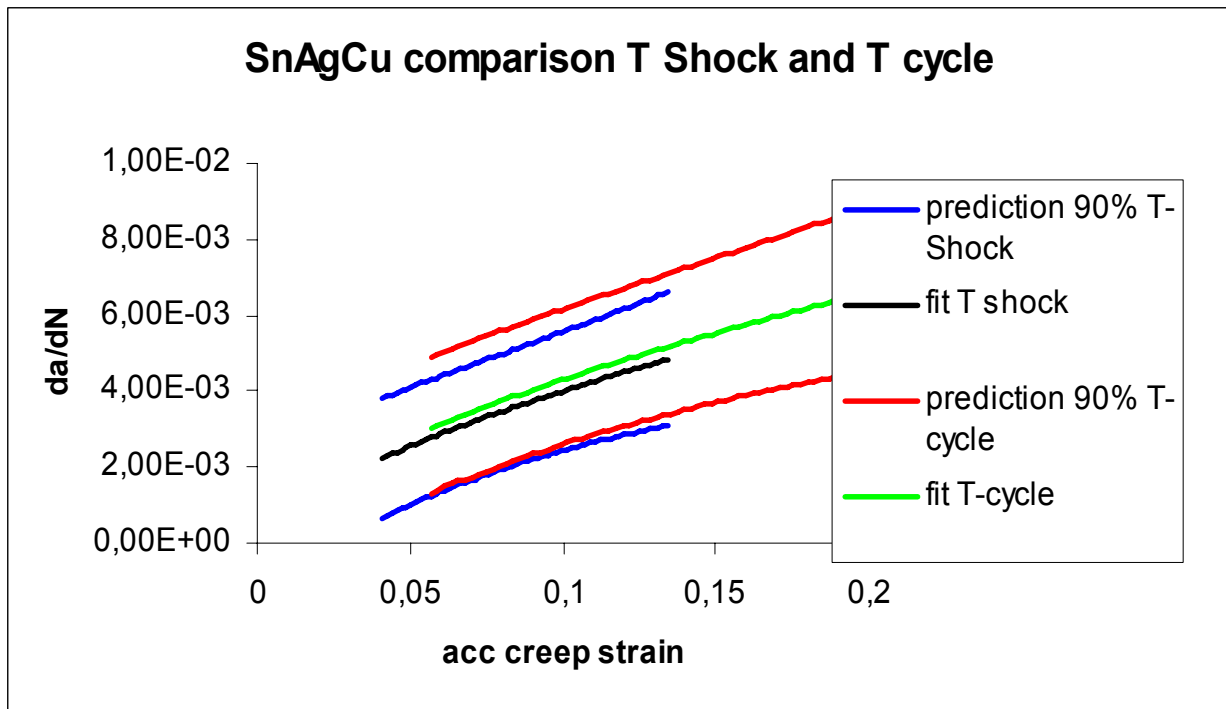


Figure 6.25. SnAgCu: model for the crack growth rate and prediction interval 90% of this model

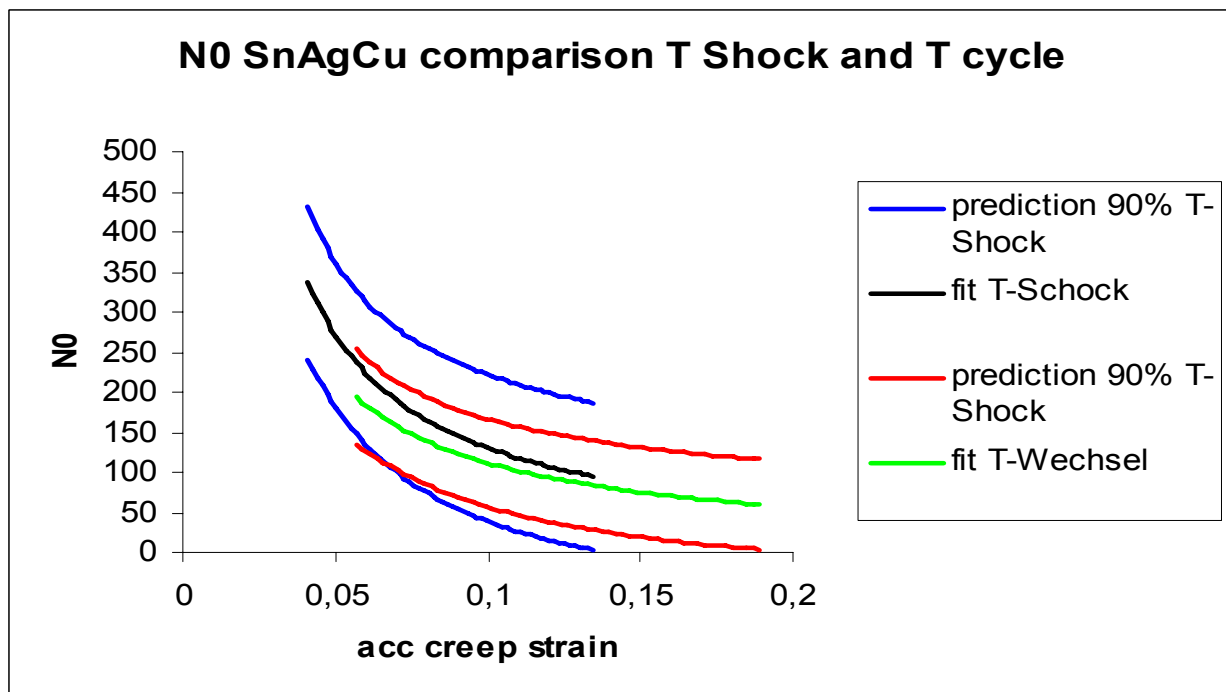


Figure 6.26. SnAgCu: model for the crack initiation and prediction interval 90% of this model

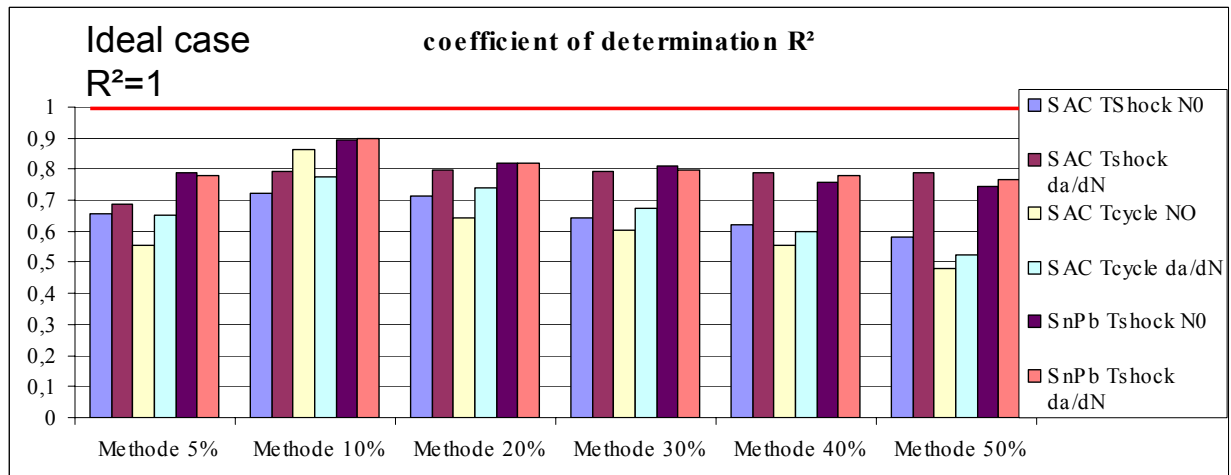


Figure 6.27. *coefficient of determination for different case and methods: the method 10% gives the best accuracy*

6.7 verification test

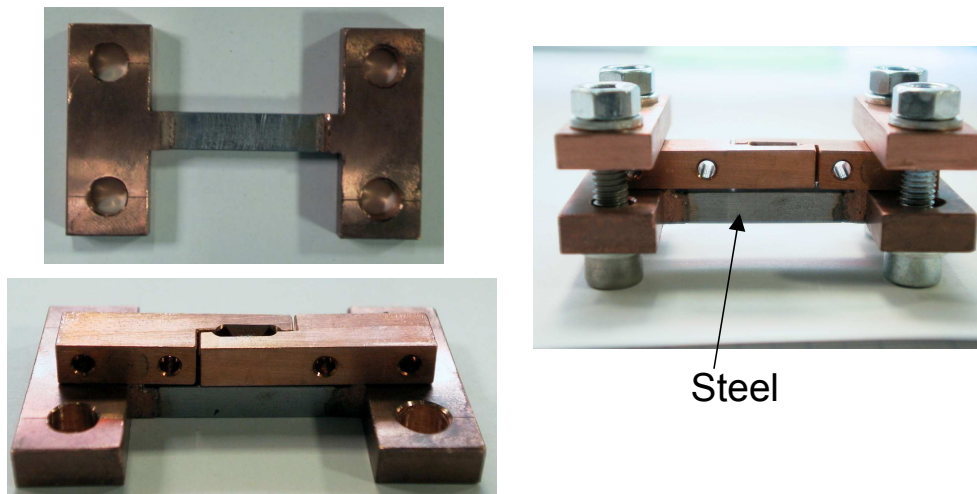


Figure 6.28. *the grooved lap test specimen on its frame*

The test which will be presented in this section is a temperature shock performed with shear test sample. The grooved lap test specimen was fixed on a frame which has a different thermal expansion from the test sample. Controlling different expansion of the frame, the accumulated creep strain can be also controlled. The frame is composed by two copper pieces and in the middle are soldered with a steel bar. The length of this steel bar, will determine the accumulated creep strain (see figure 6.28). Through the FE-simulation, this accumulated creep strain per cycle could be calculated. Two frames were used, one which gives an accumulated creep strain of 5 % and the second one 12 %.

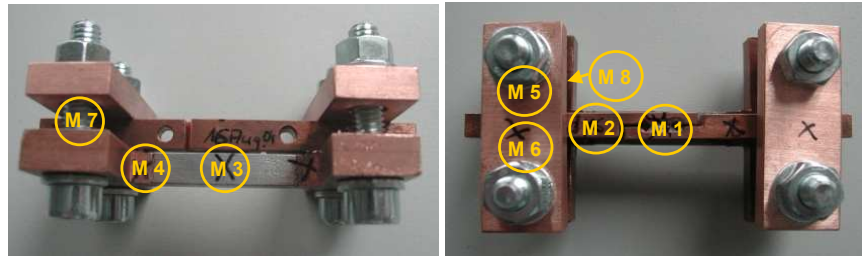


Figure 6.29. *temperature measurement places*

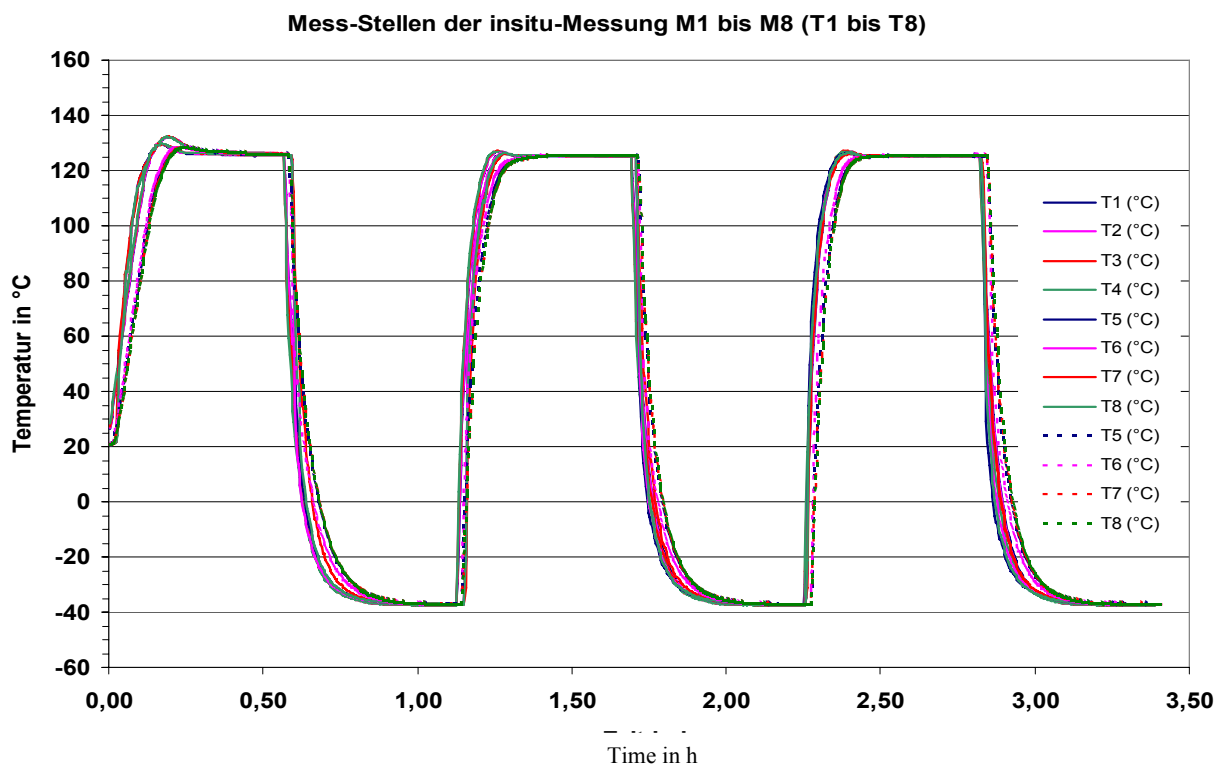


Figure 6.30. *temperature measurement results during 3 cycles*

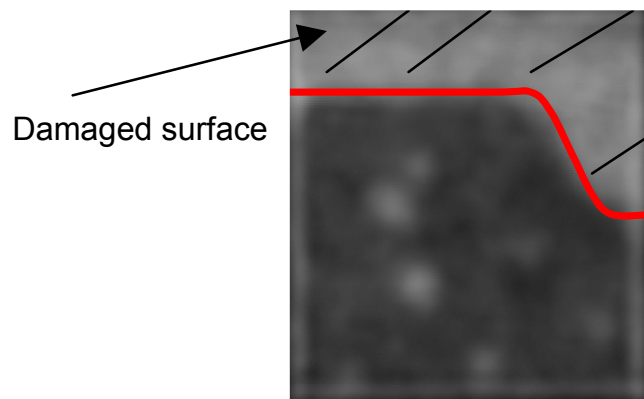


Figure 6.31. *Ultrasound picture of a shear test sample after 500 cycles*

Only SnAgCu was tested with this kind of test specimen. The objective was to verify the crack growth rate at constant accumulated creep strain level. Indeed, it was expected to have a homogenous crack distribution in the solder joint, because of the homogenous stress distribution (see Chapter III). The test samples were tested with the same thermo-shock as the chip on board (see figure 6.5). It was verify during the test that the temperature at different places (see figure 6.29 of the test sample is constant along the full test (it is necessary to maintain a homogenous stress in the solder joint)).

The results of this investigation confirms that the temperature is homogenous at all places of the specimen. A maximal temperature difference of 10 K was measured. As for the chip on board, an ultrasound picture was regularly done each 100 cycles. It was expected a homogenous crack distribution along the cross section, from the border to the center of the solder joint. Unfortunately, it was absolutely not the case. The figure 6.31 shows for example one of this picture. The crack occurs only from one side of the solder joint. So, the method measuring the crack length at 8 places as it was already presented for Chip on board is not here applicable. Since the results of shear test on frame and Chip on board could not be directly compared with the methods presented above, a new one had to be developed. The idea was not to use the crack length , but the damaged surface. From the experimental results of Chip on board, it was easy to calculate the damaged surface after the crack lengths as function of the number of cycles. Syed et al. [75] presented such a method for PBGA package. He intended, that a relationship can be found, between the number of cycle to corresponding damaged surface of solder joint and the mean accumulated creep strain along this damaged surface (it could be the full cross section surface 100 % of the surface, or a percentage of this surface. The equivalent creep strain has to be calculated along the real damage surface). The relationship was:

$$N_{x\%} = C_1 \times \varepsilon_{acc,cr,x\%}^{C_2} \quad (6.11)$$

where $N_{x\%}$ is the mean cycle to damage $x\%$ of the full surface, and $\varepsilon_{acc,cr,x\%}$ the equivalent accumulated creep strain, integrated along the damage surface (mean value), and C_2 a constant equal to -1. He gave for the constant C_1 , two values, dependant on creep law he used. These values were 0.0513 and 0.0648.

The same work was realized with the chip on board and the shear test sample. To calculate the mean value of accumulated creep strain for the die attach, the non-damaged surface was considered as an ellipse. A subroutine for ansys was written to calculate this accumulated creep strain. This work was performed for 3 cases; 5% of the full surface damaged, 10% and 20 %.

| damaged surface percentage of full surface | C_1 | C_2 |
|--|--------|---------|
| 5% | 17,458 | -1,0055 |
| 10% | 22,76 | -0,9342 |
| 20% | 33,959 | -0,8344 |
| Syed 1 | 0,0513 | -1 |
| Syed 2 | 0,0648 | -1 |

Table 6.3: parameters for equation 6.11

The comparison between the simulation data and the experimental data is presented in figure 6.32. For each case, the results of the shear test specimen are represented. The parameters of equation 6.11 are fitted and presented in table 6.3. The results of Chip on Board are very good and the damaged surface can be calculated with the Syed Method. Unfortunately the results given by the shear test sample are not so good as expected and can not confirm or infirm the developed model. From this experiment, it is not possible to take good conclusion, because the standard deviation is very large for the shear test samples, and they were not reproducible. Indeed, for each test sample, a new damaged ultrasound picture was measured (crack distribution), contrary to the chip on board (always an ellipsoidal crack distribution). This can be explained by the homogeneity of the stress and stress in the shear test sample solder joints. Indeed, the crack initiation, and growth occurred probably at void or micro-defects, which created stress concentration, which accelerate the crack growth at this place. the crack growth of the 2 test demonstrators (chip on board and shear on frame) are not comparable.

6.8 conclusion

Two methods to predict the crack propagation for chip on Copper substrate are presented. It is possible to detect the crack propagation with the Scanning Acoustic Microscope that revealed that the SnPb alloy has a better crack resistance that the SnAgCu for die attach under the same temperature cycling conditions. It was shown that it is not necessary to use complicated fracture mechanical models to be able to simulate the crack growth and propagation in this solder joint type. But it is not known yet if this model or method can be universally applied for every planar solder joint. The models can not be applied for the verification test sample which was imagined. Some questions are still open: What happens with very fine solder joints ($10\mu m$ for example), and what is the influence of the intermetallic? What is the crack propagation behaviour of very large solder joints? Is the model still valid for chip soldered on FR4?

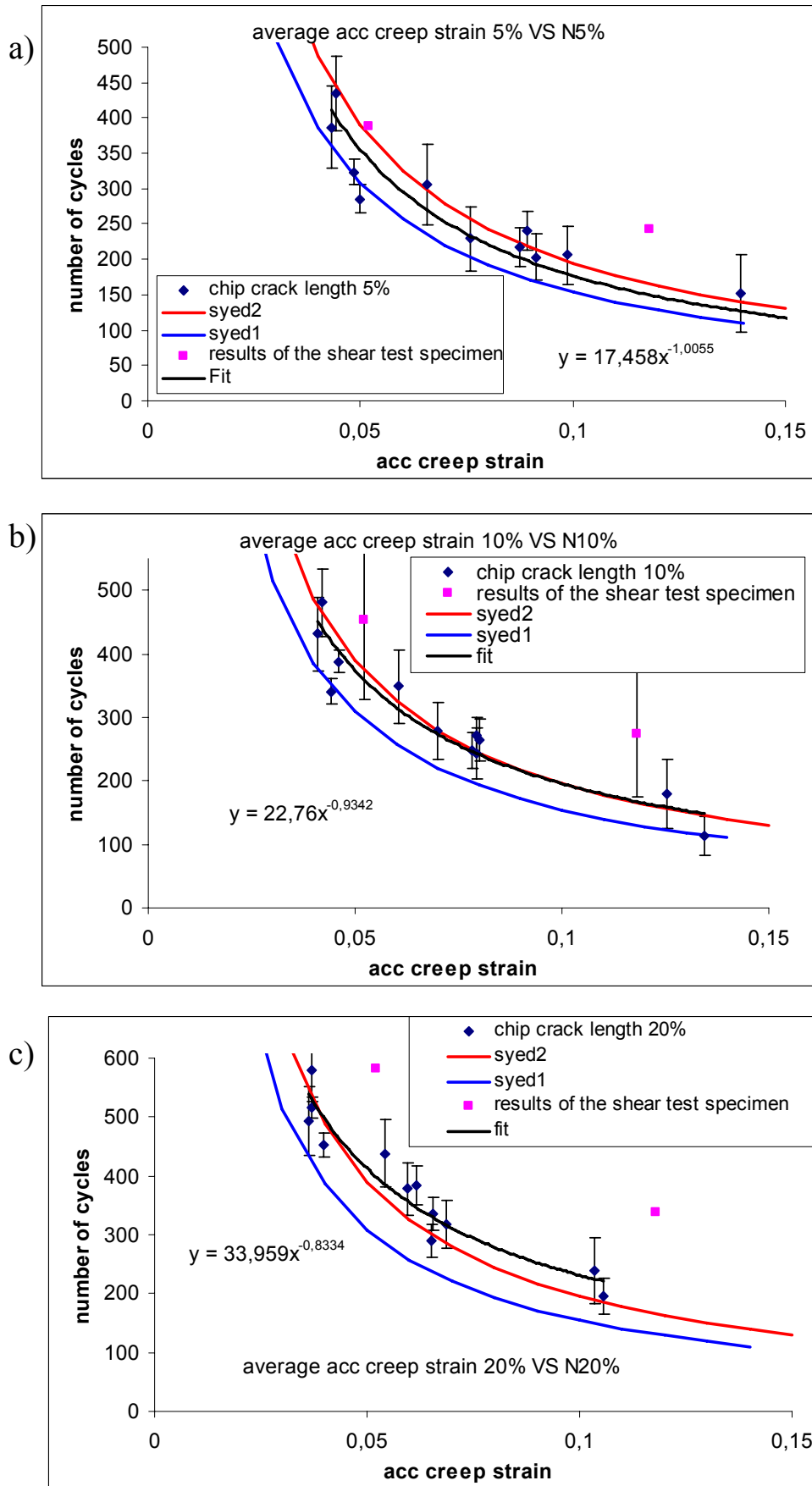


Figure 6.32. results of the surface method measurement method for SnAgCu: a) 5% b) 10% c) 20%

Bibliography

- [1] G.Q. Zhang, L.J. Ernst, and O. de Saint Leger. *Benefiting from Thermal and Mechanical Simulation in Micro-Electronics*. Proc. 1st. EuroSimE Conference. Kluwer Academic Publishers, Eindhoven, The Netherlands, March, 23-24 2000.
- [2] A. Schubert, R. Dudek, B. Michel, and H. Reichl. Package Reliability Studies by Experimental and Numerical Analysis. *Proc. 3. Int. Conf. on Micromaterials*, pages 110–119, April 17-19, Berlin, Germany 2000.
- [3] S. Wiese, A. Schubert, H. Walter, R. Dudek, F. Feustel, E.Meusel, and B. Michel. Constitutive Behaviour of Lead-Free vs. Lead-Containing Solders – Experiments on Bulk Specimens and Flip-Chip Joints. *IEEE Proc. Electronic Components and Technology Conference*, pages 890–902, 2001.
- [4] S. Wiese, E. Meusel, and K.-J. Wolter. Microstructural dependence of constitutive properties of eutectic snag and snagcu solders. *Proc. Electronic Components and Technology Conference*, May 27-30 2003.
- [5] K.P. Jen and J.N. Majerus. Stress-strain equations for some near eutectic tin-lead solders. *Journal of Engineering and materials technology*, pages 475– 484, 1991.
- [6] W.G. Plumbridge, C.R. Gagg, and S;Peter. The creep of leadfree solders at elevated temperatures. *Journal of Electronic Materials*, 9:1178–1183, 2001.
- [7] A. Schubert, R. Dudek, R. Döring, H.Walter, E. Auerswald, A. Gollhardt, B. Schuch, H. Sitzmann, and B. Michel. lead-free solder interconnects: Characterization, testing and reliability. *3rd International Conference on benefiting from Thermal and Mechanical Simulation in (Micro)-Electronics*, 2002.
- [8] J.H. Lau and Y. Pao. *Solder Joint Reliability of BGA, CSP, Flip Chip, and Fine Pitch SMT Assemblies*. Mc Graw-Hill, 1997.
- [9] E. Suhir. Calculated Thermally Induced Stresses in Adhesively Bonded and Soldered Assemblies. *International Symposium on Microelectronics*, pages 383–392, 1986.
- [10] R. Darveaux. Effect of simulation methodology on solder joint crack growth correlation. *conference ECTC, proceedings*, 2000.
- [11] W. Engelmaier and A. Attarwala. Surface-Mount Attachment Reliability of Chip-Leaded Ceramic Chip Carriers on FR-4 Circuit Boards. *IEEE Trans. Components, Hybrids, and Manufacturing Technology*, 12(2):284–296, 1989.

- [12] A. Schubert, R. Dudek, J. Auersperg, D. Vogel, B. Michel, and H. Reichl. Thermo-Mechanical Reliability Analysis of Flip-Chip Assemblies by Combined Microdac and Finite Element Method. *Conf. Proc. Interpack '97, Hawaii, USA*, pages 1647–1654, 1997.
- [13] A. Schubert, R. Dudek, H. Walter, E. Jung, A. Gollhardt, and B. Michel. *Lead-free Flip-Chip Solder Interconnects – Materials Mechanics and Reliability Issues*, pages 12–25. Micromaterials and Nanomaterials. Micro Materials Centre Berlin at the Fraunhofer Institute IZM, Germany, 1 edition, 2002.
- [14] A. Schubert, R. Dudek, R. Leutenbauer, P. Coskina, K.-F. Becker, J. Kloeser, B. Michel, H. Reichl, D. Baldwin, J. Qu, S. Sitaraman, C.P. Wong, and R. Tummala. Numerical and Experimental Investigations of Large IC Flip-Chip Attach. *Proc. of 50. Electronic Components and Technology Conference*, pages 1338–1346, 2000.
- [15] S. Rzepka, M.A. Korhonen, E. Meusel, and C.Y. Li. The Effect of Underfill and Underfill Delamination on the Thermal Stress in Flip-Chip Solder Joints. *Journal of Electronic Packaging*, 1998.
- [16] C.A. Le Gall et. al. Influence of Die Size on the Magnitude of Thermomechanical Stresses in Flip-Chips Directly Attached to Printed Wiring Board. *ASME EEP-Vol. 19-2, Advances in Electronic Packaging - Proc. Interpack 1997*, pages 1663–1670, 1997.
- [17] R. Dudek, A. Schubert, and B. Michel. Thermo-Mechanical Reliability of Microcomponents. *Proc. 3. Int. Conf. on Micromaterials*, pages 206–213, April 17-19, Berlin, Germany 2000.
- [18] C.E. Hanna, S. Michaelides, P. Palaniappan, D.F. Baldwin, and S.K. Sitaraman. Numerical and Experimental Study of the Evolution of Stresses in Flip-Chip Assemblies During Thermal Cycling. *IEEE Proc. Electronic Components and Technology Conference*, 1999.
- [19] J.H.L. Pang and D.Y.R. Chong. Flip-Chip on Board Solder Joint Reliability Analysis Using 2-D and 3-D FEA Models. *IEEE Transactions on Advanced Packaging*, 24(4):499–506, 2001.
- [20] Q.Yao and J.Qu. Three-Dimensional versus Two-Dimensional Finite Element Modelling of Flip-Chip Packages. *Journal of Electronic Packaging*, 121:196–201, 1999.
- [21] M. Spraul, W. Nüchter, B. Wunderle, and B. Michel. Fe analysis and experimental testing of a 4-pin ceramic test vehicle with tin-lead and tin-silver-copper solder joints. *proc. Eurosime*, pages 441– 447, 2005.
- [22] M. Spraul, W. Nüchter, W. Moller, B. Wunderle, and B. Michel. Reliability of snpb and pb-free flip-chips under different test conditions. *proc. Eurosime*, pages 437– 442, 2004.
- [23] M. Thoben. *Zuverlässigkeit von Grossflächigen Verbindungen in der Leistungselektronik*. PhD thesis, Universität Bremen, 2002.

- [24] B. Michel, T. Winkler, M. Werner, and H. Fecht. *Micro Materials*. Verlag DDP Goldenbogen, Dresden, Germany, 2000. Proceedings of the 3rd MicroMat.
- [25] H.D. Solomon, V. Brzozowski, and D.G. Thompson. Prediction of Solder Fatigue Life. *Proc. 40. ECTC*, pages 351–360, 1990.
- [26] K. Doi, N. Hirano, T. Okada, Y. Hiruta, and T. Sudo. Prediction of Thermal Fatigue Life for Encapsulated Flip-Chip Interconnection. *Int. Journal of Microcircuits and Electronic Packaging*, 19(9):231–237, 1996.
- [27] R. Dudek, M. Nysten, A. Schubert, B. Michel, and H. Reichl. An Efficient Approach to Predict Solder Fatigue Life and its Application to SM- and Area-Array Components. *Proc. 47. Electronic Components and Technology Conference*, pages 462–471, 1997.
- [28] A. Syed. Predicting Solder Joint Reliability for Thermal, Power & Bend Cycle within 25 % Accuracy. *Proc. 51. Electronic Components and Technology Conference*, pages 255–265, 2001.
- [29] L.F. Coffin. A Study of the Effects of Cyclic Thermal Stresses on a Ductile Material. *Trans. ASME*, 76:931–950, 1954.
- [30] S.S. Manson. Behaviour of Materials under Condition of Thermal Stresses. *NACA TN-2933, Report 1170*, pages 317–350, 1954.
- [31] P.L. Hacke, A.F. Sprecher, and H. Conrad. *Thermomechanical Fatigue of 63Sn-37Pb Solder Joints*, chapter 15, pages 466–499. van Nostrand Reinold, NY, USA. In: *Thermal Stress and Strain in Microelectronic Packaging*, edited by J.H. Lau.
- [32] Z. Guo and H. Conrad. Effect of Microstructure Size on Deformation Kinetics and Thermo-Mechanical Fatigue of 63Sn37Pb Solder Joints. *Journal of Electronic Packaging*, 118:49–54, 1996.
- [33] A. Syed. Creep Crack Growth Prediction of Solder Joints During Temperature Cycling – An Engineering Approach. *Journal of Electronic Packaging*, 117:116–122, 1995.
- [34] S.H. Ju and B.I. Sandor and M.E. Plesha. Life Prediction of Solder Joints by Damage and Fracture Mechanics. *Journal of Electronic Packaging*, 118:193–200, December 1996.
- [35] W.C. Dash. *Dislocations and Mechanical properties of Crystals*. John Wiley and sons, INC, 1 edition, 1953.
- [36] J.P. Hirth and J. Lothe. *Theory of dislocations*. John Wiley and sons, New-York, 2 edition, 1982.
- [37] A.S. Argon. *Physical metallurgy*. Elsevier, 1996.
- [38] W. Blum. *Plastic deformations and fracture*. Material Science and technologie, 1993.
- [39] F. Garafalo. *Déformation et rupture par le fluage*. Éditions Dunod, 1971.

- [40] J. Gittus. *Creep, viscoplasticity and creep fracture in solids*. Applied science Pub., London, 1975.
- [41] A.H. Cottrell. *Deformations and plastic flow in Crystals*. Oxford university Press, London, 1 edition, 1953.
- [42] R.W. Evans and B. Wilshire. *Creep of metals and alloys*. Inst. of Metals, London, 1 edition, 1985.
- [43] H.E. Evans. *Mechanisms of creep fracture*. Elsevier, 1 edition, 1993.
- [44] J.Cadek. *Creep in metallic materials*. Elsevier, Amsterdam, 1 edition, 1988.
- [45] H. Neuber. Theory of stress concentration for shear strained prismatic bodies with arbitrary non-linear stress-strain law. *ASME, American Society of Tests and Materials*, 10:625–630, 1910.
- [46] M. Kawai and Y. Ohashi. Coupled effect between creep and plasticity of type 316 stainless steel at elevated temperature. *2nd International conference on Constitutive laws for engineering Materials*, Arizon USA 1987.
- [47] E. Consteti and G. Cailletaud. Description of creep-plasticity interaction with non-unified constitutive equations in an austenitic steel. *6th. Int. Seminar on inelastic Analysis and Life prediction in High Temperature Environment*, Paris 1987.
- [48] S. Wiese. *Experimentelle Untersuchungen an SnPb37 Flip-Chip-Lotkontakten zur Bestimmung werkstoffmechanischer Modelle fuer die FEM-Simulation*. Ph.d. thesis, Fakultät Elektrotechnik der Technischen Universität Dresden, Germany, 2000.
- [49] D. Grivas, K.L. Murty, and J.W. Morris. Deformation of Pb-Sn Eutectic Alloys at Relatively High Strain Rates. *Acta Metallurgica*, 27:731–737, 1979.
- [50] M. Amagai, M. Matanabi, M. Omiya, K. Kishimoto, and T. Shibuya. Mechanical characterization of sn-ag based lead free solders. *Microelectronics Reliability*, 42, 2002.
- [51] Banerji K. Darveaux R. Constitutive relations for tin-based solder joints. *Transactions On Components, Hybrids and manufacturing technology*, 15(6):87–91, 1992.
- [52] R. Darveaux and K. Banerji. *Ball Grid Array Technologies*, chapter 13. Mc Graw-Hill, New York, USA, 1995. Edited by J.H. Lau.
- [53] J. Nottay, M Dusek, C. Hunt, C. Baley, and H. Lu. Creep properties of snagcu solder in surface mounting assemblies. *NPL Report*, August 2001.
- [54] F. Garafalo. *fundamentals of creep and creep rupture in metals*. McMillan Book Co, New-York, 1965.
- [55] J.L. Chaboche. Viscoplastic constitutive equations for the description of cyclic and anisotropic behaviour of metals. *Bull. de acad. Polonaise des Sciences*, pages 33–42, 1977.

- [56] J.L. Chaboche. Constitutive equations for cyclic plasticity and cyclic viscoplasticity. *International of plasticity*, 5:247–302, 1989.
- [57] J.L. Chaboche. On some modifications of kinematic hardening to improve the description of ratchening effects. *International of plasticity*, 7, 1991.
- [58] W. Schmitt, R. Mohrmann, H. Riedel, A. Dietsche, and A. Fischerworrungbung. Modelling of the fatigue life of automobile exhaust components. *Fatigue*, 2002.
- [59] H. Riedel. *Fracture at high temperatures*. Springer-Verlag, Berlin, Heidelberg, New-York, 1997.
- [60] J.Wilde, K. Becker, M. THoben, W. Blum, T. Jupitz, W. Guozong, and Z.N. Cheng. Rate dependant constitutive equations based on anand model for 95.2pb5sn2.5ag solder. *Soldering and surface mounting Techology*, 1:31–36, 2000.
- [61] Z.N. Cheng, G.Z. Wang, L. Chen, J.Wilde, and K. Becker. Viscoplastic anand model for solder alloys and its application. *IEEE transactions on advanced packaging*, 3:408–414, 2000.
- [62] J.H.L Pang, B.S. Xiong, and F.X. Che. Modeling stress strain curves for lead-free SnAgCu. *Eurosime 2004*, 2004.
- [63] B.A. Zahn. Finite element based solder joint fatigue life prediction for a same die size-stacked-chip scale-ball grid array package. *IEMT*, 2002.
- [64] A. Yeo, C. Lee, and J.H.L. Pang. Flip chip solder joint fatigue life model investigation. *EPTC*, 2003.
- [65] L. Anand and S. Brown. constitutive equations for large deformation of metals at high temperatures. *CSA Illumina*, 1:28, 1986.
- [66] L. Anand and M. Kothari. Elasto-viscoplastic constitutive equations for polycrystalline metals: application to tantalum. *Journal of the mechanics and physics of solids*, 46:51–83, 1998.
- [67] O. H. Basquin. The exponential law of endurance tests. *Journal of applied Mechanic, Trans ASME*, E28, 1961.
- [68] B. Wunderle. *Thermo-Mechanical Reliability of Flip-Chips with Heat-Spreaders*. PhD thesis, Technische Universität Berlin, Germany, 2003.
- [69] Bernhard Wunderle, Karl-Friedrich Becker, Olaf Wittler, Ralph Schacht, Hans Walter, Mathias Nowottnick, Bernd Michel, and Herbert Reichl. Thermo-mechanical reliability of chip-on-board assemblies with encapsulation in experiment and simulation. *Proc. Electronic Components and Technology Conference, San Diego, USA*, June 2006.
- [70] M. Spraul. *Lebensdauerprognose fr gelötete Bauteile mit Zinn-Blei und Zinn-Silber-Kupfer Lot füt Temperaturwechselprüfungen*. PhD thesis, Technische Universität Berlin, Germany, 2006.

- [71] B. Wunderle, W. Nüchter, A. Schubert, B. Michel, and H. Reichl. Lifetime Prediction of Extended Flip-Chip Packages under Thermal and Mechanical Loading. *Proc. 2nd EuroSime Conf., Paris, France*, pages 123–128, 2001.
- [72] B. Wunderle, W. Nüchter, A. Schubert, B. Michel, and H. Reichl. Parametric FE-Approach to Flip-Chip Reliability under various Loading Conditions. *Proc. 3rd EuroSime Conf., Paris, France*, pages 52–60, April 15-17 2002.
- [73] IPC. Ipc-sm-785-guidelines for accelerated reliability of surface mounting solder attachments. *IPC*, 8, 2004.
- [74] H.D. Solomon and E.D. Tolksdorf. Energy Approach to the Fatigue of 60/40 Solder: Part I – Influence of Temperature and Cycle Frequency. *Journal of Electronic Packaging*, 117:130–135, 1995.
- [75] A. Syed. Accumulated creep strain and energy density based thermal fatigue life prediction models for snagcu solder joints, corrected version. *Proc ECTC*, 2004.
- [76] R. Darveaux. Solder joint fatigue life model. *design and reliability of solders and solder interconnections, Orlando, Florida, USA*, pages 213–218, 1997.
- [77] B. Wong, D. Helling, and R. Clark. A creep-rupture model for two-phase eutectic solders. *IEEE Transactions on CHMT*, pages 284–290, 1988.
- [78] Y.H. Pao. A fracture mechanics approach to thermal fatigue life prediction of solder joints. *IEEE Transactions on CHMT*, pages 559–570, 1992.
- [79] J.M. Hu. An empirical crack propagation model and its application for solder joints. *advances in electronic packagings*, pages 1001–1005, 1995.
- [80] W.A. Logston, P.K. Liaw, and M.A. Burke. Fracture behavior of 63sn-37pb solder. *Engineering Fracture Mechanics*, pages 183–218, 1990.
- [81] H.G. Badri and B. Michel. Generalized fracture mechanical integral concept jg applied to smt components. *proc. materials week*, 2001.
- [82] H. Badri. *Einsatz bruchmechanischer Integralkonzepte zur thermomechanischen Zuverlässigkeitsbewertung in der Mikroelektronischen Aufbau- und Verbindungstechnik*. PhD thesis, Universität Berlin, 2004.
- [83] Z. Guo and H. Conrad. Fatigue crack growth rate in 63sn37pb solder joints. *Journal of electronic Packaging*, pages 159–164, 1993.
- [84] R. Dudek. internal report. 2000.
- [85] J.J. Ramon and S. F Dirnfield. a practical way to measure the shear strength of small soldered joints. *Welding journal*, 67:12–21, 1988.
- [86] Stone K.R., Duckett R., R.Muckett S., and Warwick M. mechanical properties of solders and soldered joints. *Brazing and soldering*, 4:20–24, 1983.

- [87] <http://www.anton-paar.com/physica/download/mcrserie-e.pdf>.
- [88] CADFEM. Anwendung des neuen RIGID184-Elements zur Lasteinleitung, Ausgabe. *service newsletter*, pages 3–5, 11/1993.
- [89] P. Hacke, A.F. Sprecher, and H. Conrad. Computer Simulation of Thermo-Mechanical Fatigue of Solder Joints Including Microstructure Coarsening. *Journal of Electronic Packaging*, 115:153–158, 1993.
- [90] J. Courbon. *Calcul de structures*. Dunod, 1973.
- [91] R. Dudek. Fe-untersuchungen an ring und plug proben unter torsion. 04/2003.
- [92] J.W.Jr Morris Z. Mey. Fatigue life on 60Sn/40Pb Solder joints made With different cooling rate. *Journal of Electronic Packaging*, 114:104–108, 1992.
- [93] f. K Chen. Deformation analysis of simple-shear sheet specimens. *Journal of engineering Materials and technology*, 117:269–277, 1995.
- [94] J.W Morris D. Tribula. creep in shear of experimental solder joints. *Journal of electronic Packaging*, 122:87–91, 1990.
- [95] Iosipescu N. new accurate procedure for single shear testing of metals. *Journal of Materials*, 3(2):537–566, 1967.
- [96] Iosipescu N. and Matak R. Verfahren zur prfung von gestein und einigen baustoffen unter reiner schubbeanspruchung. 1972.
- [97] Poech M. Krumm M. Reinikainen, T. and J.K. Kivilahti. A finite-element and experimental analysis of stress distribution in various shear tests for solder joints. *Journal of Electronic Packaging*, 120(2):106–113, 1998.
- [98] Wie R Reinikainen, T. An optimized shear test sample for assessing solder deformation properties. *Proc. 2nd Int. Conf. on Benefiting from Thermal and Mechanical Simulation in (Micro)-Electronics (SIME)*, 2001.
- [99] G.J.S Chou. Microstrural evolution of snpb and snagcu bga solder joints during thermal aging. *Proc. Advanced Packaging materials*, Lincolnwood 1992.
- [100] CM Lu, TL Shang, CJ Yang, and C Chen. Microstrural evolution of snpb and snagcu bga solder joints during thermal aging. *Journal of Materials Research*, 8, 2004.
- [101] S. Déplanque, H. Walter, W. Nüchter, B. Wunderle, and B. Michel. Charakterisierung des primären und sekundären kreichverhaltens von snagcu und snpb- lotwerkstoffen. *Materialsweek conference oral presentation*, Germany 2004.
- [102] Inc. Ansys. *ANSYS structural analysis guide V. 9.0*. ANSYS, Inc., 2000.
- [103] R.W. Evans and B. Wilshire. *Introduction to creep*. ISBN 0 0901462 64 0.

- [104] M. Mayazumi and T. Onchi. Creep deformation and rupture properties of unirradiated zircalloy-4 nuclear fuel cladding tube at temperature of 727 to 857 k. *Journal of Nuclear Materials*, 175:135–142, 1990.
- [105] E. Anderson, Z. Bay, C. Bishoff, S. Blackford, J. Demmel, J. Dongarra, J. Du Croz, A. Greenbaum, S. Hammarling, A. Mckenney, and D. Sorensen. Lapack users' guide. *Society for Industrial and Applied Mathematics*, 3rd Edition.
- [106] S.Y. Sokolov. An ultrasonic microscope. *J. Tech. Phys.*, pages 271–273, 1949.
- [107] R.A. Lemons and C.F. Quate. Acoustic microscope-scanning version. *Press. Oxford*, 1992.
- [108] A. Briggs. *Acoustic microscopy*. 1973.
- [109] H. Reichl. Halbleiterbauelemente, Vorlesung Skriptung. *TU Berlin Fachbereich Elektrotechnik*, October 1999.
- [110] M. Burns. Reliability testing and product qualification. *Proc. European Power Electronics Conference (EPE), Toulouse*, September 2-4 2003.
- [111] Paul C Paris and F Erdogan. A critical analysis of crack propagation laws. *Selected papers on foundations of linear elastic fracture mechanics (A99-25742 06-39)*, 1963.
- [112] R. J. Freund and W. J. Wilson. *Regression analysis: Statical Modelling of a response variable*. Academic press, ISBN 0122674758, 1 edition, 1998.

Lebenslauf

Name: Sylvain Déplanque
Geburtstag: 01.06.1979
Geburtsort: Lille in Frankreich

1985-1990 Grundschohle in Templeuve
1990-1994 Gymnasium in Pont-à-Marcq (Collège)
1994-1997 Gymnasium in Lille (Lycée)
Juni 1997 Abitur in Naturwissenschaften

1997-1999 Vorbereitungsklasse Mathematik, Physik und Technology in Armentières

1999-2002 Studium der Maschinenbau an der Universität Strasbourg
Juni. 2002 Abschluss des Studiums als Diplom-Ingenieur bei der Robert Bosch GmbH in Bühl (Deutschland)

Sept. 2002 Dez. 2002 Berechnungsingenieur bei der Robert Bosch GmbH in Bühl (Deutschland)

2003-2006 Tätigkeit als Doktorand bei der Robert Bosch GmbH in Stuttgart in Zusammenarbeit mit dem Fraunhofer Institut "Zuverlässigkeit und Mikrointegration" in Berlin

2006 Tätigkeit als Berechnungsingenieur bei Luk GmbH und Co. in Bühl

2007 Tätigkeit als Entwicklungsingenieur bei Creative Power Solutions AG (CH)

Erklärung

Ich versichere, dass ich die von mir vorgelegte Dissertation selbständig und ohne unzulässige Hilfe angefertigt, die benutzten Quellen und Hilfsmittel vollständig angegeben und die Stellen der Arbeit – einschliesslich Tabellen und Abbildungen – die anderen Werken im Wortlaut oder dem Sinn nach entnommen sind, in jedem Einzelfall als Entlehnung kenntlich gemacht habe, dass diese Dissertation noch keiner anderen Fakultät zur Prüfung vorgelegen hat, dass sie noch nicht veröffentlicht worden ist, sowie dass mit der Veröffentlichung der Dissertation bestehende Schutzrechte nicht verletzt werden.

Die Bestimmungen der geltenden Promotionsordnung sind mir bekannt. Die von mir vorgelegte Dissertation ist von Herrn Prof. Dr. Bernd Viehweger betreut worden.

Sylvain Bernard Déplanque